


Spring 1-1-2017

# Zonal Articular Cartilage Possesses Complex Mechanical Behavior Spanning Multiple Length Scales: Dependence on Chemical Heterogeneity, Anisotropy, and Microstructure

Joseph Anders Wahlquist

University of Colorado at Boulder, joseph.wahlquist@gmail.com

Follow this and additional works at: [https://scholar.colorado.edu/mcen\\_gradetds](https://scholar.colorado.edu/mcen_gradetds)

 Part of the [Biomechanics Commons](#), [Biomedical Engineering and Bioengineering Commons](#), and the [Mechanical Engineering Commons](#)

---

## Recommended Citation

Wahlquist, Joseph Anders, "Zonal Articular Cartilage Possesses Complex Mechanical Behavior Spanning Multiple Length Scales: Dependence on Chemical Heterogeneity, Anisotropy, and Microstructure" (2017). *Mechanical Engineering Graduate Theses & Dissertations*. 142.

[https://scholar.colorado.edu/mcen\\_gradetds/142](https://scholar.colorado.edu/mcen_gradetds/142)

This Dissertation is brought to you for free and open access by Mechanical Engineering at CU Scholar. It has been accepted for inclusion in Mechanical Engineering Graduate Theses & Dissertations by an authorized administrator of CU Scholar. For more information, please contact [cuscholaradmin@colorado.edu](mailto:cuscholaradmin@colorado.edu).

# Zonal Articular Cartilage Possesses Complex Mechanical Behavior Spanning Multiple Length Scales: Dependence on Chemical Heterogeneity, Anisotropy, and Microstructure

Joseph A. Wahlquist

B.S. Mechanical Engineering, Brigham Young University, Utah, 2006

M.S. Aeronautical Engineering, Air Force Institute of Technology, Ohio, 2010

A thesis submitted to the  
Faculty of the Graduate School of the  
University of Colorado in partial fulfillment  
of the requirements for the degree of  
Doctor of Philosophy  
Department of Mechanical Engineering  
2017

This thesis entitled:  
Zonal Articular Cartilage Possesses Complex Mechanical Behavior Spanning Multiple Length Scales:  
Dependence on Chemical Heterogeneity, Anisotropy, and Microstructure

written by Joseph Anders Wahlquist  
has been approved for the Department of Mechanical Engineering

---

Virginia L. Ferguson, Ph.D.

---

Corey P. Neu, Ph.D.

Date\_\_\_\_\_

The final copy of this thesis has been examined by the signatories, and we find that both the content and the form meet the acceptable presentation standards of scholarly work in the above-mentioned discipline.

# Abstract

---

Wahlquist, Joseph Anders (Ph.D., Mechanical Engineering)  
Department of Mechanical Engineering, University of Colorado

Zonal Articular Cartilage Possesses Complex Mechanical Behavior Spanning Multiple Length Scales:  
Dependence on Chemical Heterogeneity, Anisotropy, and Microstructure

Thesis directed by Professor Virginia L. Ferguson, Ph.D.

This work focused on characterizing the mechanical behavior of biological material in physiologically relevant conditions and at sub millimeter length scales. Elucidating the time, length scale, and directionally dependent mechanical behavior of cartilage and other biological materials is critical to adequately recapitulate native mechanosensory cues for cells, create computational models that mimic native tissue behavior, and assess disease progression. This work focused on three broad aspects of characterizing the mechanical behavior of articular cartilage. First, we sought to reveal the causes of time-dependent deformation and variation of mechanical properties with distance from the articular surface. Second, we investigated size dependence of mechanical properties. Finally, we examined material anisotropy of both the calcified and uncalcified tissues of the osteochondral interface. This research provides insight into how articular cartilage serves to support physiologic loads and simultaneously sustain chondrocyte viability.

## Dedication

---

To my wonderful wife, April, and my four delightful children.

## Acknowledgements

---

First, I would like to thank my advisor Ginger Ferguson for her continuous and tireless efforts in providing guidance, motivation, and knowledge. I would also like to thank my committee Dr. Neu, Dr. Bryant, Dr. Long, and Dr. DelRio for their insightful comments, encouragement, and perspective they shared with me. I am deeply indebted to my coauthors, coworkers, and collaborators for all of their efforts without which this work would have not have been possible and for the fun times we have had over the last three years. Last but not the least; I would like to thank my family: my siblings, my parents, my children, and especially my wife for all of the countless hours and time they have sacrificed toward this work.

The views expressed in this dissertation are those of the author and do not reflect the official policy or position of the United States Air Force, Department of Defense, or the U.S. Government

# Contents

Chapter 1 - Motivation and Specific Aims .....	1
1.1 Motivation .....	1
1.2 First Hypothesis and Specific Aim .....	4
1.3 Second Hypothesis and Specific Aim.....	5
1.4 Third Hypothesis and Specific Aim .....	6
Chapter 2 - Background and Literature Review.....	8
2.1 Cartilage and Osteoarthritis .....	8
2.2 Current Treatment Options.....	10
2.3 Future Treatment Options .....	14
2.3.1 Hydrogels .....	14
2.3.2 Stem Cells .....	15
2.3.3 3-D printing.....	15
2.4 Chemistry and Structure of Cartilage.....	17
2.4.1 Histology .....	18
2.4.2 Secondary Harmonic Generation and Auto-Fluorescence Imaging.....	18
2.4.3 Raman Spectroscopy .....	21
2.5 Bulk Cartilage Properties.....	22

2.5.1 Mechanical Tests .....	22
2.5.2 Deformation Tracking and Digital Image Correlation .....	23
2.5.3 Fluid Permeability .....	23
2.6 Micro-Mechanical Assessment of Cartilage .....	24
2.6.1 Indentation .....	24
2.6.2 Nanoindentation and Microindentation .....	31
2.6.3 Atomic Force Microscopy .....	32
2.6.3 Anisotropic Property Assessment via indentation .....	33
Chapter 3 – Indentation Mapping Reveals Poroelastic, but not Viscoelastic, Properties	
Spanning Native Zonal Articular Cartilage .....	35
3.1 Abstract .....	35
3.2 Introduction.....	36
3.3 Methods .....	39
3.3.1 Materials.....	39
3.3.2 Histological analysis and SHG/TPF Imaging.....	40
3.3.3 Microindentation testing.....	41
3.3.4 Microindentation Analysis.....	43
3.3.5 Atomic Force Microscopy .....	44



3.3.6 Statistical Analysis .....	45
3.4 Results .....	45
3.5 Discussion .....	57
3.6 Conclusion .....	60
Chapter 4 – The influence of contact radius on the indentation response of poroelastic materials .....	62
4.1 Abstract .....	62
4.2 Introduction.....	63
4.3 Methods .....	66
4.3.1 Sample Preparation .....	66
4.3.2 AFM Conical Probe Indentation and Imaging.....	66
4.3.3 Spherical Probe Indentation and Analysis.....	67
4.3.4 Raman Spectroscopy .....	72
4.4 Results .....	74
4.4.1 AFM Conical Probe Results.....	74
4.4.2 Spherical Probe Results .....	76
4.4.3 Raman Spectroscopy Results.....	81
4.5 Discussion .....	83

4.6 Conclusion .....	89
Chapter 5 – Time-Dependent, Anisotropic, Zonal Variation of Mechanical Properties of the Osteochondral Unit .....	90
5.1 Abstract .....	90
5.2 Introduction.....	91
5.3 Materials and Methods.....	93
5.3.1 Materials.....	93
5.3.2 X-Ray and Magnetic Resonance Imaging .....	95
5.3.4 Histology, Secondary Harmonic Generation, and Two Photon Fluorescence Imaging .....	96
5.3.5 Raman Spectroscopy Imaging .....	96
5.3.6 Soft Tissue Microindentation .....	97
5.4 Results .....	98
5.5 Discussion .....	108
5.6 Limitations.....	110
5.6 Conclusion .....	111
Chapter 6 – Discussion and Conclusion .....	112
6.1 Major Findings.....	112
6.2 Significance of Work.....	114

6.4 Recommendations and Future Directions .....	117
6.5 Concluding Remarks .....	118
Bibliography .....	120

## Tables

Table 1 – Summary of observations during dissection of knees, all samples were obtained from the medial femoral condyle. Visual observation of the pervasiveness of cartilage damage (Minor, Moderate, Severe), coloration of the synovial fluid, and assessment of fracture via X-ray are indicated. .... 99

# Figures

Figure 1 - Cartilage Types and Locations in the Human Body [49]..... 8

Figure 2 – 3-D printed cartilage structure with arches mimicking the arched Benninghoff structure of collagen in native articular cartilage. A) A bilayer cartilage structure design incorporating two layers for calcified tissues and soft cartilage. B) Single layer construct design and 3-D printed structure viewed under SEM. C) Design and D) photograph of bilayer hydrogel constructs. Scale bar = 500  $\mu\text{m}$ ..... 17

Figure 3 – image of the osteochondral unit Secondary Harmonic Generation (artificially colored red) and Two Photon Fluorescence (artificially colored green). Chondrocyte and osteocyte lacuna are easily identifiable as are the zone of calcified cartilage and subchondral bone. Images can also be employed to identify collagen fiber orientation..... 20

Figure 4 - Excise location and sample groups for articular cartilage. Dots on indentation samples represent indentation arrays performed parallel to the articular surface..... 40

Figure 5 - Microindentation relaxation test load profile, indenter probe geometry, and representative indentation curves which demonstrate matched strain fields for different sized indenters ..... 42

Figure 6 - Indentation modulus of agarose demonstrates behavior of a material with time-dependent behavior dominated by poroelasticity. Hertz analysis performed on the loading portion of the indentation curve.  $*=p<0.05$  ..... 46

Figure 7 - Indentation modulus of untreated and trypsin-treated cartilage on the articular surface and at three distances from the articular surface. Untreated cartilage behaves as a poroelastic

material at all distances from the articular surface. By contrast, the underlying cause of time-dependence in trypsin-treated samples cannot be determined. Hertz analysis performed on the loading portion of the indentation curve.  $*=p<0.05$  ..... 48

Figure 8 - The tensile and compressive modulus decrease while the permeability increases for untreated and trypsin-treated cartilage as a function of distance from the articular surface. Trypsin treatment decreases tensile and compressive modulus while increasing permeability for all cartilage zones. Parameters obtained from rate compensated HBT using indents performed at multiple displacement rates. .... 50

Figure 9 – Histology and SHG/TPF images of articular cartilage demonstrate GAG depletion due to trypsin treatment but little change to collagen matrix. Safranin-O/Fast Green histological stain on paraffin embedded samples. Fresh samples imaged with SHG for collagen type II artificially colored red and TPF artificially colored green..... 52

Figure 10 - Decreased organization of collagen matrix is observed via atomic force microscopy, topography images of untreated (a) and trypsin-treated cartilage (b). Images were taken approximately 1000  $\mu\text{m}$  from the articular surface. In (a) and (b) white indicates higher and black lower topography. Scale bar = 1  $\mu\text{m}$ ..... 54

Figure 11 - Heat maps of mechanical properties obtained from indentation rate compensated nonlinear biphasic theory (HBT) demonstrate variation in mechanical properties with distance from the articular surface and treatment for representative untreated and trypsin-treated cartilage samples. .... 56

Figure 12 – Cartoon depicting the constituents and arrangement of articular cartilage across multiple length scales. Indentation methods applicable to probe the mechanical response of tissues at these various length scale are also indicated. .... 65

Figure 13 – Demonstration of multiple indenter radii and indentation systems to obtain reliable information over a broad range of indentation depths. Mean load versus contact depth curves for spherical indentation of middle zone cartilage demonstrating the loading portion of the curve for indentation depths between 0.5% and 20% of indenter radius. .... 69

Figure 14 – Biphasic surface film model produced by piecewise combination of functions describing the behavior of a thin film on a stiff substrate. This model is composed of a logarithmic average of two thin film models [153], [220] combined with two theoretical limiting cases representing (1) a compliant substrate and (2) contact of the indenter with the substrate..... 72

Figure 15 – AFM topography images indicating heterogeneity of indentation modulus at the submicron length scale while remaining well below the indentation modulus that was observed at larger length scales. AFM (a) height and (b) indentation modulus maps of an untreated (top) and trypsin-treated (bottom) cartilage surface. Scale bar = 1  $\mu\text{m}$ . (c) Cross sectional data taken from denoted locations (dashed lines) in (a) and (b). .... 75

Figure 16 – Mean indentation modulus showing differences in indentation modulus based on the contact radius. Measured using spherical AFM ( $D = 2, 25, 49, 116, 196 \mu\text{m}$ ) and Nanoindenter ( $D = 210, 500 \mu\text{m}$ ) probes for middle zone cartilage and agarose gel. Dashed lines represent maximum and minimum modulus values measured for a given contact radius. Note, both scales are logarithmic..... 77

Figure 17 – Average piecewise biphasic surface film model fit of indentation modulus recreates key features of experimental indentation modulus as a function of contact radius. Middle zone untreated cartilage is shown as a representative case. .... 79

Figure 18 – Biphasic surface film model parameters for untreated cartilage, trypsin-treated cartilage, and agarose indicate film thickness is a function of collagen matrix prevalence and arrangement and osmotic pressure of the extracellular matrix. .... 80

Figure 19 – Representative Raman maps and of full thickness cartilage and charts of mean and standard deviation of collagen and chondroitin sulfate as a function of distance from the articular surface for all samples. Note: decreased chondroitin sulfate prevalence after trypsin treatment. Variation of collagen and chondroitin sulfate with distance from the articular surface can also be observed for both untreated and trypsin treated samples..... 82

Figure 20 - Cartoon depicting indentation for two indenters of a porous material, shaded regions indicate affected regions predicted using Hertz continuum mechanics assumptions. Soft surface layer effective thickness is indicated by green dashed line. .... 86

Figure 21 – Sample excise location, orientation, and testing sequence for soft articular cartilage and calcified tissue samples. Notional locations and directions for Indentation and Raman spectra arrays are depicted as dots on the samples. Bone depicted in gold, calcified cartilage in tan, and soft articular cartilage in white..... 95

Figure 22 – Compressive modulus, tensile modulus, and permeability indicate pronounced zonal differences in material properties in both the split line (Direction 1) and perpendicular to the split



line (Direction 2) directions. The compressive and tensile moduli increased while permeability decreased with increasing distance from the articular surface. .... 101

Figure 23 – Heat maps of nonlinear biphasic mechanical properties of a representative sample in Direction 2 demonstrate the ability of microindentation to measure property variation over large areas..... 102

Figure 24 – Ratio of compressive moduli in three orthogonal directions for superficial middle and deep zone cartilage indicate that the tissue is anisotropic. This anisotropy varies in strength and direction depending on the zone tested. The behavior of an isotropic material is indicated as a green line and all statistical comparisons are made to isotropic behavior..... 103

Figure 25 – Map of T2 relaxation time (ms) at a location approximately corresponding to the location where mechanical testing was performed (red boxes) for knees with the highest (top) and lowest (bottom) average values of T2. .... 104

Figure 26 – Average T2 and T1ρ relaxation times (ms) obtained for the femoral condyle and tibial plateau in locations approximately corresponding to locations of mechanical testing. Images from knees C170123 and C161473 indicated the highest and the lowest likelihood of osteoarthritis respectively. .... 105

Figure 27 – SHG and TPF images reveal the zonal structure of cartilage and subchondral bone. For image on the left SHG is artificially colored red and TPF is artificially colored green. The demarcation between calcified cartilage and subchondral bone is identifiable based on a pronounced change in the strength of the TPF signal. Soft cartilage zones are distinguishable

based on collagen orientation as identified using NIH imageJ software (Right side of image SHG is shown in grayscale and dominant fiber direction is shown as white line segments)..... 106

Figure 28 – Raman maps showing variation in distribution of chemical constituents as a function of distance from the articular surface for two samples. The ratio of chondroitin sulfate peaks (1380, 1342 and 1068  $\text{cm}^{-1}$ ) to collagen peaks (1271, 1246, 920, 857 and 816  $\text{cm}^{-1}$ ) shown above.  
..... 108

# Chapter 1 - Motivation and Specific Aims

## 1.1 Motivation

The study of the mechanics of biological tissues is motivated by the desire to understand the behavior of these materials in healthy and degenerated states with the end goal of preventing or remedying disease. These materials frequently possess a complex hierarchy that present differing structural arrangement at different length scales. Many of these materials serve not only a mechanical function but also act as homes for living cells as they engage in construction and remodeling of their surrounding environment. The multiscale hierarchical arrangement of these tissues produces complex mechanical behavior that can vary significantly depending on the testing method and length scale.

One biological material of particular interest is articular cartilage. Degradation of cartilage results in osteoarthritis, a painful and debilitating disease [1]–[3]. A potential method to address this disease is to create synthetic cartilage implants [4]–[8]. These implants could restore proper physiologic function while enabling the regrowth of healthy native tissue. Designing scaffolds that are adequate to support physiologic loading and potentially encourage tissue repair requires an understanding of the mechanical properties of native cartilage. One of the mechanical complexities exhibited by cartilage and many other biological materials is a pronounced time-dependence. In fact, the stiffness of a cartilage varies by up to 10 fold depending on the loading rate [9]. Previous studies have also shown that cartilage is a complex multi-scale material with

significant variation from the articular surface to the bone [10]–[13]. Unfortunately, classic bulk mechanical [14]–[22], and fluid [23]–[27] testing methods are limited in their ability to assess site-specific behavior because direct loading of a specific region of cartilage in its native surroundings is not possible.

A promising approach to understand the mechanical properties of cartilage is small-scale indentation including nanoindentation, microindentation, or Atomic Force Microscopy (AFM). These methods allow probing of specific regions of cartilage to assess properties and mechanical behavior while limiting mechanical loading of adjacent tissue. Indentation further provides the opportunity to investigate elastic, plastic, and time-dependent mechanical behavior by analyzing the material response to creep, stress relaxation, and varied loading rates. The value of indentation testing is not limited to cartilage but can be applied to many biological and synthetic biomimetic materials with complex hierarchical structures.

As we seek to understand the progression of osteoarthritis and produce engineered materials to replace or repair damaged tissue, it is of vital importance that we know how the native material behaves. One of the biggest challenges in this arena has to do with establishing a proper material model to represent cartilage behavior and then using that model to observe the material properties for each region of cartilage. There has been, and still is, vigorous debate regarding which material models best represent the mechanical behavior of cartilage and little discussion about how this might vary throughout the cartilage thickness [28]–[32]. Another major challenge is determining which material properties best represent cartilage behavior at the length scales relevant to tissue engineering. It is important to reconcile the sometimes wildly

discrepant values of material properties observed when measuring cartilage particularly at the sub millimeter length scales and indicate to material engineers and modelers which are the appropriate design targets [28], [30], [33], [33]–[40]. Further, experimental observations have indicated that cartilage behaves differently based on the direction of testing [10], [41]–[44]. Finally, an area of tissue that has been frequently neglected is the zone of calcified cartilage which plays an important role in transferring loads through the joints into the bone and may also play an important role in fluid transport into and out of the articular cartilage [45]. Understanding the native tissue properties throughout the full osteochondral region provides key insight as we seek to prevent or treat arthritis.

The overall objectives of this work are threefold. First, we have quantified the time-dependent mechanical behavior of articular cartilage and biomimetic materials. Experimental results were fit to models that account for cartilage time-dependent behavior including viscoelasticity [46], linear biphasic poroelasticity [47], and nonlinear biphasic poroelasticity [36]. A process was established which provides clear criteria for selection of the appropriate material model. Identification of a proper material model not only enabled quantitative measures of material properties but also elucidated the underlying physical phenomena that result in load rate dependent response. Using the appropriate model for cartilage, the time-dependent mechanical response was measured as a function of distance from the articular surface.

The second objective of this effort is to understand and quantify the mechanical properties of cartilage across multiple length scales. Prior researchers have observed that material properties of biological materials vary by multiple orders of magnitude depending on

the length scale of the indentation [34], [36]. We observed that these length scale dependent changes in mechanical behavior arise from the pore size of the extracellular matrix, the arrangement of the collagen matrix, and the osmotic potential of the tissue. Observations of these phenomena are important to understanding the interaction of cells with their environment and characterization of fluid filled biological materials.

Third, we observed the mechanical behavior of articular cartilage in three orthogonal directions and used these measurements to investigate the anisotropy of soft articular cartilage. We further measured the variation in anisotropy as a function of distance from the articular surface. Finally, we correlated mechanical properties with chemical properties as revealed through Raman spectroscopy and collagen matrix structure via Secondary Harmonic Generation (SHG) imaging to elucidate the relationship between mechanical behavior and chemistry for all zones of articular cartilage.

## 1.2 First Hypothesis and Specific Aim

We tested the hypothesis that a nonlinear biphasic model represents the time-dependent mechanical behavior of articular cartilage better than linear biphasic or viscoelastic models and explains the high compressive strength of articular cartilage. We utilized untreated and glycosaminoglycan (GAG) depleted cartilage resulting in increased permeability. We further hypothesized that (a) time-dependent mechanical behavior of cartilage is strongly influenced by depletion of GAG molecules and (b) mechanical response of cartilage varies with distance from the articular surface with higher permeability and lower moduli near the articular surface compared to the middle and deep zones.

### *Specific Aim 1*

*Developed a systematic process to experimentally reveal the underlying cause of time-dependent mechanical behavior in zonal articular cartilage. To achieve this aim, several sub aims were completed:*

*1a. Demonstrated that a nonlinear biphasic model best represents cartilage mechanical behavior.*

*1b. Compared the behavior of untreated and GAG depleted cartilage.*

*1c. Quantified the material properties of cartilage as a function of distance from the articular surface.*

### 1.3 Second Hypothesis and Specific Aim

We tested the hypothesis that articular cartilage exhibits significantly different modulus values when tested at millimeter, micrometer, and nanometer length scales. We also sought to explain this length-scale dependent modulus variation through a range of analytical approaches. We confirmed that this effect is only partially explained by matrix compaction, poroelastic indentation rate, and surface roughness. We proposed that the newly liberated surfaces of within tissue could be modeled as a thin film of soft material on a stiffer substrate. We then investigated the correlation between this film's thickness and the prevalence and arrangement of the extracellular matrix and the osmotic potential of the tissue. These results help to illuminate the microstructure of cartilage and the behavior of this tissue at a newly liberated surface, *i.e.* fracture. Similar mechanisms may be present at a sharp transition in material stiffness, *i.e.* cell

and extracellular matrix interface. This also has important implications regarding the applicability of continuum mechanics analysis at cell relevant length scales.

### *Specific Aim 2*

*Experimentally measured the stiffness of articular cartilage across multiple length scales. To achieve this aim, several sub aims were be completed:*

*2a. Applied closed form solutions that correct for matrix compaction, surface roughness and indentation rate effects.*

*2b. Determined the soft layer thickness and stiffness using a thin film indentation analytical model.*

*2c. Compared film thicknesses for superficial, middle, and deep zones of untreated and trypsin-treated cartilage to collagen and GAG content.*

## 1.4 Third Hypothesis and Specific Aim

We hypothesized that hyaline articular cartilage is an anisotropic material with higher stiffness that is related to the predominant collagen fiber direction. Additionally we sought to collaborate the mechanical properties observed via nanoindentation with X-Ray, Magnetic Resonance Imaging (MRI), SHG imaging, histology, and Raman spectroscopy to explore the connection between mechanical properties and the underlying chemistry and structure of the tested materials.

### *Specific Aim 3*



*Measured the anisotropic and depth dependent properties of zonal hylaine articular cartilage and relate those properties to the underlying chemistry and structure. To achieve this aim, several sub aims will be completed:*

*3a. Quantify the material properties articular cartilage as a function of distance from the articular surface.*

*3b. Quantify the material properties of zonal articular cartilage in three orthogonal directions.*

*3c. Correlate observed mechanical properties with underlying chemistry and structure observed via various methods.*

## Chapter 2 - Background and Literature Review

### 2.1 Cartilage and Osteoarthritis

Cartilage is an important biological material found in many locations throughout the body (Figure 1). It provides a supporting framework for some organs such as the airway (nose, trachea, and larynx), provides a low friction surface at the ends of articulating bones, and serves as a pattern for bone growth in maturing individuals [48]. Based on extracellular matrix and mechanical function, cartilage is grouped into three major types: fibrocartilage, elastic cartilage, and hyaline cartilage. Fibrocartilage is a major constituent of intervertebral discs, tendon insertions, and the meniscus. Elastic cartilage, as found in the outer ear, is the most deformable type of cartilage because it has a high elastin content [48]. Hyaline cartilage is the most common form of cartilage and can be found in rib ends, nose, trachea, joints, and juvenile bones [48].

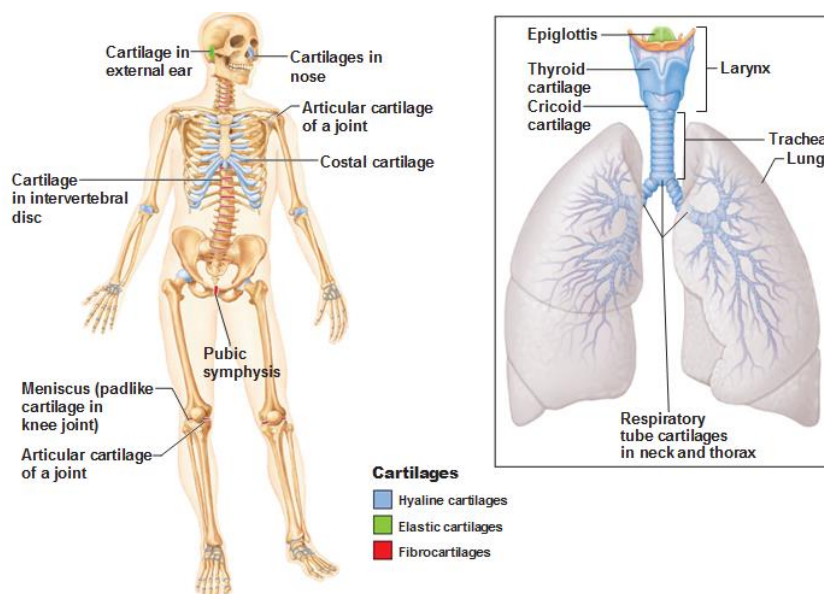


*Figure 1 - Cartilage Types and Locations in the Human Body [49]*

The most studied subcategory of hyaline cartilage is articular cartilage [50]. This type of cartilage covers the articulating ends of bones in synovial joints such as the hip or knee. A synovial joint consists of a strong and highly vascularized fibrous capsule, the cartilage covered surfaces of bones, ligaments, and in the case of the knee a meniscus. Articular cartilage is a notable biological material because it is both avascular and aneural. Thus, nutrient transfer in cartilage is accomplished solely through diffusion through the synovial fluid resulting in slowly rates of tissue repair [51]. Degradation of articular cartilage causes significant pain, as nerves in bones are exposed to stress and fretting during joint loading and articulation. Arthritis is the general term given to diseases affecting joints that result in deterioration of articular cartilage. Two of the most common types of arthritis are rheumatoid arthritis and osteoarthritis. Rheumatoid arthritis involves an autoimmune reaction within joints. Osteoarthritis is a disease that results from both chronic and acute mechanical damage to cartilage. Arthritis affects between 27 and 50 million people in the United States [1]–[3] causing indirect and direct medical costs in excess of \$86 billion [52]. This disease is predominantly experienced by elderly individuals but also can occur in children or active individuals in their twenties and thirties [3]. While the details of osteoarthritic progression are still being studied, impact loading of cartilage frequently leads to early onset of osteoarthritis [53]–[56]. The form of the disease resulting from acute injury is referred to as posttraumatic osteoarthritis (PTOA). Prompt intervention following damage has the potential to prevent PTOA by quickly restoring proper joint function. However, current repair methods leave significant room for improvement [57].

It has long been noted that when articular cartilage is damaged, normal biological processes fail to adequately repair wounds [58]. In fact, the inability of cartilage to repair damage was noted as early as 370 BC by Hippocrates [48]. Cartilage damage can result from traumatic injury, chronic usage, or due to genetic or metabolic conditions. Frequently, lesions occur at the articulating surface of the cartilage and progressively increase in width and depth until the lesion reaches the full cartilage thickness. When the underlying bone layer is breached, stem cells, growth factors, and blood may form a clot in the cartilage layer. This process is capable of repairing damages 1-2 mm in size, but larger and smaller damage is not innately repaired [57]. Additionally, this repair produces fibrocartilage that possesses inferior mechanical properties to articular cartilage. This repair tissue quickly deteriorates resulting in progression of osteoarthritis.

## 2.2 Current Treatment Options

There are multiple clinical treatment options which attempt to address cartilage deterioration for both small and large defects [59], [60]. These options will be briefly discussed in ascending order of invasiveness along with the advantages and limitations of each approach. The least aggressive method of treatment for osteoarthritis is through oral medication. At early stages of the disease, patients typically resort to the use of analgesics like acetaminophen or Nonsteroidal Anti-Inflammatory Drugs (NSAIDs) like ibuprofen or celecoxib. While these medicines alleviate some of the pain associated with osteoarthritis they are frequently insufficient to fully mask the symptoms. Clinicians also recommend glucosamine and chondroitin sulfate supplements in an attempt to slow the progression of osteoarthritis. The effectiveness of

these supplements is disputed with some sources showing mild positive effects while others find little to no effect [61]–[63].

In an attempt to rid the affected joints of debris created through the progression of arthritis, some clinicians perform joint irrigation or lavage. This is accomplished either through a needle or during other arthroscopic procedures. The effectiveness of this approach is still under debate with some studies showing improvement in patient symptoms for up to one year [64], [65] while others indicate no improvement over placebo treatments [66], [67]. While this procedure may be helpful in relieving symptoms for a short period, it appears to be ineffective in resolving the root causes of cartilage degeneration and pain.

Fibrillated cartilage can also be removed from osteochondral defects. These methods include shaving and debridement. Unfortunately, these approaches have not produced healing of articular cartilage and may actually cause further damage cartilage adjacent to the lesion [68]–[71]. A potential improvement on these methods is the use of laser ablation; however, this method likewise has not been shown to produce positive outcomes in prospective clinical trials [57], [72]. Additionally, there does not exist a clear biological rationale for expecting that these treatments would induce lesion healing.

A more helpful alternative involves stimulation of the body's natural clotting and fibrocartilage response. These methods rely on disruption of the subchondral bone plate to induce bleeding into the cartilage defect. In abrasion chondroplasty, the surgeon uses a burr to disturb the bone and inducing bleeding. Alternately, Pridie drilling uses a 2-2.5mm drill to create perforation of the bone inducing marrow to flow into the region of damaged cartilage. A study

on rabbits has shown that Pridie drilling produces superior fibrocartilage to abrasion chondroplasty [73]. If the entire subchondral bone plate is removed and only underlying trabecular bone and marrow are left below the defect this is called spongification. This technique is clinically uncommon, has been primarily used on patellar cartilage, and had not been studied in animal models [74], [75]. Microfracture represents a variation on Pridie drilling in which small 0.5-1 mm diameter holes are punched 3-4 mm apart to a depth of approximately 4 mm [76]. This procedure has the advantage that it can be performed arthroscopically, causes less disruption to the natural bone plate geometry, and may be performed with simple instruments such as an awl. Animal models have shown that this procedure results in the formation of fibrocartilage [77]. This procedure has produced good results with functional improvements and defect filling for patients who were young or had a low BMI [78]–[81]. However, there are limitations to this repair as approximately one third of patients undergoing this procedure have radiographic evidence of early arthritis only five years after surgery [82]. Clinical outcomes were also found to worsen 18-24 months following surgery [83].

Autologous chondrocyte implantation is a two-part procedure. The first procedure involves arthroscopically obtaining a biopsy of cartilage tissue from the patient. This tissue is then processed to isolate the chondrocytes and placed in media that induces cellular proliferation. These cultured cells are re-inserted into the patient six to eight weeks following the first surgery either arthroscopically using fibrin glue or via open surgery wherein a periosteal patch is used to cover the defect and the expanded chondrocytes are injected under the patch. Some studies

show that this approach produces better results when compared to microfracture while others show no significant difference or worse outcomes [83].

Osteochondral autograft and allograft involves removal of the damaged region of cartilage and the underlying bone plate. In autograft, osteochondral plugs from an undamaged (and less critical) portion of the joint are extracted and used to fill in the damaged location. Allograft involves obtaining the osteochondral plugs from a donor rather than the patient. This process can use a single plug to fill a small defect or multiple smaller plugs to fill a large defect (mosaicplasty). Autologous grafts produced similar outcomes as autologous chondrocyte implantation or microfracture and all three procedures produced improvement when compared to perioperative outcomes [83].

The final treatment option for osteoarthritis is total joint replacement. This is frequently performed on knee and hip joints with approximately 267,000 hip and 571,000 knee replacements occurring annually in the United States [84]. It is expected that the number of joint replacement surgeries will increase sharply in the coming years [84], [85]. Total joint replacements are highly invasive procedures with long recovery times. Even after total joint replacement pain may still be a persistent problem with 6-15% of patients reporting severe or extreme pain 3-4 years after surgery [86]. Additionally, revision rates for these surgeries is approximately 6% at 5 years and 12% at 10 years [87].

## 2.3 Future Treatment Options

Because the body is unable to repair severely damaged articular cartilage and current treatments present significant drawbacks, researchers have turned to synthetic materials in an attempt to find a solution. This has proven to be a very difficult task as native cartilage is capable of sustaining up to 20% strain [15], [88]–[93] which allows it to distribute compressive loads over a large portion of the subchondral bone. It also provides an extremely low friction surface and is capable of supporting compressive loads between 6 and 18 MPa [94]–[97]. Additionally, the repair material would ideally integrate in with surrounding tissue as researchers have noted that the native articular cartilage adjacent to an induced injury frequently becomes necrotic [98]. For these reasons, it is desirable to fill cartilage defects with a material that would be biocompatible, restore mechanical function, and incorporate with adjacent undamaged cartilage.

### 2.3.1 Hydrogels

One promising group of materials for biomimetic implants are hydrogels. These materials are both compositionally and structurally similar to many native tissues. They are composed of hydrophilic polymers formed into three-dimensional networks. These networks can be formed by either covalent bonds or physically intermolecular interactions. Hydrogels can absorb large amounts of water similar to biological materials and reach an equilibrium swelling balance as osmotic forces pulling fluid into the material come into balance with the cohesive forces of the matrix. This allows hydrogel swelling ratio to be adjusted by varying the crosslink density and the hydrophilicity of the polymer. Hydrogels have also proven suitable to cellular survival and proliferation [4]–[8]. These materials are highly customizable allowing synthesis with varying



stiffness, porosity, and permitting tethering of chemical cues to affect biological incorporation [4], [6]. Hydrogels have been explored for direct use as a replacement for articular cartilage but significant challenges have been encountered. One of the primary issues is that hydrogels that have proven suitable for cellular survival and proliferation have moduli much less than 1 MPa [4]–[8]. This is problematic for application to articular cartilage because many joints experience stress that greatly exceeds the load carrying capacity of these gels.

### 2.3.2 Stem Cells

Use of stem cells in scaffolds has been proposed as a method whereby a synthetic construct would be replaced over time by healthy native tissue. One promising source of stem cells is mesenchymal stem cells (MSCs) derived from bone marrow. These MSCs are multipotent and can be induced to differentiate into either chondrocytes or osteocytes. Differentiation can be induced using chemical cues like transforming growth factor- $\beta$  (TGF- $\beta$ ) [99] or Arginylglycylaspartic acid (RGD) [7]. Additionally, fluid shear stress [100] or mechanical loading in have been shown to be effective in producing either chondrogenesis or osteogenesis [4], [5], [101]. As the chondrogenic cells thrive and mature in these synthetic environments, they produce extracellular matrix (ECM) with the expectation that this will eventually result in recreation of healthy articular cartilage.

### 2.3.3 3-D printing

Because chondrocytes thrive in very soft matrix environments but those same materials are insufficient to support normal joint loading a multiphase system is desirable. Using this approach, one material phase can be tailored to provide an optimal cellular niche while the other

phase can be synthesized to support mechanical loading. There are various strategies for organizing these phases but one of the most promising is the use of 3-D printing. 3-D printing allows the stiff and soft phases to be arranged in structural patterns mimicking native cartilage structure (Figure 2). 3-D printing is a relatively new innovation in bioengineering and various materials are being investigated for suitability including alginate [102], fibrin [103], [104], and PEGDM [105], [106]. One of the important challenges of creating 3-D scaffolds mimicking native tissue behavior is to understand the behavior of native tissue. By having a clear understanding of the properties within healthy native zonal articular cartilage, calcified cartilage, and subchondral bone, design targets for tissue engineering can be established. This will enable tissue engineers to prescribe properties and develop printing geometries to capture the complexities of native osteochondral tissues. These 3-D systems show great promise and are a very active area of research.

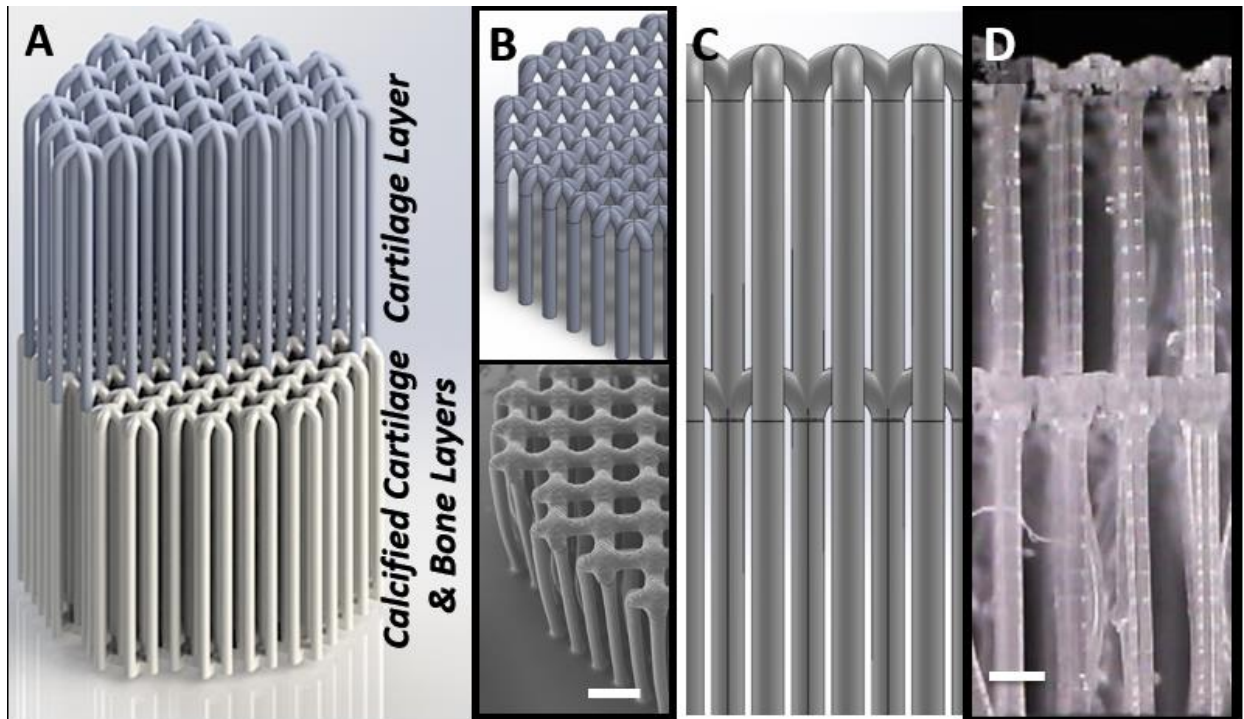


*Figure 2 – 3-D printed cartilage structure with arches mimicking the arched Benninghoff structure of collagen in native articular cartilage. A) A bilayer cartilage structure design incorporating two layers for calcified tissues and soft cartilage. B) Single layer construct design and 3-D printed structure viewed under SEM. C) Design and D) photograph of bilayer hydrogel constructs. Scale bar = 500  $\mu$ m*

## 2.4 Chemistry and Structure of Cartilage

The chemical composition of cartilage was investigated as early as the 1940's with Hirsch establishing a correlation between the mechanical response of cartilage and the chondroitin sulfate content [107]. Early researchers also noted that depletion of chondroitin sulfate was one of the early signs of osteoarthritis [108]. Cartilage was also found to have different chemical composition at varying depths from the articular surface [19], [109], [110] which resulted in non-

uniform fluid permeability and mechanical properties [26], [27]. Later work has confirmed the initial findings that cartilage has a higher water and collagen content near the articular surface and has an increasing GAG and glycoprotein concentration with increasing depth [111].

#### 2.4.1 Histology

While not a quantitative method of evaluating cartilage. Histology has proven invaluable to understanding cartilage composition and structure [112], [113]. One of the most common histological stains in cartilage is safranin-o/fast green. Fast green serves as a background stain while safranin-o is a cationic dye that stains proteoglycans and glycosaminoglycans [114]. Staining for collagen can be accomplished with picosirius red and when used in conjunction with polarization microscopy this stain can identify predominant collagen fiber orientation[115]. Staining for additional ECM components can be accomplished via Immunohistochemistry which reveals both their prevalence and spatial distribution [116]–[118].

#### 2.4.2 Secondary Harmonic Generation and Auto-Fluorescence Imaging

Another method that allows for observation of chemical constituents in cartilage is Secondary Harmonic Generation (SHG) imaging (Figure 3). The SHG phenomenon was first observed in 1961 in shortly after the invention of the laser. When non-centrosymmetric molecules are excited by two coherent photons they produce a single output signal at half the wavelength of the excitation photons [119], [120]. Because this imaging modality requires two input photons to produce a single output photon, it is an inherently confocal technique and exhibits a high spatial resolution. This technique can be used to image non-centrosymmetric molecules including type I and type II collagen molecules [121]–[123]. Further, signal strength

has a strong dependence on the crystallinity and alignment of the collagen fiber bundles that provides the opportunity to visualize collagen fibers and discern their orientation. Two-photon fluorescence (TPF) is similar to SHG in that it requires two photons to impinge on a molecule. However, unlike SHG that produces a signal via harmonic resonance, TPF results from autofluorescence of molecules in which the excitation wavelength is longer than the emission wavelength.

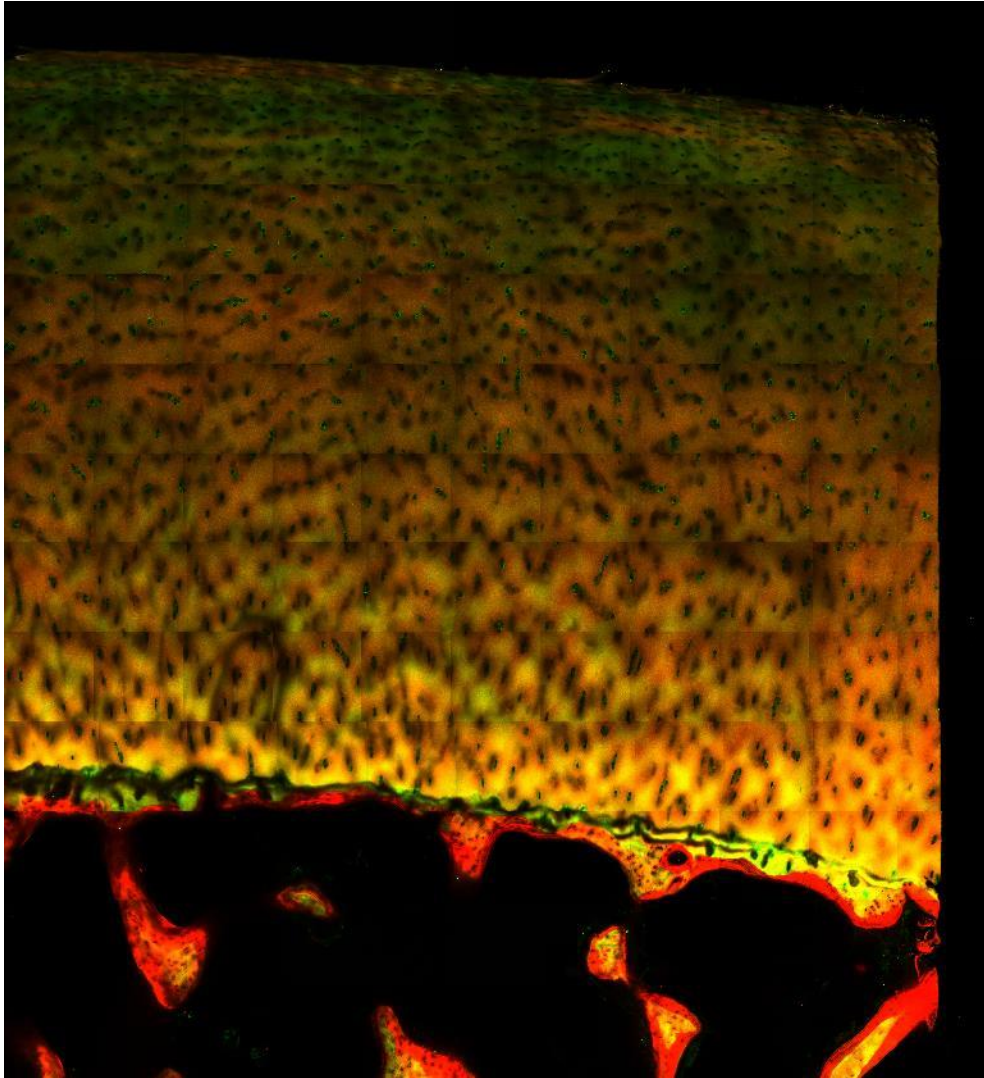


*Figure 3 – image of the osteochondral unit Secondary Harmonic Generation (artificially colored red) and Two Photon Fluorescence (artificially colored green). Chondrocyte and osteocyte lacuna are easily identifiable as are the zone of calcified cartilage and subchondral bone. Images can also be employed to identify collagen fiber orientation.*

Yeh *et al.* used SHG and TF to obtain two and three dimensional images of articular cartilage [123]. They noted that excitation with an 800 nm wavelength laser produced SHG and

TPF signals that were spectrally separable. They also found that, in contrast to type I collagen as found in bones, type II collagen does not exhibit polarization dependence. Type II collagen fiber arrangement was observable via SHG signal and the elastin and cellular nuclei were observed in TPF. One of the advantages of imaging using these modalities is that no stains or dyes are required [122]. Additionally, samples can be imaged as thick samples in immersion fluids consistent with physiological conditions. This allows for observation of constituent arrangement in near native surroundings with few preparation artifacts.

### 2.4.3 Raman Spectroscopy

Another imaging technique which can be used to identify chemical constituents within a material is Raman spectroscopy [124]. When monochromatic light is directed onto the sample, most of the interactions result in elastic scattering events wherein light is reflected at a wavelength equal to the excitation wavelength. However, for a small portion of the interactions, the photons are inelastically scattered resulting in a shift either to either a lower (stokes) or higher (anti-stokes) energy wavelength. The wavelength shift observed due to this inelastic scattering is characteristic of the molecular bonds of the investigated material. This provides a “fingerprint” whereby chemical constituents can be identified. Bonifacio *et al.* investigated dried sections of articular cartilage via Raman spectroscopy and analyzed their results using univariate and multivariate methods [125]. They were able to identify and localize DNA, chondroitin sulfate, collagen, and non-collagenous proteins using both analytical methods. The univariate method applied by Bonifacio *et al.* actually used three to five peak intensities per constituent to reduce noise, in contrast to a standard univariate analytical approach that utilizes a single peak for each

constituent. Both of these analytical methods allow Raman spectroscopy provides a semi-quantitative measure of chemical species with resolution capable of distinguishing single cells.

In bone, Raman spectral measurements have been employed to observe mineral and collagen matrix. The mineral phase has primary peaks at  $960\text{ cm}^{-1}$  (v1 phosphate),  $430\text{ cm}^{-1}$  (v1 phosphate), and  $1070\text{ cm}^{-1}$  (B-type carbonate). The collagen matrix has prominent peaks at  $1670\text{ cm}^{-1}$  (amide I),  $1270\text{ cm}^{-1}$  (amide III) [126], and  $855\text{ cm}^{-1}$  (proline). Because, Raman signals arising from these molecules are polarization dependent it is important to select mineral to matrix ratios for phase matched signals which include v2 phosphate/amide III and v1 phosphate/proline [127], [128]

## 2.5 Bulk Cartilage Properties

### 2.5.1 Mechanical Tests

Bulk mechanical testing of cartilage has been performed on articular cartilage sections and full thickness osteochondral plugs. Test configurations have included unconfined compression [9], [14], [15], confined compression [12], [16]–[18], tension [19]–[22], and large scale indentation [129]–[132]. These bulk tests have investigated not only the equilibrium modulus of cartilage but also the instantaneous modulus and the time dependence of the response. Significant work has been invested in understanding the creep and relaxation behavior and elucidating the underlying processes involved in causing this time dependence [133], [134]. Mao *et al.* proposed linear biphasic and triphasic models for cartilage behavior where the solid phase produces an elastic response and the transportation of the fluid phase is responsible for



the material time dependence [29], [48], [135], [136]. This method was further expanded to address nonlinear tension and compression behavior [28].

### 2.5.2 Deformation Tracking and Digital Image Correlation

One method to measure the differential zonal behavior of cartilage while maintaining an intact osteochondral structure is to take images of the cartilage during loading. By staining cells, these images show movement of chondrocytes and thus provide information about the relative stiffness of cartilage zones. The Sah group pioneered this effort and its application has led to a greater understanding of the effects of zonal differences on the mechanical response of cartilage [11], [17]. If these images are acquired digitally, software can be used to extract strain maps of the loaded region via digital image correlation [137], [138]. In addition to tracking the two dimensional movement of cells, confocal microscopy allows for the tracking of cell motion in three dimensions and even deformation of individual chondrocyte lacuna [139].

### 2.5.3 Fluid Permeability

The permeability of articular cartilage to fluid flow has been measured by various methods. The most straightforward technique has been to immerse the cartilage or osteochondral samples in a solution containing dye then observe the progression of this dye into the cartilage [23]. It was observed that diffusion into cartilage with fluid agitation was significantly greater than penetration without stirring suggesting the importance of joint mobility in nutrient transport within cartilage. Fluid permeability was also measured in conjunction with compressive loading and it was found that as compressive loads increased, there was a densification of the extracellular matrix and the permeability of the cartilage decreased [24]. Additionally, solute size

has been found to be an important factor in determining cartilage permeability as cartilage behaves as a nearly impenetrable membrane to large molecules like serum albumin [23]. Alterations in cartilage permeability with age, excise location, and osteoarthritis have been studied [26]. Finally, cartilage permeability has been directly measured by placing plugs in a pressure differential permeability test apparatus [25]. By slicing subsequent thin sections of cartilage parallel to the articular surface, Maroudas found that permeability decreased with increasing distance from the articular surface [27].

## 2.6 Micro-Mechanical Assessment of Cartilage

### 2.6.1 Indentation

Extraction of material properties from indentation was first investigated by Hertz [140], [141] who developed equations which represent the contact radius of two elastic spheres. Throughout this dissertation, it is assumed that the probe is much stiffer than the tested material. The indented material is treated as an infinite half space simplifying Hertzian contact problem and resulting in Equations 1 and 2.

$$E^* = \frac{E}{1 - \nu^2} = \frac{3}{4} \frac{F}{R^{0.5} h^{1.5}} \quad (1)$$

$$a = \sqrt{Rh} \quad (2)$$

Here, the indentation modulus ( $E^*$ ) is related to the elastic modulus ( $E$ ) and the poisons ratio ( $\nu$ ) of the tested material. Indentation modulus is also given as a function of the contact force ( $F$ ) the radius of the indenter ( $R$ ) and indentation depth ( $h$ ). The contact radius ( $a$ ) is directly related to the indenter radius by assuming the material behaves elastically.

This method has been expanded to account for elastic-plastic behavior [142], [143]. This approach asserts that during the loading portion of the indentation curve there are contributions to deformation from both elastic and plastic mechanisms. However, during unloading the material behaves only elastically. This approach isolates the elastic response of the material and enables measurement of reduced modulus ( $E_R$ ). To employ this approach, a relationship between contact depth ( $h_c$ ) and contact area ( $A$ ) is established via fitting constants ( $C_0, C_1, C_2$ , etc.) (Equation 3). This tip area function can be quantified by repeated indentation in a material of a known modulus and Poisson's ratio. Having established this relationship between indentation depth and contact area, the unloading load ( $P$ ) versus depth ( $h$ ) can be fit resulting in material stiffness ( $S$ ) by using Equations 4 and 5 where  $\varepsilon = 0.75$  for a paraboloid of revolution. This reduced modulus can then be converted to elastic modulus of the tested material ( $E_1$ ) if the elastic modulus of the probe ( $E_{tip}$ ) and the Poisson's ratio of the tested material ( $\nu_1$ ) and probe ( $\nu_{tip}$ ) are known (Equation 6) [144].

$$A = C_0 h_c^2 + C_1 h_c + C_2 h_c^{1/2} + C_3 h_c^{1/4} \dots \quad (3)$$

$$E_R = \frac{dP}{dh} \frac{\sqrt{\pi}}{\sqrt{A}} = S \frac{\sqrt{\pi}}{\sqrt{A}} \quad (4)$$

$$h_c = h_{max} - \varepsilon \frac{P_{max}}{S} \quad (5)$$

$$\frac{1}{E_R} = \frac{(1 - \nu_1^2)}{E_1} + \frac{(1 - \nu_{tip}^2)}{E_{tip}} \quad (6)$$

Elastic contact mechanics has also been expanded to include time-dependent behavior [46], [145], [146]. The methods used to explain time-dependent behavior are based on two broad categories of underlying physical causes of rate dependence. The first is viscoelastic behavior; these models assume the tested material acts as a single-phase continuum with time-dependence arising from changes in molecular arrangement. In polymers, this occurs via breaking and reformation secondary bonds. For indentation, testing two common methods are employed to observe this phenomenon. First, the probe is maintained at a constant indentation depth and the relaxation of load is observed. Second, the load applied to the indenter is maintained constant and the increase in indentation depth is observed. Mattice *et al.* [147] developed a method of analyzing indentation data to extract material characterization parameters using these assumptions and common testing approaches. This technique can incorporate an unlimited number of parameters to model material response at multiple time scales. However, in this work, we apply only the most basic form of this model as follows:

$$G(t) = C_0 + C_1 \exp(-t/\tau_1) \quad (7)$$

$$G_0 = \frac{G(0)}{2} = \frac{C_0 + C_1}{2} \quad (8)$$

$$G_\infty = \frac{C_0}{2} \quad (9)$$

Where ( $G$ ) is the shear relaxation modulus of the tested material, the constants ( $C_0$ ) and ( $C_1$ ) are material parameters obtained through fitting the relaxation curve and ( $\tau_1$ ) is the time constant. The instantaneous ( $G_0$ ) or long-term shear modulus ( $G_\infty$ ) and Poisson's ratio ( $\nu$ ) can be used to find  $E$  through the equation  $E = 2G (1 + \nu)$ .

The second category of models used to explain time-dependent deformation are based on the assumption that a tested material is made up of two or more distinct components [29], [46], [135], [145]. The simplest of these, the biphasic model, assumes these components can be divided into a compressible elastic solid phase and an incompressible fluid phase. The further assumption is made that all electrostatic and physical interactions between the fluid and the solid phase can be incorporated into a single permeability term. Two of the analytical methods that have been developed to investigate biphasic poroelastic material behavior using indentation testing were proposed by Hu *et al.* [47] and the Burriss research group [30], [36], [148], [149]. The model proposed by Hu *et al.* was formed by creating a master curve representing material behavior based on a large number of runs of a finite element model spanning a broad spectrum of material parameters. It assumes that the solid phase behaves as a linear elastic material and that all the time-dependent response can be attributed to the flow of the fluid phase through the material. The equations applicable to displacement controlled relaxation test using a spherical indenter are:

$$\frac{F(t) - F(\infty)}{F(0) - F(\infty)} = g(\tau) \quad (10)$$

$$F(0) = \left(\frac{16}{3}\right) Gha \quad (11)$$

$$g(\tau) = 0.491 \exp(-0.908\sqrt{\tau}) + 0.509 \exp(-1.679\tau) \quad (12)$$

$$\tau = Dt/a^2 \quad (13)$$

$$D = \left[ \frac{2(1-\nu)}{1-2\nu} \right] Gk \quad (14)$$

Here,  $F$  measured as a function of time ( $t$ ) is related to the force measured immediately upon reaching the indentation depth when relaxation begins ( $t=0$ ) and the force measured at a very long time after relaxation ( $t=\infty$ ) by the empirical equation  $g(\tau)$ . Where the normalized time ( $\tau$ ) is related to  $t$ ,  $a$ , and the diffusivity ( $D$ ).  $D$  is in turn related to  $\nu$ , the permeability ( $k$ ) of the matrix specific to the fluid permeating the matrix. Fitting the relaxation curve provides measures of  $G$ ,  $\nu$ , and  $k$ .

Alternately, closed form solutions for material response can be obtained by assuming that the Poisson's ratio of the tested material is near zero and that the solid phase behaves linear elastically in tension and compression separately but with different tensile and compressive moduli. This nonlinear biphasic approach was proposed by Soltz and Ateshian [28] and applied to indentation by the Burris group [30], [36], [148], [149] This model is known as the Hertz-Burris Theory (HBT) and can be represented as follows:

$$F' = \frac{F - F_s}{F} = \left( \frac{E_t}{E_t + E_{c0}} \right) \left( \frac{\dot{\delta}R}{\dot{\delta}R + E_{c0}k} \right) \quad (15)$$

$$E_c = \frac{E_{c0}}{1 - \left( \frac{E_t}{E_t + E_{c0}} + \frac{\dot{\delta}R}{\dot{\delta}R + E_{c0}k} \right)} \quad (16)$$

The portion of the total load supported by resistance to movement of the fluid phase is called the fluid load fraction ( $F'$ ). The total load is ( $F$ ) and the load present due to the solid matrix ( $F_s$ ). It should be noted that if the tensile modulus ( $E_t$ ) and compressive modulus ( $E_c$ ) are equal then  $F'$  is limited to a value of 0.5 for indentation, even at very fast loading rates. The effective contact modulus ( $E_c$ ) can be found for any point during the test using the Hertz equation ( 1 ) and

includes contributions from both the fluid and solid components. After a sufficient creep or relaxation hold time, the equilibrium contact modulus ( $E_{co}$ ) can be found.

Indentation provides an intriguing method to test whether the time-dependent mechanical response of articular cartilage, or other soft tissues, results from viscoelastic or poroelastic origins. Because viscoelastic models assume that materials act as a single continuum, the mechanical response should be independent of indenter size if the maximum strain level and strain rates are kept constant. For indentation testing this means that if the indentation time and the ratio of indenter depth to indenter radius are kept constant, the extracted material parameters should not vary with indenter size. On the other hand, because poroelastic models assume the time-dependent response is due to fluid transport, the size of the indenter has a nonlinear impact on the behavior of the tested material. For these models a characteristic indentation time can be established which is proportional to the square of the indentation radius. This dissertation uses a novel method by performing indentation tests with multiple sized indenters at rates matched via viscoelastic or poroelastic assumptions, thus determining whether the primary cause of time-dependent behavior is due to fluid transport or physical rearrangement of the solid material.

One of the limitations of the poroelastic indentation models is that they are based on the assumption that loading occurs very quickly. Rapid loading produces a pressure differential as the fluid is forced out of the region under the indenter. The poroelastic models then use the time-dependent flow to characterize the moduli of the solid phase and the permeability of the material. The fluid pressurization and flow depends on the size of the indenter, the depth of

indentation, and the indentation rate. The rate of fluid transport through a biphasic material can be quantified using the non-dimensional Peclet Number ( $Pe$ ).

$$Pe = \frac{\dot{\delta} R}{E_{c0}k} \quad (17)$$

Because the Peclet number is a function of indenter radius, when the indenter size is small, a very rapid loading rate is required to extract reliable material parameters. When loading occurs at a rate that is not fast enough to create significant fluid pressure, the poroelastic models are cannot directly assess material properties. Specifically, the HBT model underestimates the tensile modulus and does not produce a consistent value for permeability using data from a single indent. The linear biphasic model proposed by Hu *et al.* will also overestimate the Poisson's ratio and give a poor estimate of permeability. The equipment used to perform nanoindentation in this study was unable to indent at rates fast enough to consistently measure the material parameters using the poroelastic models with data from a single test. However, by performing indentation tests at multiple loading rates and with different sized indenters the material response at varying Peclet numbers can be used to predict the material parameters that would be observed if the test were performed at a sufficiently fast loading rate. This approach follows the methods outlined in [36] using the following equation.

$$F' = F'_{max} \frac{Pe}{Pe + 2} \quad (18)$$

Here the fluid load fraction for a particular test ( $F'$ ) are related to the maximum attainable fluid load fraction ( $F'_{max}$ ) and the Peclet number ( $Pe$ ). By performing multiple tests while varying



the indentation rate and/or the radius of the indenter, the fluid load fraction for each particular test can be used to determine the  $F'_{max}$ , and  $k$ .

Large-scale indentation of cartilage has been performed on extracted tissue plugs and even whole joints. These tests have been used to investigate the influence of osteoarthritis [107], immersion fluid [14], [150], age [151], and indentation site [131]. While some testing has been performed in quasi-static conditions, many researchers have also investigated the time dependence of the indentation response [30], [36], [131]. Testing cartilage with large indenter tips has some inherent challenges. Foremost among these issues is that the indentation response is frequently affected by the presence of the subchondral bone plate. While there are analytical solutions which attempt to correct for this effect, many assumptions are required to obtain material properties [152]–[156].

### 2.6.2 Nanoindentation and Microindentation

The analytical framework for indentation analysis applies equally to large and small length scale if continuum mechanics assumptions are met. To enable analysis of very small material samples, indentation devices have been developed which are capable of indentation depths less than one micrometer. Nanoindentation specifically refers to indentations of depths less than 1 micrometer of but is also a commonly used term for indentation testing performed on systems which have that capability even if the actual test may reach greater than one micrometer in depth which is more properly termed microindentation.

Nanoindentation has been used to study cartilage because it offers the ability to test very small volumes of materials and avoid substrate effects inherent when testing cartilage with larger

indenters. Nanoindentation testing of cartilage is a relatively new field of study but valuable preliminary work has already been done [157], [158]. Researchers have investigated the properties of native and repair cartilage [159], [160], combined experimental and finite element results [161], [162], performed testing in the frequency domain [163], performed creep testing [164], explored applications of biphasic theory [31], [36], and investigated posttraumatic osteoarthritis [165]. Nanoindentation continues to be an area of significant research in bioengineering.

### 2.6.3 Atomic Force Microscopy

Atomic Force Microscopy (AFM) can be employed to perform mechanical testing at even smaller length scales. AFM was developed in the 1980's and is capable of measuring forces as small as  $5 \times 10^{-9}$  N with a vertical displacement resolution of less than one angstrom [166], [167]. AFM testing is typically performed with cantilevers having a sharp pyramidal or conical tip geometry (frequently with tip radii of curvature less than 10 nm). A common approach to analyze load vs depth data obtained through AFM testing using sharp tips is to apply Sneddon's model of an axisymmetric punch assuming the probe behaves as a conical punch [168]. Alternately AFM indentation can be performed with colloidal probes and the indentation data can be analyzed using appropriate spherical indentation models as explained above [36], [46], [140], [147].

Investigation of cartilage using AFM has revealed significant information about the physical arrangement of cartilage constituents at small length scales and progression of osteoarthritis [165]. Researchers were able to obtain images of the collagen fibril arrangement on the articular surface through enzymatic digestion [169] and measure frictional forces [33],

[169]. The elastic modulus of cartilage was also measured via AFM using both sharp and spherical tips and it was noted that the modulus was much lower than when measured at macroscopic length scales [35]. Researchers also found that cartilage specimen appeared to increase in stiffness with increasing indentation depth within a single indentation test [34]. Indentation of the articular surface with sharp tips also led to the observation that there was a bimodal distribution of stiffness perhaps corresponding to collagen and proteoglycan constituents [170]. AFM indentation was also performed on cryo-sectioned surfaces of cartilage cut in three directions enabling observation of anisotropic stiffness variation in the superficial, middle, and deep zones [10]. Additionally, confirming results observed with bulk tissues, the time-dependent response of cartilage was investigated using dynamic nanomechanical testing and dynamic modulus was observed to increase with increasing indentation rate [171]. These systems provide valuable information about the structure and behavior of articular cartilage but frequently observe properties that differ markedly from tests performed at larger length scales.

### 2.6.3 Anisotropic Property Assessment via indentation

The anisotropy of elastic mechanical properties of many practical materials, including biological and biomimetic materials, are an important factor in their function. Probing these directionally varying properties via indentation has long been a goal of material scientists [172]. While the mechanics involved in modeling this contact are daunting, the complex partial differential equations have been converted to algebraic equations via integral transforms [173]. These solutions have been applied to orthotropic and transversely isotropic materials and allow prediction of contact forces and areas if the material properties are known [174]. Because of the

number of elastic constants involved, (*i.e.* 5 for a transversely isotropic material, 9 for an orthotropic material, and 21 for an anisotropic material) compliance matrices for these materials cannot be populated via indentation perpendicular to the three principal axis (only three independent measures). However, if some material properties are obtained through other testing approaches, indentation can be used to complete the characterization of an orthotropic material like bone [175]. Even if sufficient material property measures are not available to enable full material property characterization, indentation provides important information regarding material anisotropy [176].

# Chapter 3 – Indentation Mapping Reveals Poroelastic, but not Viscoelastic, Properties Spanning Native Zonal Articular Cartilage

## 3.1 Abstract

Osteoarthritis is a debilitating disease affecting millions, yet engineering materials for cartilage regeneration has proven difficult because of the complex microstructure of this tissue. Articular cartilage, like many biological tissues, produces a time-dependent response to mechanical load that is critical to cells' physiological function in part due to solid and fluid phase interactions and property variations across multiple length scales. Recreating the time-dependent strain and fluid flow may be critical for successfully engineering replacement tissues but thus far has largely been neglected. Here, microindentation is used to accomplish three objectives: (1) quantify a materials time-dependent mechanical response, (2) map material properties at a cellular relevant length scale throughout zonal articular cartilage, (3) and elucidate the underlying viscoelastic, poroelastic, and nonlinear poroelastic causes of deformation in articular cartilage. Untreated and trypsin-treated cartilage samples were sectioned perpendicular to the articular surface and indentation was used to evaluate properties throughout zonal cartilage on the cut surface. The experimental results demonstrated that within all cartilage zones, the mechanical response was well represented by a model assuming nonlinear biphasic behavior and did not follow conventional viscoelastic or linear poroelastic models. Additionally 10% (w/w) agarose was tested and, as anticipated, behaved as a linear poroelastic material. The approach outlined here provides a method, applicable to many tissues and biomaterials, which reveals and quantifies the underlying causes of time-dependent

deformation, elucidates key aspects of material structure and function, and that can be used to provide important inputs for computational models and targets for tissue engineering.

### 3.2 Introduction

Biological tissues, e.g. cartilage, present significant property differences over small (i.e., nano- to micrometer) length scales and marked time-dependent behavior. Accurate determination of properties and their variation throughout tissues is vital to engineer materials that effectively recapitulate the property gradients that are present in native tissues, *e.g.* to match cellular level strains particularly under dynamic mechanical loading and to provide appropriate mechanical cues to cells. Much work thus far has focused on creating simple constructs that match bulk tissue properties at very slow loading rates, yet this approach neglects the markedly different properties observed at higher physiological loading rates and the complex, hierarchical organization of most tissues that spans multiple length scales (*e.g.*, nanometers to centimeters).

Articular cartilage is particularly compelling due to the prevalence of osteoarthritis and as a complex material possessing significant mechanical property variation, underlying chemistry, and extracellular matrix organization from the articular surface to the underlying bone [10]–[13], [17], [135], [177]. While articular cartilage possesses a pronounced time-dependent response [15], [36], classic methods for mechanical property assessment [133], [134] and evaluating fluid-structure interactions [23], [136], [178] poorly assess behavior within small regions of tissue, *e.g.*, within individual cartilage zones. Displacements of chondrocytes in cartilage sections have been mapped via digital image correlation [11], [17], [137], or through the use of displacement-

encoded magnetic resonance imaging [179], [180]; however, these methods apply loads to bulk sections of tissue and prevents direct loading of specific cartilage zones. Thus while inverse methods have been applied to estimate properties, the quantification of time-dependent mechanisms remains daunting and prone to error. In contrast, microindentation provides a facile way to directly observe the mechanical response of cartilage *in situ* without altering the zonal arrangement, while enabling investigation of both elastic and time-dependent material behaviors.

The time-dependent response in articular cartilage has been attributed to viscoelasticity, poroelasticity, or a combination of these phenomenon [16], [161], [164], [181]–[183]. Yet it is likely that these behaviors vary with the underlying chemistry and extracellular matrix organization in zonal cartilage. Indentation of the articular surface has evaluated equilibrium properties of native, diseased, and repair cartilage [157]–[160], [165] and begun to explore the time-dependent response [31], [36], [163], [164]. Results were combined with finite element models [161], [162] and correlated with chemistry in maps spanning osteochondral tissues [184]–[186]. However, property measures have been inconsistent because analytical models have not been established for each cartilage zone.

Microindentation uniquely provides the ability to assess both time-dependent behavior in small tissue volumes and the underlying causes of this deformation at length scales relevant to cells. Because viscoelastic models assume that materials act as a continuum, mechanical response is assumed to be independent of indenter probe radius if the applied strain and strain rates are kept constant [187]. Thus if the rise (i.e. indentation) time and the ratio of indenter

depth to indenter radius are maintained, then the measured material parameters should not vary with indenter size. On the other hand, because poroelastic models assume that a time-dependent response is due to fluid transport, the size of the indenter has a nonlinear impact on the behavior of the tested material. For this poroelastic case, a characteristic rise time can be established which is proportional to the square of the indentation radius if relative indentation depth is kept constant. Thus, testing at various indentation rates using multiple sizes of indenter probes with rates matched via viscoelastic or poroelastic assumptions can determine whether time-dependent material behavior is due physical arrangement of the solid material (*i.e.* viscoelasticity) or fluid transport (*i.e.* poroelasticity). With data obtained by performing experiments using multiple sized probes we can now evaluate the best analytical model [36], [47], [147], [188] to describe cartilage behavior in each zone.

Using a novel microindentation-based approach, we test the hypothesis that a nonlinear biphasic model best represents the time-dependent mechanical behavior of articular cartilage. Trypsin treatment was also employed to increase permeability through glycosaminoglycan (GAG) depletion [189], [190] to evaluate changes in the time-dependent mechanical response, with increased permeability of cartilage, with the goal of deconvoluting viscoelastic and poroelastic behavior. Evaluating zonal material properties obtained using this approach provides an important target for tissue engineering to match deformations and fluid flows experienced by cells in native tissue, to improve accuracy of computational finite element models of cartilage, and may provide novel insight into osteoarthritis progression.



### 3.3 Methods

#### 3.3.1 Materials

Agarose samples were prepared using 10% (w/w) agarose (Sigma, A9539), dissolved into phosphate buffered saline (PBS) with a pH of 7.4, heated to 90°C in a double boiler while being continuously mixed with a magnetic stir rod, and centrifuged (2500 RPM, 5 minutes) to eliminate bubbles. Eight specimens were sectioned using a vibratome (Technical Products International, Vibratome 1000) to 1 mm thick slices and mounted to 1 mm thick steel testing pucks using a thin layer of cyanoacrylate.

Separately, cartilage samples were collected from three Yorkshire pigs of 2.5-4 months in age from the lateral femoral condyle using an 8.5 mm mosaicplasty tubular chisel (Smith & Nephew, 7207494). The Massachusetts General Hospital (MGH) Institutional Animal Care and Use Committee (IACUC) approved all procedures. The split-line direction was determined by inserting a pin in the center of the cartilage plug [191]. Cartilage was cut from the bone and sectioned to ~500 µm thick slices parallel to the split-line direction using a vibratome. Subsequent slices were set apart for microindentation, Secondary Harmonic Generation (SHG) and Two Photon Fluorescence (TPF) imaging and histology (Figure 4). Cartilage sections were indented or prepared for histology without further treatment (n=6) or subjected to enzymatic degradation for three hours in 0.5% Trypsin (Life Technologies, 15090046) in calcium and magnesium free Hanks Balanced Saline Solution (Life Technologies, 14175079) and thoroughly rinsed in PBS (n=6). For mechanical testing, samples were mounted on 1mm thick steel testing pucks using a thin

cianoacrylate layer and submerged in with 1X PBS containing 1% (v/v) Protease Inhibitors (PI) (Halt, Thermo Fisher 78438).

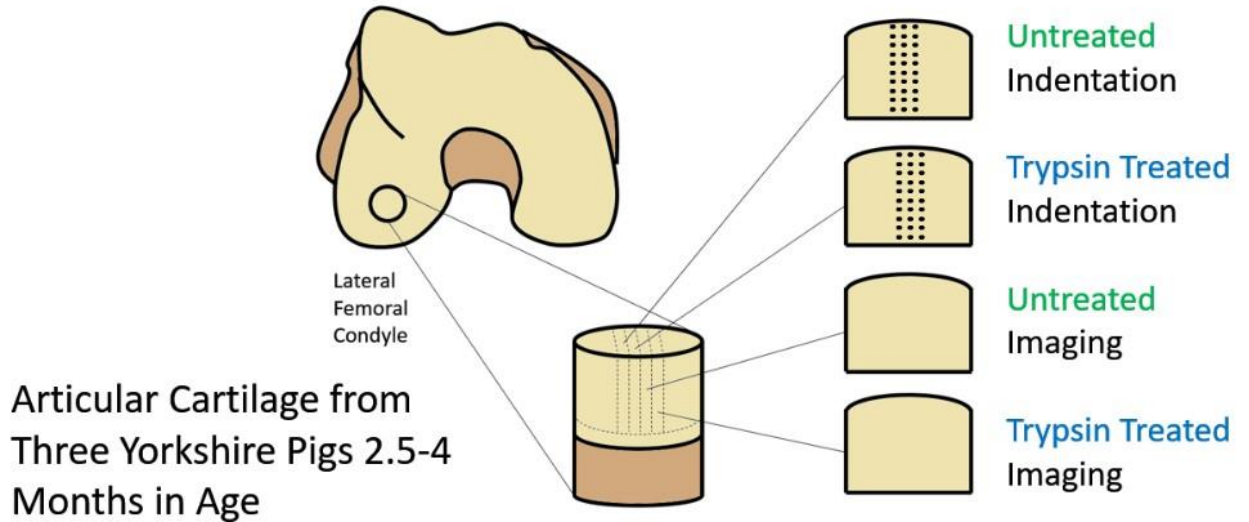


*Figure 4 - Excise location and sample groups for articular cartilage. Dots on indentation samples represent indentation arrays performed parallel to the articular surface.*

### 3.3.2 Histological analysis and SHG/TPF Imaging

Cartilage sections were fixed in 4% paraformaldehyde, dehydrated, paraffin embedded, and sectioned to 10  $\mu\text{m}$  thick slices using a microtome. These slices were stained with safranin-O/Fast Green to visualize sulfated GAGs. The prevalence of type II collagen in cartilage was investigated using SHG and TPF (Coherent Chameleon Ultra II laser tuned to 800 nm wavelength). A dichroic mirror was used to separate the output onto a non-descanned QUASAR Detection Unit with two detectors enabling the observation of SHG and two photon emissions separately. Imaging was performed on 500  $\mu\text{m}$  thick samples without staining or contrast agents.

### 3.3.3 Microindentation testing

Microindentation was performed on a Hysitron TI-950 nanoindenter. Indent arrays using cono-spherical probes ( $R = 104.7 \mu\text{m}$  and  $250.1 \mu\text{m}$ ) were spaced at a minimum of  $3 \times$  the indenter contact radius. Two 25 indent arrays were performed for each test condition in agarose, whereas in cartilage arrays spanned from the articular surface toward the bone ( $R = 104.7 \mu\text{m}$ :  $4 \times 18$  array at  $100 \mu\text{m}$  spacing in x- and y-;  $R = 250.1 \mu\text{m}$ :  $3 \times 11$  array at  $170 \mu\text{m}$  spacing). Additionally, 25 indents were placed on the articular cartilage gliding surface in treated ( $n = 4$ ) and untreated ( $n = 4$ ) samples.

All indents were performed in displacement control to a max indentation depth of 5% of the probe radius (Figure 5). Multiple load rates were tested with each indenter using a trapezoidal load-hold unload function. The rise times ( $t_R$ ) were 0.32, and 2 s for the  $R = 104.7 \mu\text{m}$  probe and 2 and 12.5 s for the  $R = 250.1 \mu\text{m}$  radius probe. The samples were then subjected to a 40-second stress relaxation hold and unloaded at the same rate as they had been loaded.

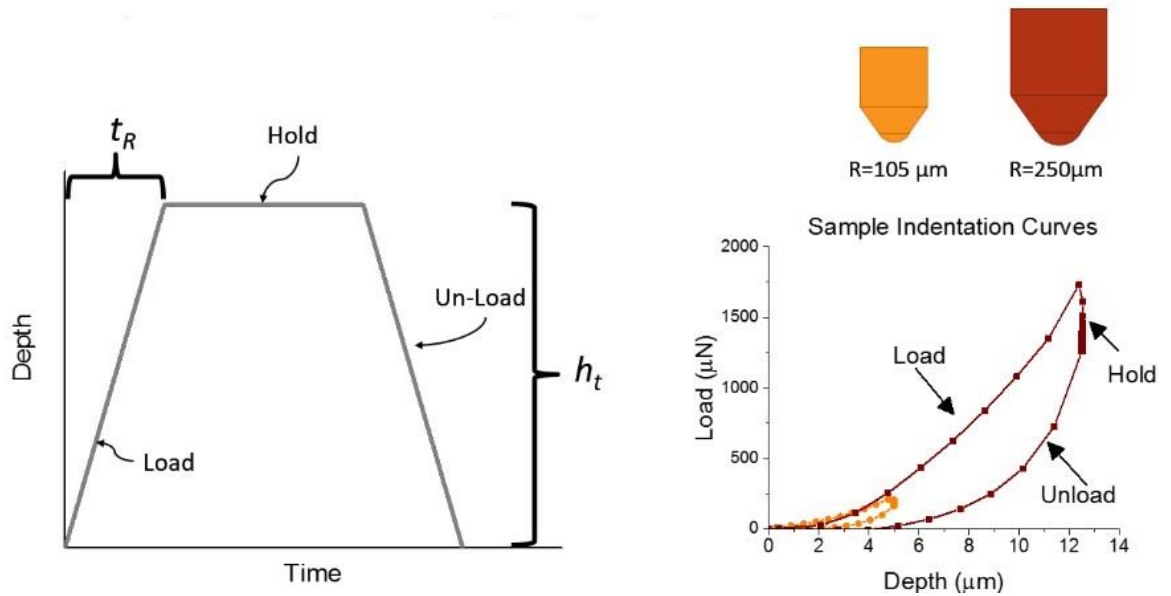


*Figure 5 - Microindentation relaxation test load profile, indenter probe geometry, and representative indentation curves which demonstrate matched strain fields for different sized indenters*

All indents were accomplished at large indentation depths and we assumed a perfect spherical geometry for the indenters. To determine the exact point of initial surface contact, we followed the method outlined by Guo [192]. In brief, a small ( $5 \mu\text{N}$ ) load was used to determine when the probe made contact with the sample but this creates a non-negligible deformation in the sample. The Hertz formula was rearranged for contact between two elastic materials assuming that the material modulus remained constant with indentation depth. Indentation load was then fit to the two-thirds power versus indentation depth to predict the indenter position at zero load.

### 3.3.4 Microindentation Analysis

For comparison between viscoelastic and poroelastic model assumptions, Hertz [140], [141] analysis of the initial loading curve was performed. The indentation modulus ( $E^*$ ) is reported without conversion to the elastic modulus ( $E$ ) via the Poisson's ratio ( $\nu$ ) of the tested material. Because no appreciable plastic deformation was observed, elastic-plastic [142], [143] models were not applied. Rather, three time-dependent models were investigated [46], [145], [146] which incorporate two broad categories of underlying physical mechanisms: viscoelastic, single phase with time-dependence resulting from changes in molecular arrangement, and poroelastic, the tested material is made up of separate solid and fluid phases [29], [46], [135], [145] where time-dependence results from fluid transport.

To evaluate for viscoelastic behavior, we utilized a method that relates the shear relaxation modulus of the tested material ( $G$ ), to the instantaneous ( $G_0$ ) and long-term shear modulus ( $G_\infty$ ) using the Poisson's ratio ( $\nu$ ), relaxation coefficients and time constants [147]. For biphasic poroelastic behavior, two models that have been previously applied to cartilage were considered. The first model, proposed by Hu *et al.* [47], assumes that the solid phase behaves as a linear elastic material and that all the time-dependent response can be attributed to the flow of the fluid phase through the material. Fitting the relaxation curve produces measures of  $G$ ,  $\nu$ , and permeability ( $k$ ). An alternate assumption is that the Poisson's ratio of the tested material is near zero and that the solid phase behaves linear elastically in compression and tension but with different moduli for each. This latter approach was proposed by Soltz and Ateshian [28] and

applied to indentation by Burris *et al.* [30], [36], [148], [149], termed “the Hertz Burris Theory” (HBT), and produces measures of tensile modulus ( $E_t$ ), equilibrium contact modulus ( $E_{co}$ ) and  $k$ .

The poroelastic indentation models are based on the assumption that loading occurs very quickly. If loading occurs at a rate that is not fast enough to create significant fluid pressure, the poroelastic models are not able to directly assess material properties from one single indentation test. Under this scenario, the HBT model underestimates the tensile modulus while the linear biphasic model overestimates the Poisson’s ratio. To overcome this limitation, we performed indentation tests at multiple loading rates and with different sized indenters. This approach enabled us to determine the portion of the load supported by the fluid, or fluid load fraction, which was then used to predict the material parameters following methods developed by Bonnevie *et al.* [36].

### 3.3.5 Atomic Force Microscopy

Atomic force microscopy (AFM) was performed on an Asylum Cypher AFM to visualize and measure the topography of the untreated and trypsin-treated cartilage surfaces. Measurements were conducted in PBS at 25 °C using the droplet cantilever holder and stage. Triangular SiN cantilevers (Bruker SNL-10) with sharp Si tips ( $R \approx 2$  nm) were used to maximize the spatial resolution of the images. Each probe was calibrated using the thermal fluctuation method [193]; the resulting values for the spring constant of the probe varied from 0.07 N/m to 0.18 N/m. Moreover, we utilized the Fast Force Mapping Mode to concurrently minimize acquisition times, such that  $10 \mu\text{m} \times 2.5 \mu\text{m}$  images with  $256 \text{ pixels} \times 64 \text{ pixels}$  ( $\approx 40$  nm pixel size) were possible in about 30 min. The maximum force and ramp rate for image acquisition were 10

nN and 20 Hz, respectively. Cross-sectional height data were taken from selected locations to compare the surface topography before and after the trypsin treatment.

### 3.3.6 Statistical Analysis

Statistical analysis was performed using Minitab v.17 (State College, PA). For agarose, one-way ANOVA compared poroelastic or viscoelastic test conditions.  $E^*$  was transformed to the power of -2 to satisfy model assumptions of normally distributed residuals and homoscedasticity. Post-hoc comparisons were performed with Bonferroni's test with critical alpha set as  $0.05/2 = 0.025$ . For cartilage, three-factor ANOVA evaluated factors of treatment (trypsin or untreated), region (superficial, middle, or deep) and test condition (baseline, viscoelastic, or poroelastic), as well as interactions.  $E^*$  was log-transformed to satisfy model assumptions of normally distributed residuals and homoscedasticity. Post-hoc comparisons were performed with Bonferroni's test with critical alpha set as  $0.05/12 = 0.004$ . Numerical results are presented as mean  $\pm$  SD; graphical results are mean with SD as error bars.

## 3.4 Results

Initial indentation modulus was used to compare matched strain rates (*i.e.* viscoelastic assumptions) or matched characteristic poroelastic indentation rate (*i.e.* poroelastic assumptions) using two cono-spherical indenters of different radii. Indentation of agarose gels produced an indentation modulus of  $1.82 \pm 0.16$  MPa for the  $R = 105$   $\mu\text{m}$  probe. When tested with the  $R = 250$   $\mu\text{m}$  probe at an equal strain rate the indentation modulus was significantly

higher at  $2.32 \pm 0.24$  MPa,  $p < 0.001$ . However, testing using a matched poroelastic indentation rate for the  $R = 250 \mu\text{m}$  probe produced a modulus of  $1.84 \pm 0.16$  MPa which is nearly identical to that found using the smaller probe (Figure 6).

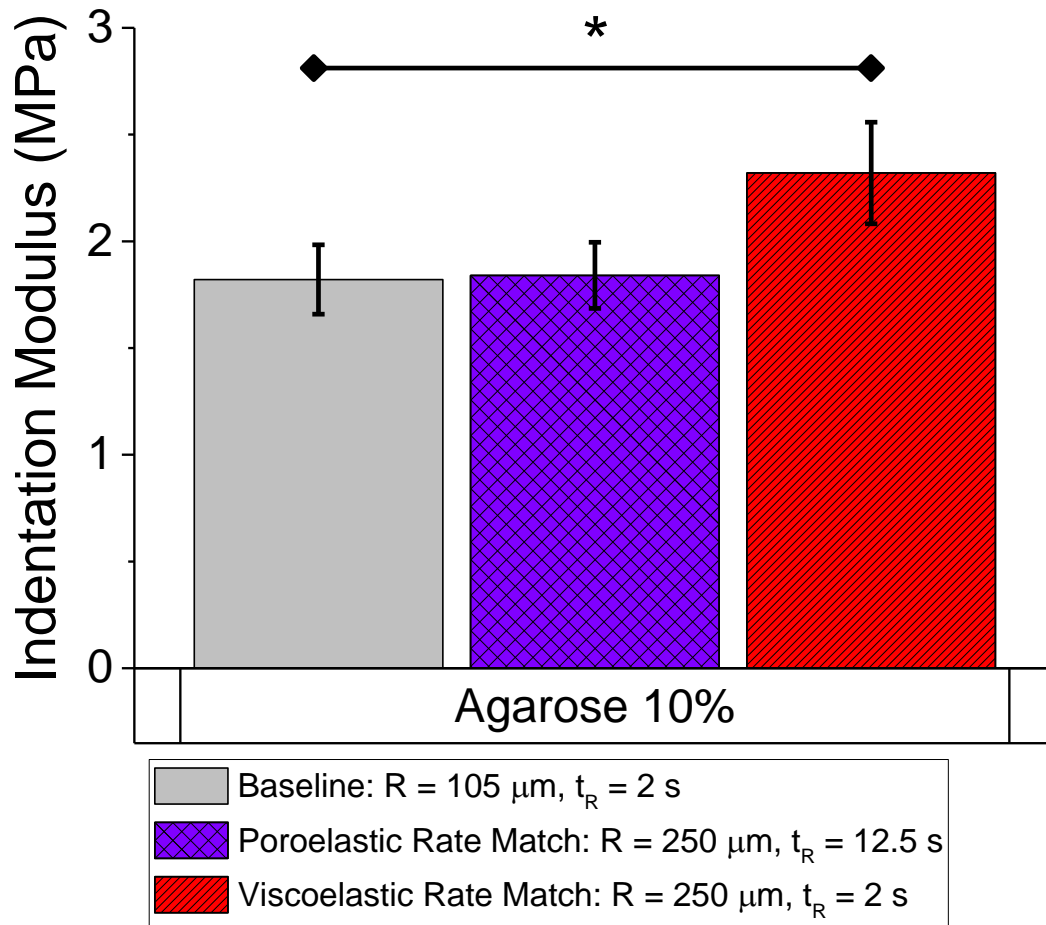


Figure 6 - Indentation modulus of agarose demonstrates behavior of a material with time-dependent behavior dominated by poroelasticity. Hertz analysis performed on the loading portion of the indentation curve.  $*=p < 0.05$



For the cartilage samples, the indentation modulus was mapped over a 400 x 1800  $\mu\text{m}$  field. For clarity, properties at four test locations will be presented first (i.e. on the articular surface, and at  $\sim 250$ ,  $\sim 1050$ , and  $\sim 1750$   $\mu\text{m}$  from the articular surface). Matched strain rates produced significantly different indentation moduli for the untreated cartilage throughout the cartilage thickness (i.e.  $p=0.02$ ,  $0.002$ , and  $0.004$  for  $\sim 250$ ,  $\sim 1050$ , and  $\sim 1750$   $\mu\text{m}$  locations, respectively) (Figure 4). By contrast, when poroelastic indentation rates were matched, the indentation moduli were not significantly different from the values measured with the smaller indenter. Indentation modulus obtained from testing the trypsin-treated cartilage showed a response with minimal time-dependence. The indentation modulus for trypsin-treated cartilage measured using the larger indenter did not provide a better correlation using matched strain rates or matched poroelastic indentation rate (Figure 7).

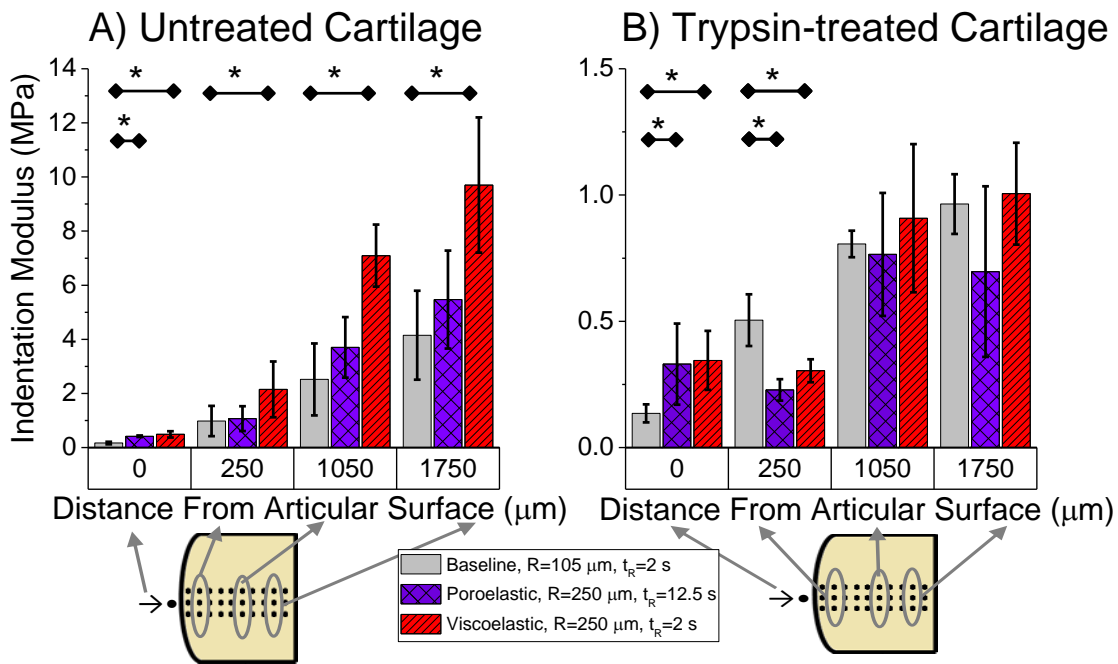


Figure 7 - Indentation modulus of untreated and trypsin-treated cartilage on the articular surface and at three distances from the articular surface. Untreated cartilage behaves as a poroelastic material at all distances from the articular surface. By contrast, the underlying cause of time-dependence in trypsin-treated samples cannot be determined. Hertz analysis performed on the loading portion of the indentation curve. \*=p<0.05

Investigation of time-dependent material properties was performed by fitting the various models to the relaxation data. Evaluating viscoelastic behavior alone produced inconsistent material parameters for agarose, untreated, and trypsin-treated cartilage (results not shown). Conversely, the Hu poroelastic model [47] provided stable measures for agarose material properties with a shear modulus ( $G$ ) of  $0.52 \pm 0.17$  MPa, Poisson's ratio ( $\nu$ ) of  $0.26 \pm 0.11$ , and permeability ( $k$ ) of  $4.66 \pm 4.26 \times 10^{-10} \text{m}^2$ . No model proved superior for trypsin-treated cartilage

samples (results not shown). The viscoelastic model produced inconsistent results when evaluating micromechanical behavior of untreated cartilage. Results obtained from the linear biphasic and HBT models were more consistent but still suffered from limitations when applied using only load relaxation data. In the linear biphasic model, the Poisson's ratio dropped as the indentation rate was increased. At maximum displacement rates, the Poisson's ratio was found to approach the theoretical limit of negative one. By contrast, as expected, the HBT model applied using relaxation data alone produced an increasing tensile modulus as the testing rate was increased.

The HBT model was also applied using an approach to compensate for the finite loading rate, with material parameters for both untreated and trypsin-treated specimens in Figure 8. The tensile and compressive moduli of the untreated cartilage were markedly higher than the moduli of the trypsin-treated samples. The compressive and tensile moduli increased in both treatment groups at greater distances from the articular surface. The permeability for both untreated and treated samples decreased rapidly for approximately the first 500  $\mu\text{m}$  from the articular surface and then decreased more slowly throughout the remainder of the thickness, whereas permeability of the trypsin-treated cartilage was significantly greater than untreated cartilage at all test locations.

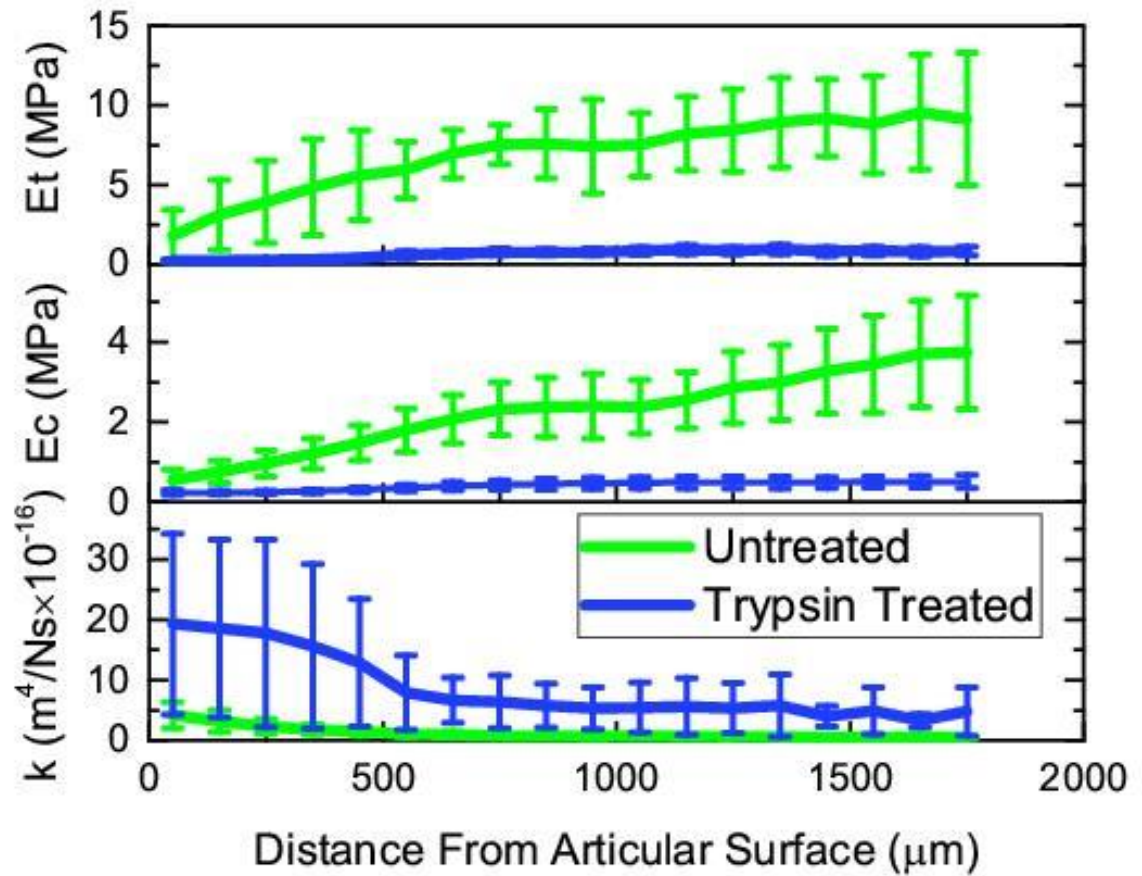
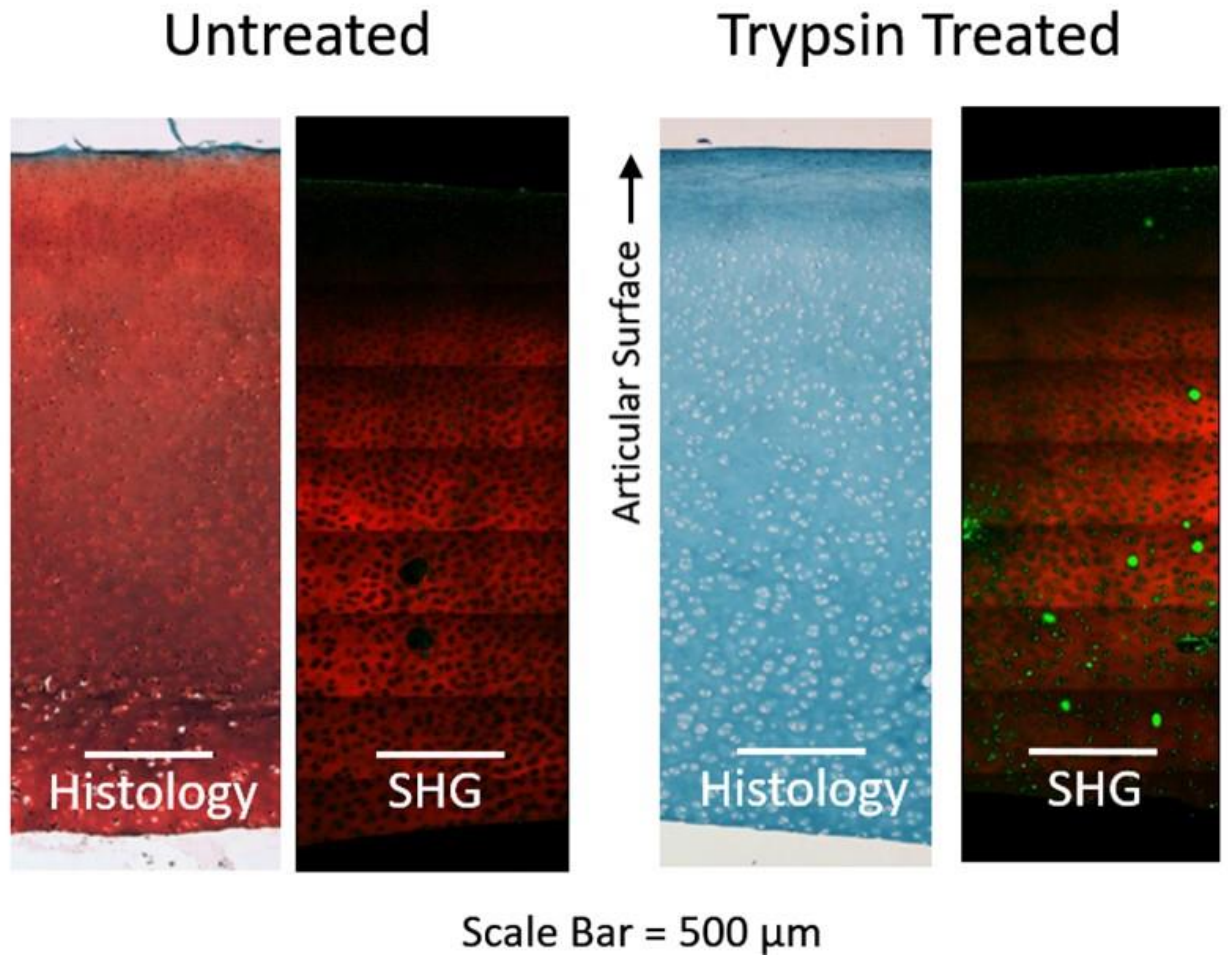


Figure 8 - The tensile and compressive modulus decrease while the permeability increases for untreated and trypsin-treated cartilage as a function of distance from the articular surface. Trypsin treatment decreases tensile and compressive modulus while increasing permeability for all cartilage zones. Parameters obtained from rate compensated HBT using indents performed at multiple displacement rates.

Histological staining of cartilage samples provided a qualitative measure of the effects of trypsin digestion. The safranin-O/Fast Green stain showed substantially less GAG content in the trypsin-treated samples when compared to the untreated cartilage (Figure 9). However, staining indicating GAG and collagen content varied little with distance from the articular surface. While not quantitative, SHG imaging of cartilage demonstrated no difference in the prevalence of signal from type II collagen (Figure 9).



*Figure 9 – Histology and SHG/TPF images of articular cartilage demonstrate GAG depletion due to trypsin treatment but little change to collagen matrix. Safranin-O/Fast Green histological stain on paraffin embedded samples. Fresh samples imaged with SHG for collagen type II artificially colored red and TPF artificially colored green.*

Due to the high spatial resolution of AFM, topography scans of small regions of cartilage were used to evaluate features of the collagen matrix that would be unresolvable using microindentation with large spheres. Indentation modulus testing was not performed using the AFM because the small scan size did not permit evaluation of the entire region of interest. Scans of the middle zone of untreated and trypsin-treated cartilage revealed differences in collagen network alignment and linearity (Figure 10). Collagen fibers in untreated samples appear more uniformly aligned and tightly packed compared to the trypsin treated samples.

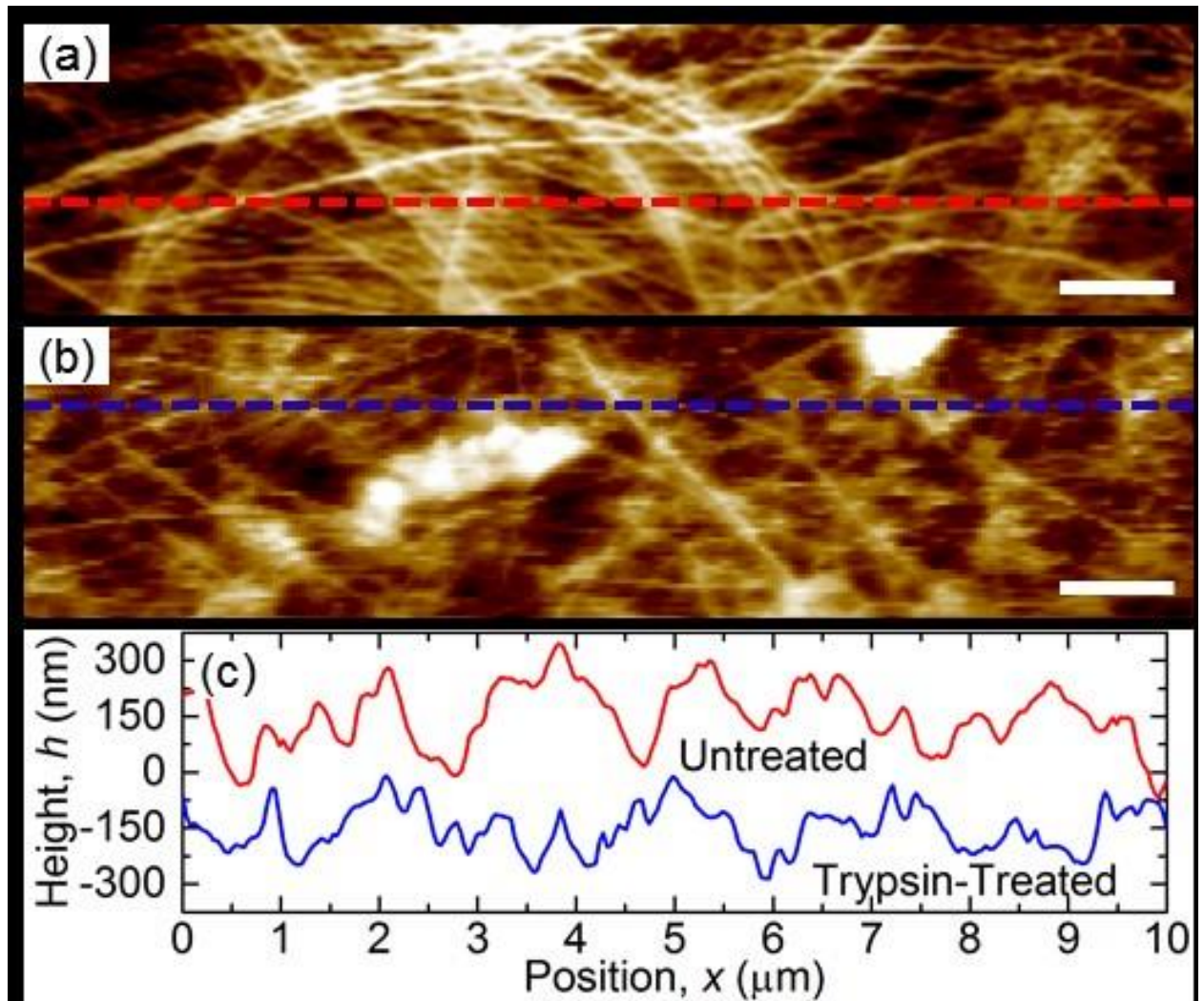
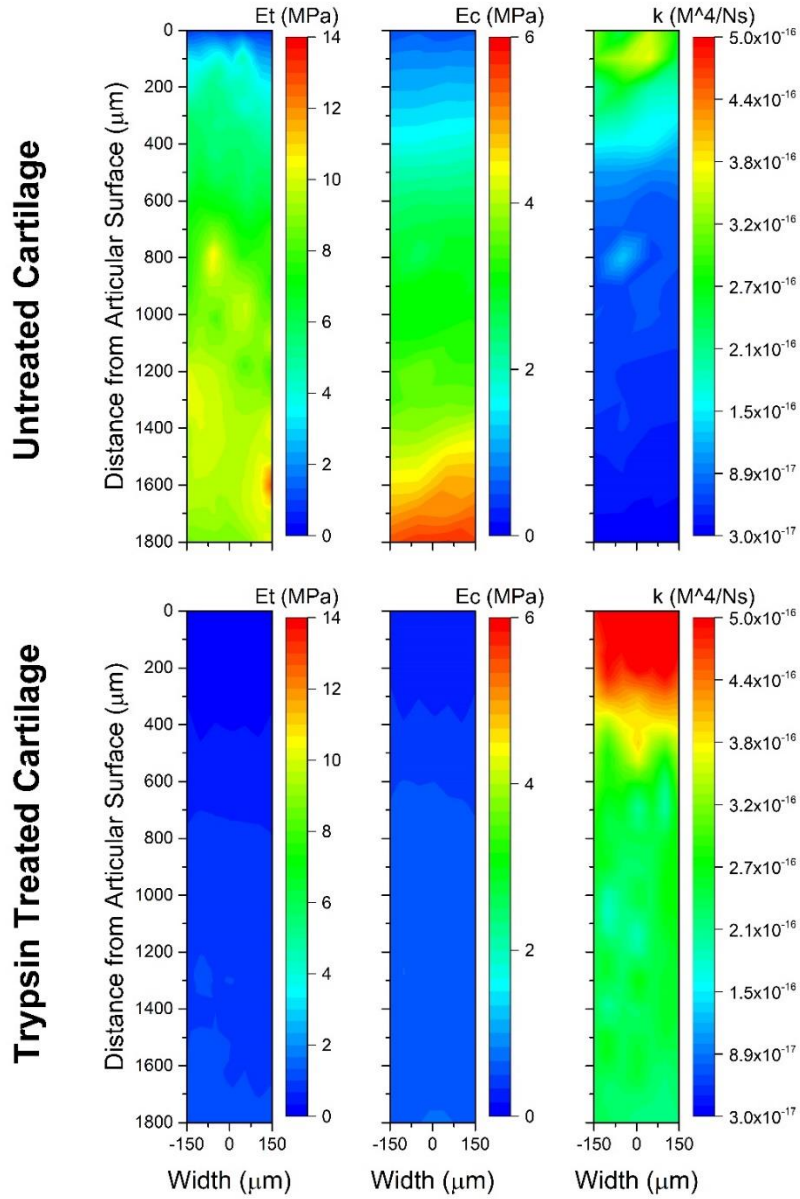


Figure 10 - Decreased organization of collagen matrix is observed via atomic force microscopy, topography images of untreated (a) and trypsin-treated cartilage (b). Images were taken approximately  $1000 \mu\text{m}$  from the articular surface. In (a) and (b) white indicates higher and black lower topography. Scale bar =  $1 \mu\text{m}$



Additionally, heat maps representing tensile modulus, compressive modulus, and permeability of a representative sample were produced are shown in Figure 11.



In agreement with the trends observed in averaged data, these maps show functional gradients in  $E_t$  and  $E_c$  and  $k$  and changes resulting from trypsin treatment. In addition, these

figures demonstrate the capability of nanoindentation to provide maps of material properties with high spatial resolution over a large area even for soft materials.

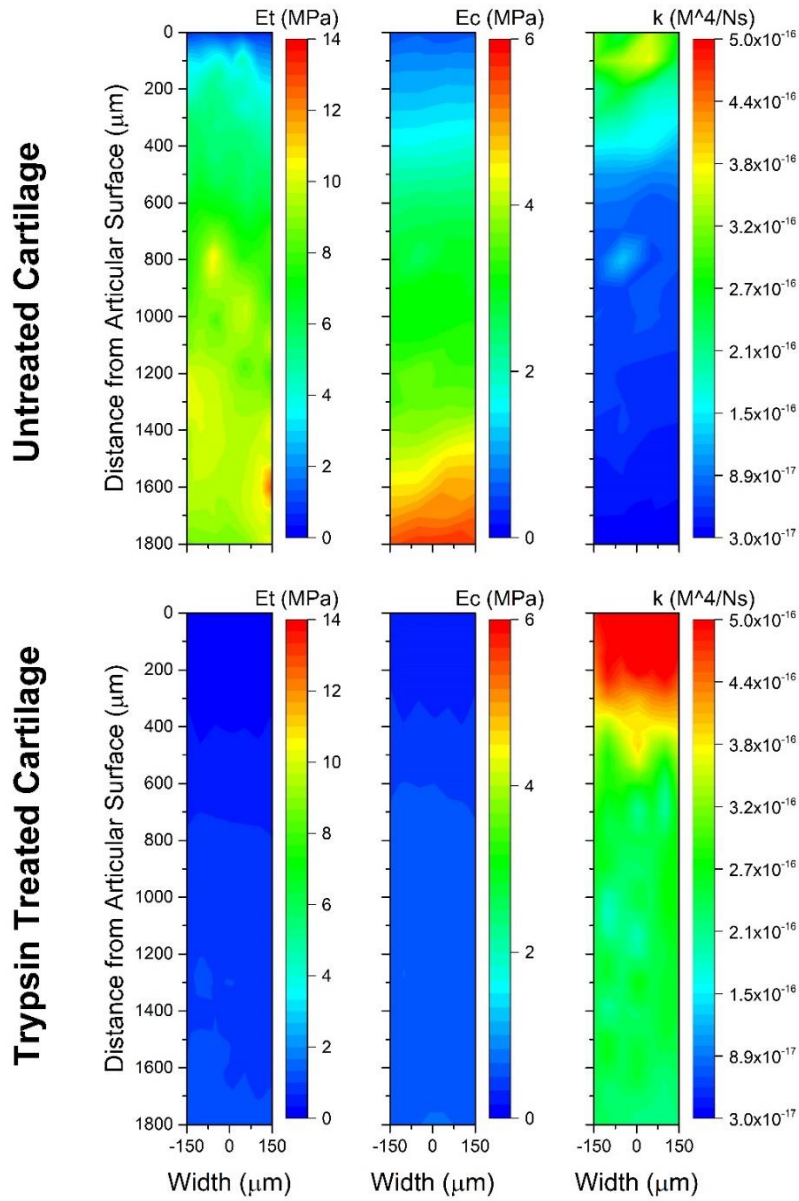


*Figure 11 - Heat maps of mechanical properties obtained from indentation rate compensated nonlinear biphasic theory (HBT) demonstrate variation in mechanical properties with distance from the articular surface and treatment for representative untreated and trypsin-treated cartilage samples.*

### 3.5 Discussion

Biological and biomimetic materials frequently present significant property differences over small length scales and a pronounced time-dependent response producing vastly different mechanical properties at physiological loading rates compared to equilibrium properties. The approach presented herein represents a systematic method to investigate and quantify these properties to provide invaluable information for those seeking to recapitulate native mechanosensory cues for cells. Using microindentation, we mapped tensile modulus, compressive modulus, and permeability of articular cartilage at sub-millimeter length scales with an intact zonal structure. We also addressed a longstanding question that has previously been difficult via bulk mechanical testing: we found that the time-dependent behavior in articular cartilage results from a predominately poroelastic, rather than viscoelastic, mechanisms throughout all cartilage zones. This work provides important design targets for approaches attempting to reproduce physiological conditions via tissue engineering.

To establish the validity of these methods a material known to possess linear poroelastic behavior was tested. In agreement with the findings of Strange *et. al.* [188], agarose was best modeled as a linear biphasic material and experimental results directly contradict viscoelastic assumptions. While the equilibrium modulus of agarose is similar to that of cartilage, the short

time response is markedly different. Agarose provides an ideal example of why small scale, complex properties may impact mechanobiology. Even if equilibrium modulus and permeability were tailored to match cartilage tissue properties, encapsulated cells would experience markedly different strains and fluid flow during dynamic loading. Similar results would be anticipated with most hydrogels and other materials commonly used for tissue engineering, thus highlighting the critical importance of accurately measuring native tissue and reproducing mechanical properties in synthetic materials for tissue engineering.

Despite the common notion that cartilage behaves viscoelastically, microindentation clearly demonstrated poroelastic behavior throughout all cartilage zones. Further, the poroelastic linear biphasic model is also insufficient as it produces an increasingly negative Poisson's ratio with increasing strain rate. This negative Poisson's ratio is not consistent with linear biphasic theory [194] or macroscopic cartilage testing which produces a Poisson's ratio of 0 - 0.2 [28], [195], [196]. The non-linear biphasic, or HBT model, overcomes this limitation by fixing the Poisson's ratio at zero and allowing the tensile modulus of the material to exceed the compressive modulus and allow for higher load support at fast loading rates. The properties measured for cartilage were found to be well represented by the HBT model in all zones.

The material properties observed herein for tensile modulus, compressive modulus, and permeability of cartilage are similar to those found for bulk cartilage via multiple other testing methods. These methods include time-dependent properties observed through macro scale indentation testing by Bonnevie *et al.* [36], fluid load fraction observed by Park *et al.* [9], and permeability observed by Soltz and Ateshian [28]. Additionally, equilibrium properties of

cartilage compressive [15], [28], [30], [42] and tensile moduli [28], [36], [41], [42] are similar to values found for bulk cartilage testing. These comparisons are notable because testing was not only performed at different length scales but also on cartilage from different ages and species and ages of animals.

In addition to validating previous measures, this work quantified changes in nonlinear poroelastic properties with distance from the articular surface. This zonal variation in mechanical behavior may be important to reproduce for engineered tissues. Specifically, the tensile and compressive moduli increased through the thickness of the cartilage, and the permeability decreased (Figure 5). These property variations with distance may result from zonal differences in chemistry and structure. One measure of chemical heterogeneity is observed in the decreased SHG signal present in the superficial zone, which confirmed observations from picosirius red stain/helium ion microscopy [197]. The decreased SHG signal indicates reduced crystallinity and collagen fibril alignment, and correlates with the lower moduli and increased permeability observed in the superficial zone. To facilitate translation to tissue engineering and computational modeling, mathematical functions representing the property variation were fit to the experimental results (supplementary data).

Further insight into the chemical and structural characteristics responsible for the time-dependent behavior of cartilage was gained by evaluating trypsin treated samples. The tensile and compressive moduli were decreased in addition to substantially increased permeability with trypsin treatment. These changes can directly be attributed to the absence of GAGs [134]. Further, one potential explanation for decreased tensile modulus lies in the high osmotic

pressure in untreated cartilage, which exerts a static tensile load on the collagen network. Conversely, in enzyme-treated cartilage, GAG depletion and low osmotic pressure allows relaxation of the collagen network. GAG depleted cartilage has been shown to exhibit a pronounced “toe” region in the stress-strain response which is absent in untreated cartilage [19]. This hypothesis is further supported herein by AFM topography images that reveal a more tightly aligned collagen network in untreated samples compared to trypsin-treated samples confirming prior observations [198]. Moreover, GAG depletion, which parallels tissue changes in osteoarthritis, would likely result in increased compressive strain and fluid flow which may attribute to cell death and further progression of the disease [58]–[60].

This work produced key insights into the zonal behavior of articular cartilage and was an important step toward establishing design targets for tissue engineering. Further efforts should be put forward to apply these methods to tissues from a statistically representative number of skeletally mature human subjects. Additionally, as trypsin treatment may have resulted in degradation of the collagen network and removal of GAGs that may not precisely mimic disease, evaluating arthritic tissue would provide valuable insight. Finally, due to load rate limitations of the indenter, a more direct method of assessing material properties would be desirable by extending the HBT model to dynamic mechanical analysis or by incorporating a ramp correction factor. Collectively, these efforts represent critical advances toward creating tissue engineered constructs that can recreate the mechanical environment of native cells.

### 3.6 Conclusions

This study demonstrated a method to measure the time-dependent behavior of biological and biomimetic materials. This understanding is important to recreate the mechanical environment of native tissue and stimulate cells with physiologically relevant strains and fluid flow. Using indentation, we mapped property variation over cell relevant length scales within a tissue. Further, this approach illuminated the underlying poroelastic and or viscoelastic causes of time-dependence in articular cartilage where viscoelastic and linear biphasic models were insufficient. Instead, cartilage is best modeled as a nonlinear biphasic material. Additionally, tensile modulus, compressive modulus, and permeability of untreated and trypsin treated cartilage were quantitatively measured in zonal cartilage as a function of distance from the articular surface. These measurements provide invaluable information for tissue engineers seeking to recreate cartilage zonal structure, understand disease progression, and as inputs for computational finite element models.

## Chapter 4 – The influence of contact radius on the indentation response of poroelastic materials

### 4.1 Abstract

Biological and biomimetic materials, such as articular cartilage and other soft tissues, generally consist of complex hierarchical structural elements that span multiple, hierarchical length scales and possess pronounced mechanical heterogeneity. At the sub-micron length scale, these materials are composed of a solid matrix with chemically driven osmotic potential and fluid-filled pores that lead to complex mechanical behaviors including poroelasticity. Yet the inherent structural hierarchy within biological materials produces vastly different mechanical behavior depending on the length scale of the test, even when the testing method is the same, *i.e.* indentation. Using a range of probe sizes, indentation uniquely enables elucidation of the multi-scale mechanical response of biological materials and potential for critical insight into tissue changes with aging and disease and design of materials for tissue engineering. Here, cartilage, trypsin-treated cartilage, and agarose were selected as characteristic biphasic biological and biomimetic materials with varying osmotic pressures and permeability. Indentation modulus was evaluated using various-sized probes (conical  $R < 2$  nm, and spherical  $D = 2 - 500$   $\mu\text{m}$ ) which demonstrated a transition from a soft response ( $\sim 0.01$  MPa in healthy cartilage) at small length scales to a stiffer response at large length scales ( $> 1$  MPa). These length-scale dependent moduli were not explained by compensating for indentation rate, surface roughness, or matrix compaction. However, we propose a biphasic surface film model that



effectively replicates this phenomenon and provides insight into the local environment that is sensed by cells.

## 4.2 Introduction

Biological tissues exhibit hierarchy across multiple length scales as has been observed and well documented in tendon [202], cortical bone [203], bamboo [204], and cartilage [205]. When specimens are tested using indentation, the hierarchical variation in material organization produces a mechanical response that depends on the size of the probe. For example, bone properties have been measured at both the small and large length scales and in various environmental conditions [206], [207] where modulus varies from 23 to 27 GPa even for the same specimen under equivalent test conditions with different sized indenter probes [208]. These measurements provides important insight into the contribution of bone microstructure to bone's overall function [208], [209]; however, the relationship between hierarchical structure and the resulting mechanical behavior has not been comprehensively explored in soft tissues.

Due to the prevalence of osteoarthritis [3], a painful and debilitating joint disorder, the behavior of articular cartilage has been studied extensively to understand its behavior in health and disease [29] and in producing materials that mimic its mechanical behavior [4], [210]. Interestingly, articular cartilage properties vary with the length scale of the test, significantly complicating the task of producing replacement materials. Specifically, indentation testing of cartilage using an Atomic Force Microscope (AFM) with a single micron-diameter probe results in a modulus of approximately 50 kPa [33], [35], [171] while indentation with a millimeter-diameter probe produces a higher indentation modulus of 0.93 – 5.21 MPa [36], [37]. Modulus

values produced with large probes ( $> 1$  MPa) are comparable to those obtained from bulk compression testing [28], [40]. The relationship between tissue hierarchical structure and the resulting modulus differences of roughly two orders of magnitude is poorly understood. Here, we demonstrate a method that is applicable to many biological materials, which provides insight into the structure mechanical function relationships of tissues at the microscale.

Indentation testing enables investigation of how mechanical properties relate to hierarchical levels within articular cartilage due to the ability to perform the same experiment across multiple length scales. Spherical probes produce a relatively uniform strain field [140], [154], and can range in diameter from  $\sim 0.1$  to 100's of micrometers. Additionally, sharp conical probes are employed to investigate properties with high spatial resolution allowing visualization of the solid matrix and modulus measurements at very small length scales (Figure 12).

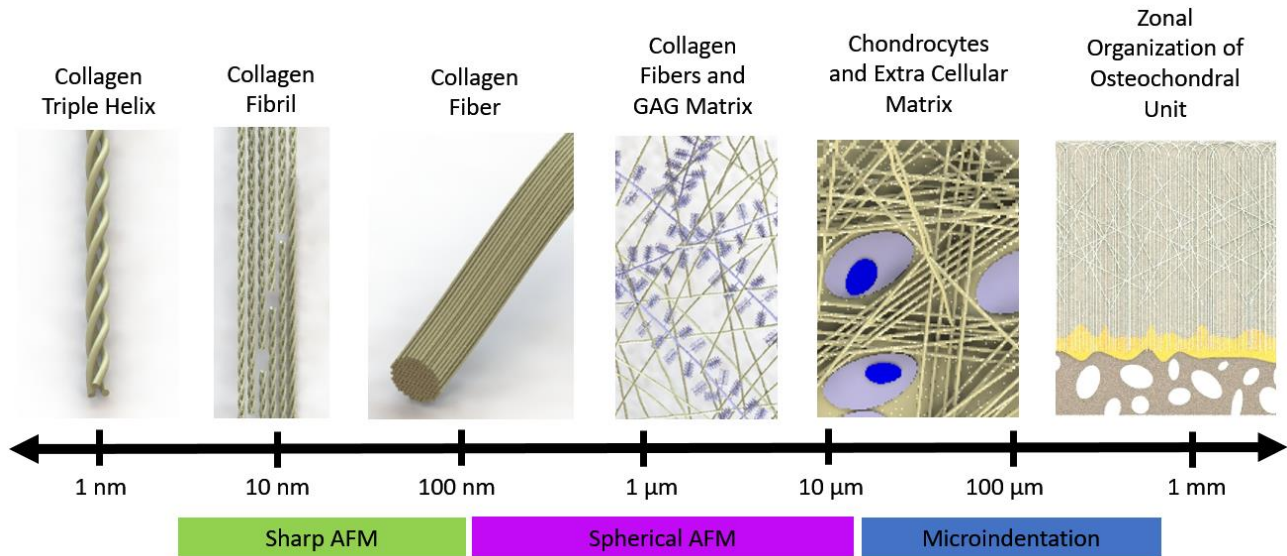


*Figure 12 – Cartoon depicting the constituents and arrangement of articular cartilage across multiple length scales. Indentation methods applicable to probe the mechanical response of tissues at these various length scale are also indicated.*

This work tests cartilage, trypsin-treated cartilage, and agarose at multiple length scales to investigate the resulting variation in mechanical behavior. These three materials enable a controlled study of the contributions of soft tissue solid matrix and fluid, solid matrix organization, and osmotic pressure using hyaline articular cartilage. Trypsin treatment was performed to reduce the sulfated glycosaminoglycan (sGAG) content within cartilage [200] which isolated the collagen matrix behavior by minimizing osmotic pressure and electrostatic interaction with the fluid [211]. Additionally, agarose was chosen as a common synthetic biomimetic material with physical cross-linking and pores spaces at a the ~200 nm length scale [212]. Collectively, these materials and the comparative use of AFM and microindentation

enabled the evaluation of relationships between tissue microstructure and structural hierarchy and the resulting mechanical behavior at both cell and tissue relevant length scales.

## 4.3 Methods

### 4.3.1 Sample Preparation

Cartilage samples, collected from the lateral femoral condyle from two 3-4 month old male Yorkshire pigs, were left untreated (Phosphate Buffered Saline (PBS) + protease inhibitors, n=4) or were enzymatically degraded (0.5% trypsin, 3h, n=4). Samples were cut to ~500  $\mu\text{m}$  thick sections along the split lines using a vibratome for indentation testing in a direction parallel to the articular surface. This sample thickness was selected to be greater than seven times the maximum contact radius and thus minimize substrate effects [213]. Agarose (Sigma, A9539) was mixed in PBS to 10% (w/w), sectioned using the same process as the cartilage, and allowed to equilibrate overnight in PBS in free swelling conditions.

### 4.3.2 AFM Conical Probe Indentation and Imaging

Atomic force microscopy (AFM) was performed on an Asylum Cypher AFM to visualize and measure the topography of the untreated and trypsin-treated cartilage surfaces. The measurements were conducted in PBS at 25°C using the droplet cantilever holder and stage. Triangular SiN cantilevers (Bruker SNL-10) with sharp Si tips ( $R \approx 2 \text{ nm}$ ) were used to maximize the spatial resolution of the images. Each probe was calibrated using the thermal fluctuation method [193]; the resulting values for the spring constant of the probe varied from 0.07 N/m to 0.18 N/m. Fast Force Mapping Mode was utilized to concurrently minimize acquisition times, such that 5  $\mu\text{m}$   $\times$  5  $\mu\text{m}$  images with 64 pixels  $\times$  64 pixels ( $\approx 80 \text{ nm}$  pixel size) were possible in

about 30 min. The maximum force and ramp rate for image acquisition were 10 nN and 20 Hz, respectively. Cross-sectional height data were taken from selected locations to compare the surface topography before and after the trypsin treatment. At each location the indentation modulus was assessed from the loading portion of the load depth curve by fitting an analytical model of contact assuming a rigid indenter and treating the sample as an infinite half space [168].

#### 4.3.3 Spherical Probe Indentation and Analysis

Microindentation was performed using a TI-950 (Hysitron, Minneapolis, MN) in 2 x 3 arrays spaced at three times the contact radius for sites located approximately 250  $\mu\text{m}$ , 1000  $\mu\text{m}$ , and 1750  $\mu\text{m}$  from the articular surface of each cartilage sample. Microindentation employed a trapezoidal load-hold unload function (max depths 5% of probe radius), with rise/unload times of 0.32 s and 2 s for 210  $\mu\text{m}$  and 500  $\mu\text{m}$  diameter tips respectively both with a 40 s hold. An initial load of 5  $\mu\text{N}$  was applied to find the sample surface that created displacement into the tested material. To account for this initial load, it was assumed that the material behaved linear elastically with a modulus equal to that measured at large depths and a displacement due to the imaging load was computed and used to correct initial indentation depths.

AFM indentation was performed (Keysight 5500, Keysight Technologies) using colloidal spheres ranging from 2  $\mu\text{m}$  to 196  $\mu\text{m}$  in diameter in locations matching those tested with the nanoindenter. Cantilevers were selected, that produced maximum indentation depth between 1.4% and 20% of the probe radius (stiffness 0.92 N/m to 46 N/m). To identify the initial contact point a median value and standard deviation for noise in the load signal was observed prior to contact. The median load was set to zero and when the observed load exceeded six times the

standard deviation of the pre-contact noise, a maximum time point was established for surface contact. The preceding load vs depth record was then reviewed to identify the latest time the load signal was zero and that point was set as the initial contact time. This process was automated for all indentation data and reviewed manually to ensure proper identification of initial contact. It should be noted that the automated software packages frequently used with indenters misidentify initial contact because the algorithms assume testing occurs on a material of uniform stiffness. This error results in an artificially high modulus and can obscure observation of the soft surface response.

Indentation modulus was determined for spherical indentation from load and depth measurements using the methods first proposed by Hertz [140] treating the tested material as an infinite half space and the indenter as a rigid sphere. Because Poisson's ratio was not independently measured, the indentation modulus ( $E^*$ ) and not elastic modulus is reported. To control for the effects of matrix compaction, the ratio of indentation depth to indenter radius was maintained across the various tip sizes producing equivalent strain fields and thus equivalent levels of matrix compaction. In addition to computing a modulus at maximum load the modulus as a function of contact radius was also computed [34], [214]. For measures of modulus as a function of contact radius, data from depths less than 0.5% of radius was excluded (Figure 13).

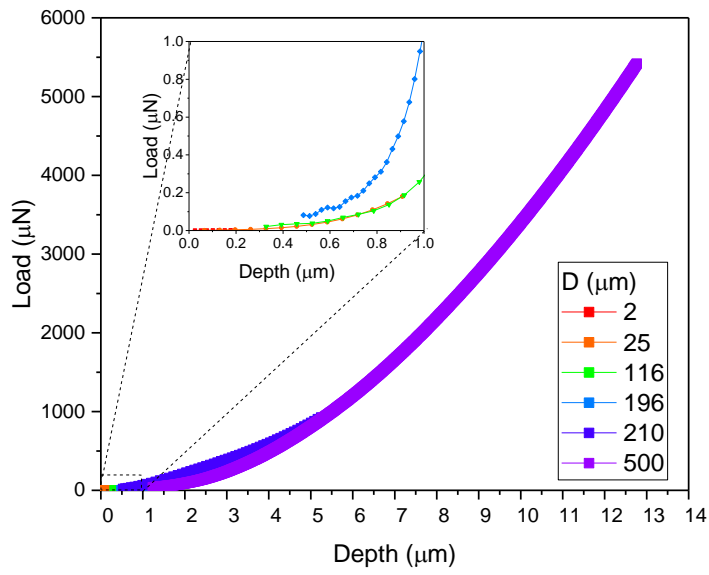


*Figure 13 – Demonstration of multiple indenter radii and indentation systems to obtain reliable information over a broad range of indentation depths. Mean load versus contact depth curves for spherical indentation of middle zone cartilage demonstrating the loading portion of the curve for indentation depths between 0.5% and 20% of indenter radius.*

Biphasic materials such as cartilage and agarose display pronounced time-dependence. Therefore, tests were performed at a constant poroelastic indentation rate by matching the ratio of indentation time over the square of the indenter radius [47], [215]. Rates used here correspond to fluid fractions of approximately 60% and 80% for untreated and trypsin-treated cartilage respectively [215]. While these rates are not fast enough to reach the max fluid load fraction of the cartilage of approximately 90% [36], they present a significant time-dependent response. Additional slower indentation rates were explored on a subset of samples and showed results consistent with observations at faster rates (data not presented). The poroelastic indentation rates used in this testing are slightly faster than the work presented by [171] which demonstrated pronounced time-dependent behavior using dynamic microindentation. Because these fluid filled materials exhibit time-dependent behavior, the poroelastic rate of the test was accounted for when comparing experimental results at different length scales.

To quantify the surface roughness of each tested region, topographical maps were obtained using contact mode with a sharp AFM probe. We measured Root Mean Squared (RMS) roughness for a representative sample from each experimental group over a  $25 \mu\text{m}^2$  area. Measured indentation modulus was corrected for surface roughness by assuming the asperities had a Gaussian distribution of heights. An analytical model was then applied which treated asperities as having spherical peaks which deformed under the applied load through elastic or elastic-plastic mechanisms [213], [216], [217]. The surface roughness corrected indentation depth and contact area were then used to compute the indentation modulus using linear elastic assumptions as described above.



The surface of other biological materials exhibit a thin compliant layer [206] and the sliding surface present in superficial zone articular cartilage has a fibrillated irregular surface [218], thus changes in indentation modulus were modeled as a thin film of soft material on a more rigid substrate. Multiple thin film analytical models were reviewed [152], [154], [155], [219] and two were selected as being best matched to this testing configuration [153], [220]. These models were rearranged to allow for simultaneous optimization of both film thickness and film modulus based on experimental data. Further, because these models assume that the substrate is infinitely stiff, they predict nonrealistic results once the contact radius approaches the film thickness. To correct for this nonphysical prediction, two theoretical bounds were established. The first asserts that the observed indentation modulus ( $E^*$ ) cannot exceed the indentation modulus of the substrate ( $E^*_{substrate}$ ) (Equation 3).

$$E^* \leq E^*_{substrate} \quad (3)$$

The second holds that the indentation modulus ( $E^*$ ) cannot be less than the case of an infinitely soft layer of thickness ( $T_{film}$ ) on a substrate of modulus ( $E^*_{substrate}$ ) (Equation 4).

$$E^* \geq \frac{E^*_{substrate}(h - T_{film})^{1.5}}{(h)^{1.5}} \quad (4)$$

By averaging of the two thin film models and combining the results with the two limiting cases, a piecewise model of indentation response was constructed which we term the biphasic surface film model (Figure 14). The biphasic surface film model was fit to the experimental data using a logarithmic least squares optimization and a film stiffness, substrate stiffness, and film

thickness were computed. Properties produced by fitting each of the individual thin film models independently can be found in the supplemental data.

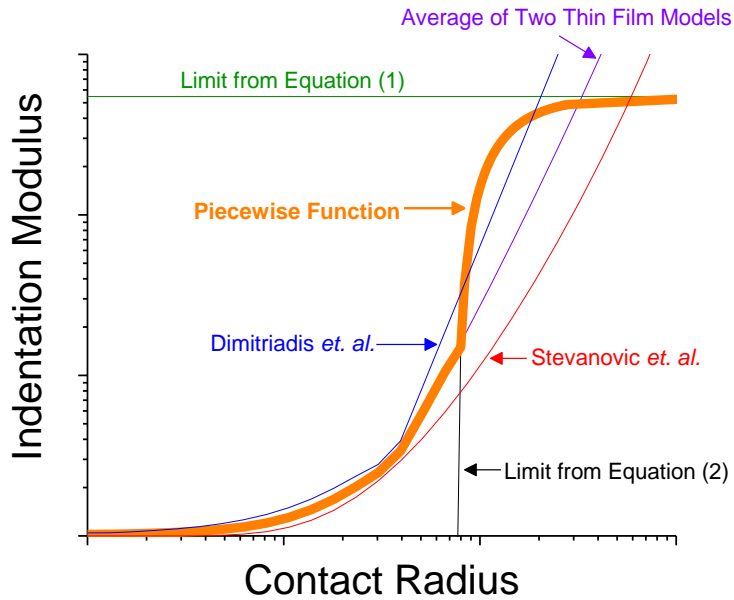


Figure 14 – Biphasic surface film model produced by piecewise combination of functions describing the behavior of a thin film on a stiff substrate. This model is composed of a logarithmic average of two thin film models [153], [220] combined with two theoretical limiting cases representing (1) a compliant substrate and (2) contact of the indenter with the substrate.

#### 4.3.4 Raman Spectroscopy

To observe the tissue biochemistry at the indentation locations, Raman spectroscopy was performed on cartilage sections. Raman spectra were collected in backscatter mode with an upright InVia microscope (Renishaw plc, Wotton-under-Edge, UK) supplying 10.9 mW to the

sample. The sample was excited by a 785 nm laser (Innovative Photonic Solutions, I0785SR0090B-IS1) without polarization filters. An immersion 63x microscope objective with a NA of 0.9 (Leica) provided an approximately 1  $\mu\text{m}$  spot size. A 1200 l/mm grating and a charge coupled device (CCD) camera yielded a spectral resolution of approximately 1  $\text{cm}^{-1}$  for wavelengths from 720 to 1811  $\text{cm}^{-1}$ . The system was calibrated using both internal and external silicon standards, by setting the primary silicon peak to 520  $\text{cm}^{-1}$ .

Preprocessing of Raman spectra was performed as described in [125]. Briefly, cosmic rays were identified and removed, a linear baseline was subtracted, intensity was normalized, and outliers were detected and removed using principal component analysis. The intensities observed at 1578, 1488 and 782  $\text{cm}^{-1}$  were summed for DNA, those at 1380, 1342 and 1068  $\text{cm}^{-1}$  were summed for chondroitin sulfate, those at 1271, 1246, 920, 857 and 816  $\text{cm}^{-1}$  were summed to represent collagen and those at 1555, 1127 and 1004  $\text{cm}^{-1}$  were summed for non-collagenous proteins.

Raman maps were created of full thickness cartilage sections. Cartilage samples were frozen at  $-20^{\circ}\text{C}$  until testing, then were thawed, submerged in PBS, and mounted to steel pucks for analysis. Maps of the cartilage from articular surface to bony surface were sampled at 10  $\mu\text{m}$  x 10  $\mu\text{m}$  spacing to visualize tissue chemistry spanning the full cartilage thickness. Additionally, to correspond with microscale indentation response, Raman maps were taken at 1  $\mu\text{m}$  by 1  $\mu\text{m}$  resolution at locations corresponding to indentation locations.

## 4.4 Results

### 4.4.1 AFM Conical Probe Results

Topography mapping with a sharp tip revealed a complex micrometer length scale structure within cartilage (Figure 15). The collagen network appears to be clearly defined in the untreated samples yet the definition is lost following trypsin treatment. The Root Mean Square (RMS) surface roughness taken over a 25  $\mu\text{m}^2$  area was found to be  $96 \pm 10$  nm for untreated cartilage,  $102 \pm 17$  nm for trypsin-treated cartilage, and  $78 \pm 6$  nm for agarose. The indentation modulus observed ranged from approximately 10 kPa to 200 kPa in untreated cartilage and 10 kPa to 100 kPa for trypsin treated samples. There was also a high degree of spatial variation of indentation modulus when observed at the small length scale (Figure 15). This variation was not explained by topography indicating that the inconsistency in measured modulus is due to actual changes in the cartilage stiffness, and not changes in the contact geometry.

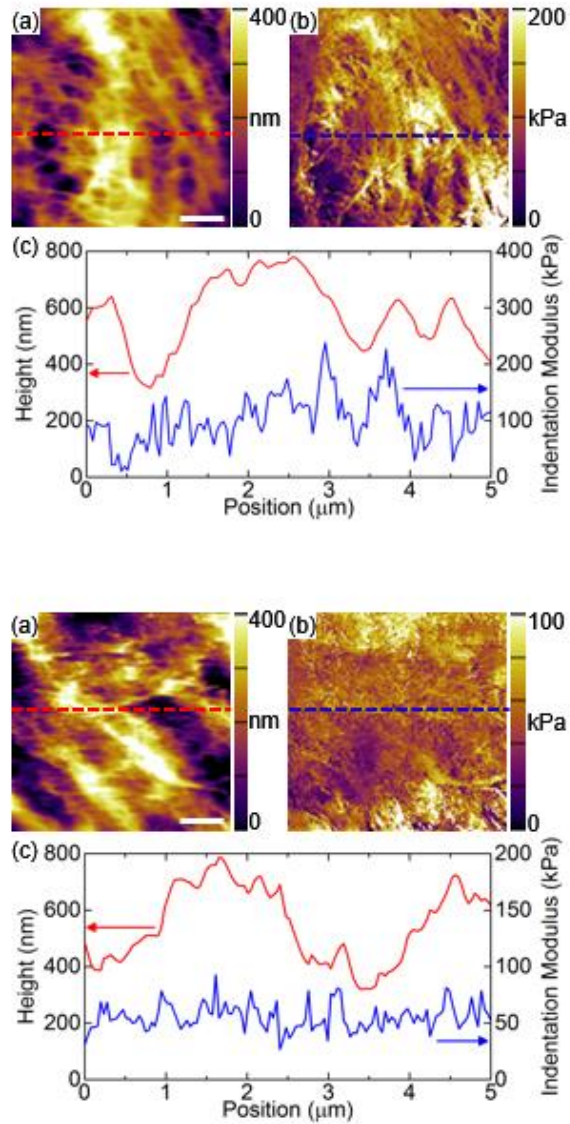


Figure 15 – AFM topography images indicating heterogeneity of indentation modulus at the submicron length scale while remaining well below the indentation modulus that was observed at larger length scales. AFM (a) height and (b) indentation modulus maps of an untreated (top) and trypsin-treated (bottom) cartilage surface. Scale bar = 1  $\mu\text{m}$ . (c) Cross sectional data taken from denoted locations (dashed lines) in (a) and (b).

#### 4.4.2 Spherical Probe Results

The indentation modulus of untreated cartilage ranged from tens of kilopascals at small contact radii ( $< 1 \mu\text{m}$ ) to single megapascals for large contact radii ( $> 20 \mu\text{m}$ ) representing moduli spanning nearly three orders of magnitude. For trypsin-treated tissue, the increase was approximately 100 fold over the same span of contact radii. Indentation modulus was approximately ten times greater at locations further from the articular surface when measured using both microindenter and AFM probes. This modulus variation was observed at all tested regions of the cartilage, where representative curves for the middle zone articular cartilage and agarose are shown in Figure 16. Agarose samples also demonstrated a two order of magnitude difference in indentation modulus over the same span in contact radii.

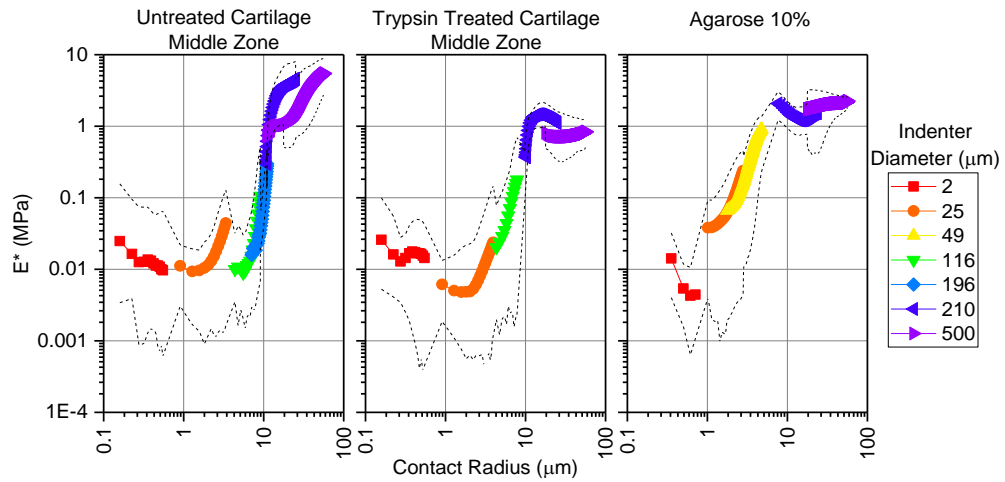


Figure 16 – Mean indentation modulus showing differences in indentation modulus based on the contact radius. Measured using spherical AFM ( $D = 2, 25, 49, 116, 196 \mu\text{m}$ ) and Nanoindenter ( $D = 210, 500 \mu\text{m}$ ) probes for middle zone cartilage and agarose gel. Dashed lines represent maximum and minimum modulus values measured for a given contact radius. Note, both scales are logarithmic

To evaluate the influence of surface roughness on modulus measurements, an analytical surface roughness compensation was performed on data obtained using all spherical indenters. For agarose samples, the compensation for surface roughness produced modulus values that were nearly constant with contact radius with values ranging from 0.5 MPa to 2.6 MPa over all tested contact radii. However, for untreated and trypsin-treated cartilage this surface roughness correction did not produce consistent indentation moduli with values which still varied by greater than 40x for all cartilage zones (*i.e.* 15 kPa to 8.9 MPa for untreated and 11 kPa to 2.1 MPa for trypsin treated middle zone cartilage).

Apparent thin film thickness, film modulus, and substrate modulus were computed for each of the test groups by fitting the proposed biphasic surface film model to the experimental data, where a representative example is shown in Figure 17. We observed that the apparent film thickness of the agarose samples was approximately 370 to 700 nm, which is likely due to surface roughness alone. In contrast, the apparent film thickness of both untreated and trypsin treated cartilage samples was much larger than was explicable by surface roughness. By comparing the trypsin-treated samples in the middle and deep zones of articular cartilage, we find that the apparent film thickness is greater in materials regions that have a high sGAG content (Figure 18). For the middle zone the apparent film thickness differs-between treatment groups, however this difference is not statistically significant ( $p=0.085$ , Student's-t test). In the deep zone, the apparent film thickness for the untreated samples is significantly larger than for the trypsin-treated samples ( $p<0.0001$ , Student's-t test). Within untreated samples, the superficial zone presents the



smallest apparent film thickness whereas for trypsin-treated samples the film is thickest near the surface and thinner in the middle and deep zones.

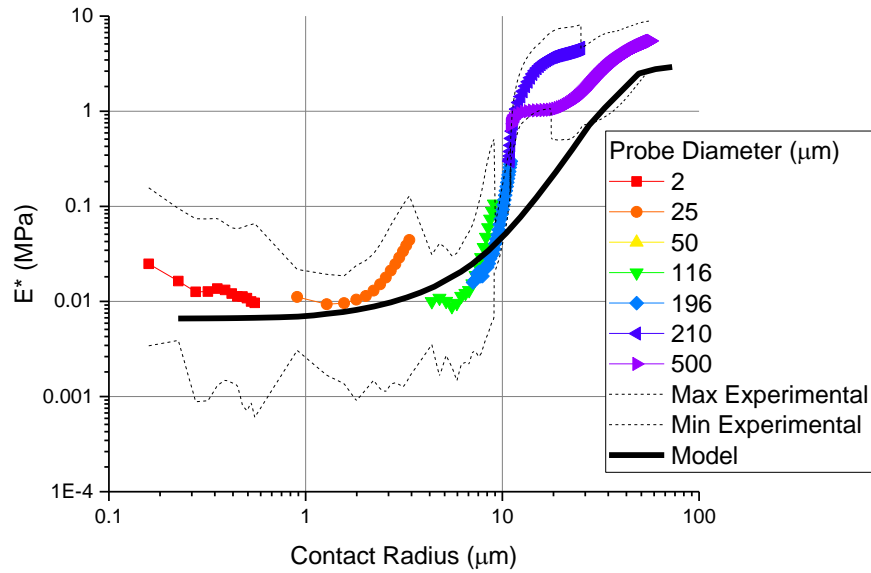


Figure 17 – Average piecewise biphasic surface film model fit of indentation modulus recreates key features of experimental indentation modulus as a function of contact radius. Middle zone untreated cartilage is shown as a representative case.

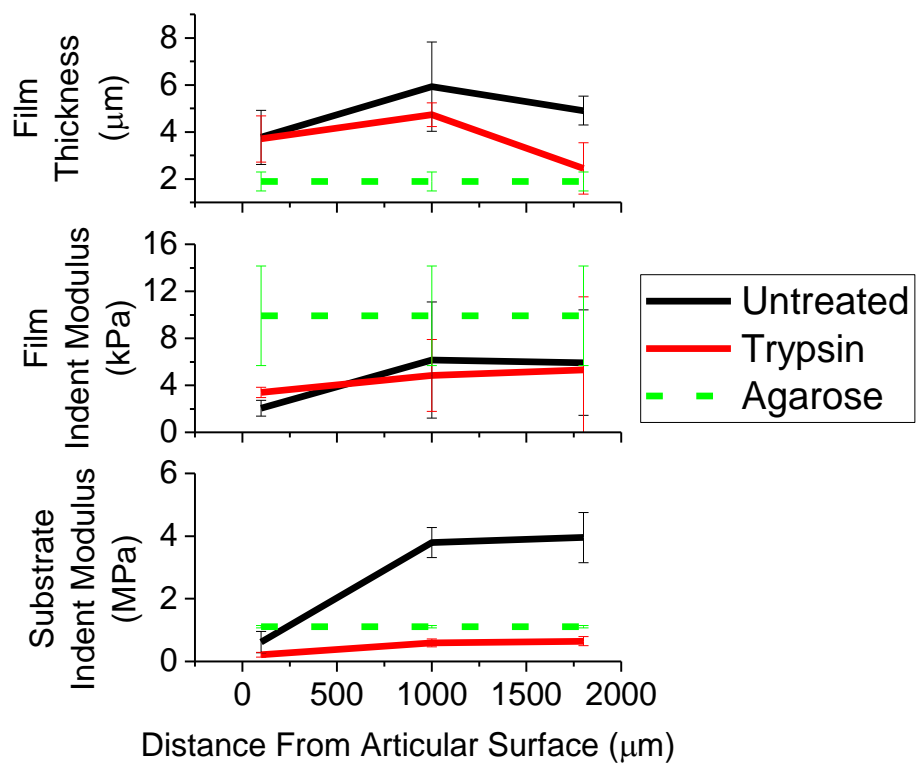
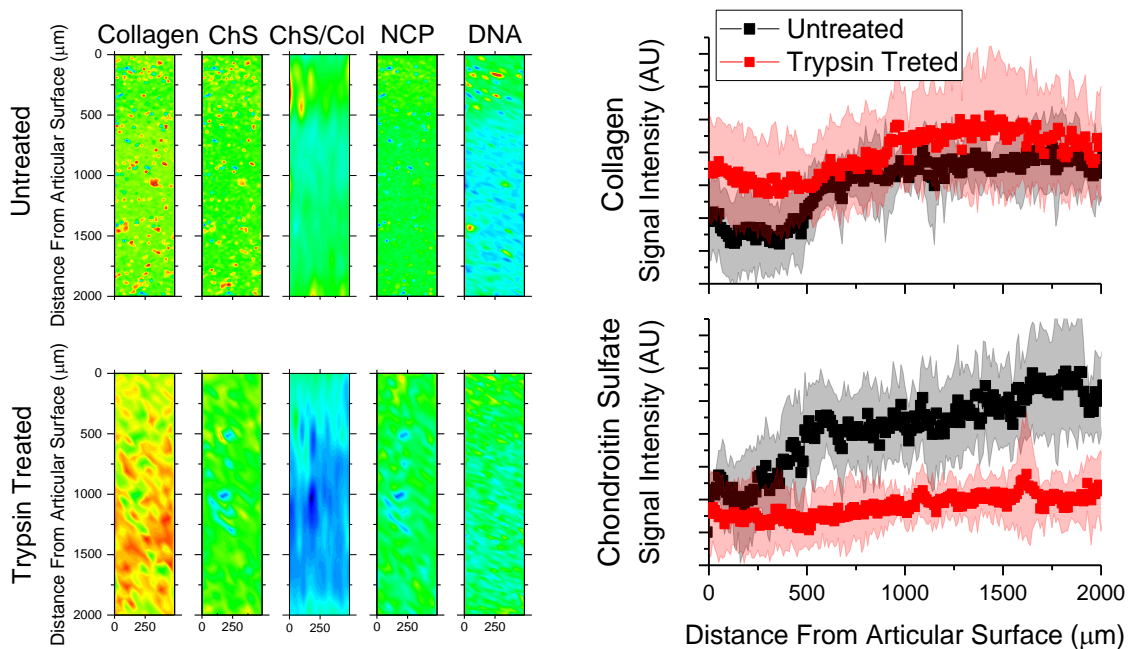


Figure 18 – Biphasic surface film model parameters for untreated cartilage, trypsin-treated cartilage, and agarose indicate film thickness is a function of collagen matrix prevalence and arrangement and osmotic pressure of the extracellular matrix.

#### 4.4.3 Raman Spectroscopy Results

Raman spectroscopy assessment indicated that collagen concentration increased with distance from the articular surface for both untreated and trypsin-treated samples, with the largest changes occurring within the first 500  $\mu\text{m}$  from the articular surface (*Figure 19*). For untreated samples, the signal scattering intensity produced by sGAG molecules also increased with distance from the articular surface whereas trypsin treatment resulted in marked decrease in sGAG signal overall, which was particularly pronounced in the middle and deep zones. The ratio of sGAG to collagen type II further demonstrates the sGAG depletion occurred after trypsin treatment, whereas the non-collagenous proteins and DNA showed no differences between the treated and untreated cartilage.



*Figure 19 – Representative Raman maps and of full thickness cartilage and charts of mean and standard deviation of collagen and chondroitin sulfate as a function of distance from the articular surface for all samples. Note: decreased chondroitin sulfate prevalence after trypsin treatment. Variation of collagen and chondroitin sulfate with distance from the articular surface can also be observed for both untreated and trypsin treated samples.*

## 4.5 Discussion

Indentation testing is ideally suited to probe the complex hierarchical structural arrangements in biological and biomimetic materials across multiple length scales. Soft tissues are structurally heterogeneous and biphasic, and possess complex mechanical properties (*e.g.*, visco- and poroelasticity) that vary markedly with aging and disease. Moreover, vastly different indentation moduli are observed in biological tissues, *e.g.*, *cartilage*, depending on the length scale at which the test is performed, *i.e.*, an indenter size effect [221]. Thus, indentation holds potential to reveal the relationships between the structure and function of these highly complex materials. Here, we investigated untreated hyaline articular cartilage, and cartilage that was enzymatically digested (*i.e.*, using trypsin ) to remove sGAGs and consequently reduce osmotic pressure [211], as characteristic materials due to their clinical relevance in osteoarthritis [3] and as they present compelling natural variations in matrix structure and osmotic pressure within a well-characterized hierarchical soft tissue.

We observed indenter probe size effects in both untreated and digested cartilage, and in agarose that served as a poroelastic reference material, where modulus values ranged over multiple orders of magnitude. To explain why modulus values differed with the probe contact radius, experimental methods were designed to minimize effects from poroelasticity and matrix compaction and analytical methods were implemented to compensate for surface roughness of the samples. Moreover, we utilized natural (*i.e.*, cartilage zones) and experimentally controlled variations in tissue constituents (*e.g.*, sGAGs) were evaluated in conjunction with results from

AFM and microindentation testing to elucidate both compositional and microstructural contributions to mechanical behavior. While these experimental and analytical adjustments corrected for the varied indentation moduli that were observed with varying probe sizes in the agarose samples, these same corrections proved inadequate to explain modulus values observed in both untreated and trypsinized cartilage. We thus surmised that an additional physical phenomenon contributed to the low modulus of the cartilage when indenting with small probes.

One contributing factor to low modulus values observed at small contact radii arise when the pore size of the tested material is on the same length scale as the contact radius. This effect was first proposed by Stolz *et al.* [35] and produces localized stress fields which depart significantly from the continuum mechanics assumptions inherent in the Hertzian-based contact mechanics applied herein. Support for the concept that microscale material heterogeneity contributes to a lower modulus when testing with small probes was observed in cartilage via topographical mapping using AFM. The resulting images revealed a collagen network within cartilage that possesses micron length scale gaps between fibers and marked microstructural heterogeneity.

However, matrix pore size alone does not completely explain the size-effect observed herein. By computing the indentation modulus when contacted with a sharp indenter, the modulus for all tested regions were highly variable and, even when adjusted, remained at several orders of magnitude below the macroscale stiffness. To explain this intriguing result, we suggest an additional physical mechanism. When a new surface is formed within a porous material with an inherently high osmotic potential, *e.g.* when sectioning cartilage or when cartilage undergoes

fracture, a soft layer is created at the newly liberated surface that consists of severed matrix components (*e.g.*, collagen fibrils and sGAGs). Internal stresses are then likely relieved with diminished osmotic pressure at the newly formed surface. In the case of cartilage, the new surface enables fluid efflux, sGAG migration, and severed collagen fibers that had previously been loaded in tension (proposed mechanism shown in Figure 20). Unloading the collagen matrix thus disables the normal, nonlinear relationship between tension and compression moduli that is observed in cartilage and collagen networks [19]. Under indentation, we model this newly liberated surface as a single thin film with a characteristic film thickness and film indentation modulus. The resulting apparent film thickness is assumed to be affected by the pore size of the solid matrix, the arrangement of this matrix, and by the osmotic potential of the material.

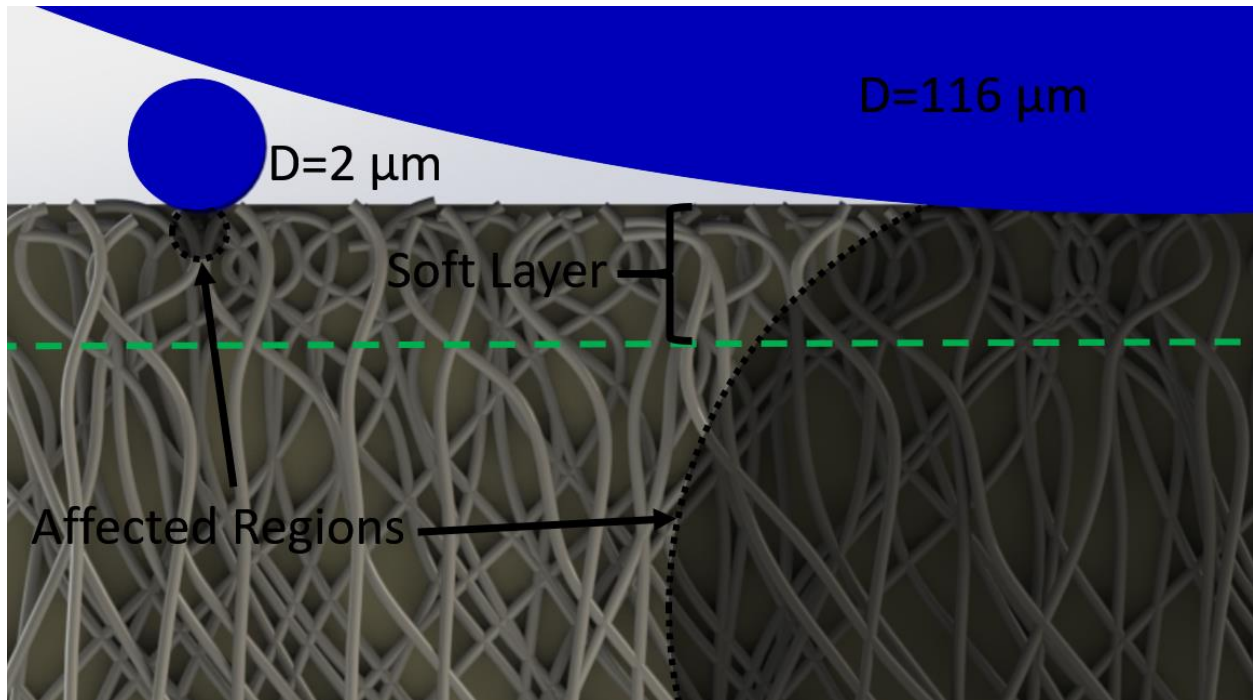


*Figure 20 - Cartoon depicting indentation for two indenters of a porous material, shaded regions indicate affected regions predicted using Hertz continuum mechanics assumptions. Soft surface layer effective thickness is indicated by green dashed line.*

The naturally occurring variation in collagen and sGAG prevalence in articular cartilage provides an ideal forum to evaluate the proposed thin film mechanism. In trypsin-treated cartilage, low sGAG and collagen were observed within the superficial zone, indicating a less dense matrix as compared to the middle and deep zones. The larger pore size present in the superficial region should result in a thicker film being observed, which is in line with our experimental findings. In addition to the pore size of the material, the arrangement of the collagen matrix appears to play an important role in determining the film thickness. Because the deep zone cartilage consists of more highly aligned collagen fibers than the middle zone [197],



the importance of collagen alignment can be observed. Despite the similar collagen content in the middle and deep zones, as observed *via* Raman spectroscopy [125] and histology [115], the apparent film thickness was diminished in deep zone of cartilage where a highly aligned collagen network exists as compared to the middle zone, which possesses less uniformly aligned collagen.

For untreated cartilage samples, the apparent film thickness is influenced by both the aforementioned collagen prevalence and arrangement and, additionally, the prevalence of sGAGs. In the superficial zone, we observed a film thickness that was very similar to the film estimated for indentation of trypsin-treated samples, which is consistent with the low sGAG content within that region. In contrast, the film thickness revealed a non-significant increase in the sGAG-rich middle zone and a significant increase in the deep zone implicating sGAG expansion, swelling, or migration at the newly liberated surface. This increased thickness is consistent with the high osmotic pressure in the deep and middle zones and the presence of a thin layer of tissue experiencing relief of residual stress when cut. This stress relief appears to be influenced by both changes in osmotic potential and the arrangement of the structural collagen matrix.

Observation of the indentation response at small length scales informs our understanding of the interactions of sGAGs and collagen fibers and the importance of collagen alignment in physiological function. We found that a newly liberated surface results in altered physical properties through a film thickness of multiple microns. In living tissue, a disturbance (*e.g.*, fracture) in the matrix may influence cellular mechanosensitivity in the immediate vicinity of damaged tissue. For example, fissures have been observed due to impact loading of cartilage

[222] and may be partly responsible for chondrocyte necrosis adjacent to damaged cartilage [223], [224]. These results also provide important information regarding the loads experienced by cells in healthy tissue. Due to their low modulus relative to the matrix [225], the cell-matrix interface (*i.e.*, chondrocyte lacuna) presents a situation very mechanically similar to a free surface. Thus in native cartilage tissue, cells likely experience an immediate matrix which is significantly softer than the bulk matrix properties.

In addition, at the micron-length scale the cartilage matrix appears to be markedly heterogeneous and brings into question the applicability of conventional continuum mechanics assumptions at small length scales and in evaluating cell-matrix interactions. This multiscale behavior may also play a critical role in the cellular response of a range of non-orthopedic materials, *e.g.* cardiovascular or brain tissue, which respond to mechanical loading and are often placed into contact with implants, foreign materials, and biomedical devices [226], [227]. Finally, the low modulus observed at small length scales, and the noted departure from conventional assumptions required for continuum mechanics analysis, may have profound implications for biomechanical computational modeling, understanding of disease progression, and our approach to creating hierarchical biomimetic materials in hyaline cartilage as well as other soft tissues that, similarly, possess compositional heterogeneity and structural hierarchy.

Some of the limitations of this work are that only a small number of immature porcine samples were used in this study as it is expected that zonal differences would be more pronounced in older individuals. While the untreated and treated cartilage samples produced mechanical behavior consistent with the presence of a thin film of soft material at the surface

this thin film was not directly measured. The hypothesis that a soft thin layer is present at the surface should be further tested using other investigative methods to confirm its presence. Further, testing on other biological and biphasic synthetic materials with varying osmotic pressure and matrix pore size could be used to establish a relationship between these factors and the apparent soft film thickness of a material.

#### 4.6 Conclusions

This study demonstrated that indentation modulus of porous materials is a strong function of the size of the indenter probe. Indentation moduli of hyaline cartilage, trypsinized (digested) cartilage, and agarose that were obtained from indentation using small contact radii probes were several orders of magnitude lower than that obtained from larger probes. This discrepancy in modulus values for untreated and trypsin treated cartilage was not explained by compensating for indentation rate, matrix compaction, and surface roughness. Yet this phenomenon was recapitulated when assuming a thin film of soft matter lay on top of the indented materials, where the film thickness was influenced by collagen prevalence and organization, sGAGs and osmotic pressure, and relief of internal residual stress at a newly liberated surface. These factors result in departure from continuum mechanics assumptions and result in properties that vary by multiple orders of magnitude with the length scale of interaction. These differences in modulus should be accounted for when analyzing small-scale interactions of biological tissues and may play an important role in the behavior of cells in both healthy and damaged tissue.

# Chapter 5 – Time-Dependent, Anisotropic, Zonal Variation of Mechanical Properties of the Osteochondral Unit

## 5.1 Abstract

The osteochondral unit consists of articular cartilage, calcified cartilage, and subchondral bone and works together to support physiological loading while maintaining tissue viability. It has become increasingly apparent that to restore proper joint function following damage or disease the functionality of all of these tissues must be reestablished. To accomplish this end, it is important to understand the mechanical behavior of these tissues. Yet osteochondral tissues are difficult to study as they are time-dependent and anisotropic with significant zonal variation. We used microscale indentation to quantify the time-dependent and anisotropic properties of osteochondral tissues as a function of distance from the articular surface. Soft articular cartilage demonstrated marked time-dependent and elastic behavior that varied with distance from the articular surface, and demonstrated different anisotropic behavior in each cartilage zone. These measures of mechanical behavior were compared to the chemistry and structure of these tissues as observed via Raman spectroscopy, Secondary Harmonic Generation (SHG) imaging, Two Photon Fluorescence (TPF), and Magnetic Resonance Imaging (MRI). This work provides important targets for tissue engineers and modelers as they seek to recreate the complex mechanical, chemical, and structural environment of the osteochondral unit.

## 5.2 Introduction

The osteochondral unit works together to distribute mechanical loads, transfer nutrients into and out of the joint to sustain chondrocyte viability, and perform repair of damaged tissues [228]. Unfortunately, when cartilage is injured it frequently fails to repair this damage, which can lead to progression of osteoarthritis producing detrimental changes from the subchondral bone through the articulating surface [229]. As we develop new remedies, it is critical to elucidate the characteristics of native tissue throughout the full osteochondral unit so a healthy native environment can be recreated. It has been suggested that to develop a successful repair approach, the interactions across the full osteochondral unit must be restored. These tissues present a mechanically, structurally, and chemically complex environment with changes in composition and function even at the sub millimeter length scale. Two of the complexities relating to the mechanical behavior of this tissue are: a time-dependent response [15] and mechanical anisotropy [42], both of which present variation with distance from the articular surface [10], [215]. Understanding these mechanical complexities will enable tissue engineers and computational modelers to reconstruct a complete and healthy osteochondral unit.

Recent studies have demonstrated that soft articular cartilage time-dependent mechanical behavior is dominated by transport of fluid within the tissue (poroelasticity) with a pronounced nonlinear tensile compressive modulus [28], [36]. We recently extended this observation to illuminate the zonal specific material properties of soft articular cartilage from juvenile animals [215]. In addition to time-dependent behavior, soft articular cartilage has been shown to exhibit pronounced mechanical anisotropy in both tension and compression [41], [42],

[230]. Due to the variation in collagen arrangement throughout the thickness the anisotropy also varies within each cartilage zone in order to facilitate the unique zonal mechanical environment [231]. This zonal specific anisotropy serves to distribute joint loads.

Results from Atomic Force Microscopy (AFM) testing of soft articular cartilage in three orthogonal directions revealed that anisotropy differed when comparing results obtained within the superficial middle and deep zones [10]. However while such measures are valuable, the small length scale at which AFM probes interact with the constituents within the cartilage extracellular matrix are poorly reflective of mechanical properties from macroscale testing [232]. While properties of individual articular cartilage zones have been evaluated using small, excised samples from within each zone [233], [234], these tests are complicated by testing *ex situ* in a non-native stress environment, imperfect sample geometry, and the inability to obtain large enough samples to evaluate anisotropy. In contrast, microindentation testing enables mechanical property assessment within biological tissues (i.e., *in situ*), thus allowing observation of spatial variation in behavior with nearly intact zonal structure.

Beyond just quantifying the mechanical behavior of the osteochondral tissues, it is important to observe chemical and structural arrangement of these materials to elucidate the structure function relationship of native tissues. This both provides insight to tissue engineers seeking to reproduce native properties and aids in assessment of disease progression. Various tools exist to explore the chemistry and structure of these tissues two of the most valuable of which are Secondary Harmonic Generation (SHG) imaging and Raman spectroscopy. Another important aspect of treating osteoarthritis is clinically assessing the severity of the disease.

Ideally, this is performed in a noninvasive manner such as through Magnetic Resonance Imaging (MRI). MRI is a powerful tool to assess the health or disease state of osteochondral tissues [235]. The advantages of using this noninvasive assessment technique can be further strengthened by correlating the signals observable via MRI with invasive measure of tissue health that more directly measure mechanical behavior, chemistry, and structure. This correlation will enable translation of MRI images to specific changes with osteochondral tissues that result in progression of osteoarthritis or restoration of function via repair approaches.

In this work, we sought to extend our prior work to reveal the zonal variation in time-dependent behavior by measuring the tensile modulus ( $E_t$ ), compressive modulus ( $E_{co}$ ), and permeability ( $k$ ) in human skeletally mature soft articular cartilage. Further, we observed the anisotropic behavior of soft tissues throughout the osteochondral unit. Additional experimental work was also performed to assess the behavior of the calcified tissues but the results of that testing will not be reported in this dissertation. The mechanical measures of soft tissue behavior were then associated with measures of tissue organization observed via SHG, chemical composition observed via Raman spectroscopy, and MRI measurements indicating cartilage health. This work serves to help better characterize the mechanical, chemical, and structural environment in skeletally mature human articular cartilage.

## 5.3 Materials and Methods

### 5.3.1 Materials

Cartilage was obtained from two male and two female human donors 55-61 years in age without clinical history of osteoarthritis. Specimens were fresh frozen, and experienced two

additional freeze thaw cycles throughout the imaging mechanical testing process. During dissection, cartilage surfaces were carefully observed to identify regions of potential cartilage degeneration and the synovial fluid was assessed for discoloration (*e.g.* blood). Three specimens were obtained from each individual from the center of the medial femoral condyle (cubes approximately 5 mm on each edge) and adjacent slices were set apart for histology (Figure 21). The split-line direction was determined by inserting a pin dipped in die the center of the extracted cartilage specimen [191] to establish orientation was for each specimen. Osteochondral samples were mounted using cyanoacrylate onto 20 mm by 20 mm Delrin blocks that had been machined to support the tissue specimen and aid in polishing and to preserve sample orientation. During all preparation, samples were maintained hydrated with PBS and all mechanical testing was performed with samples submerged in 1X PBS containing 1% (v/v) Protease Inhibitors (PI) (Halt, Thermo Fisher 78438) which was replaced with fresh fluid every three days.



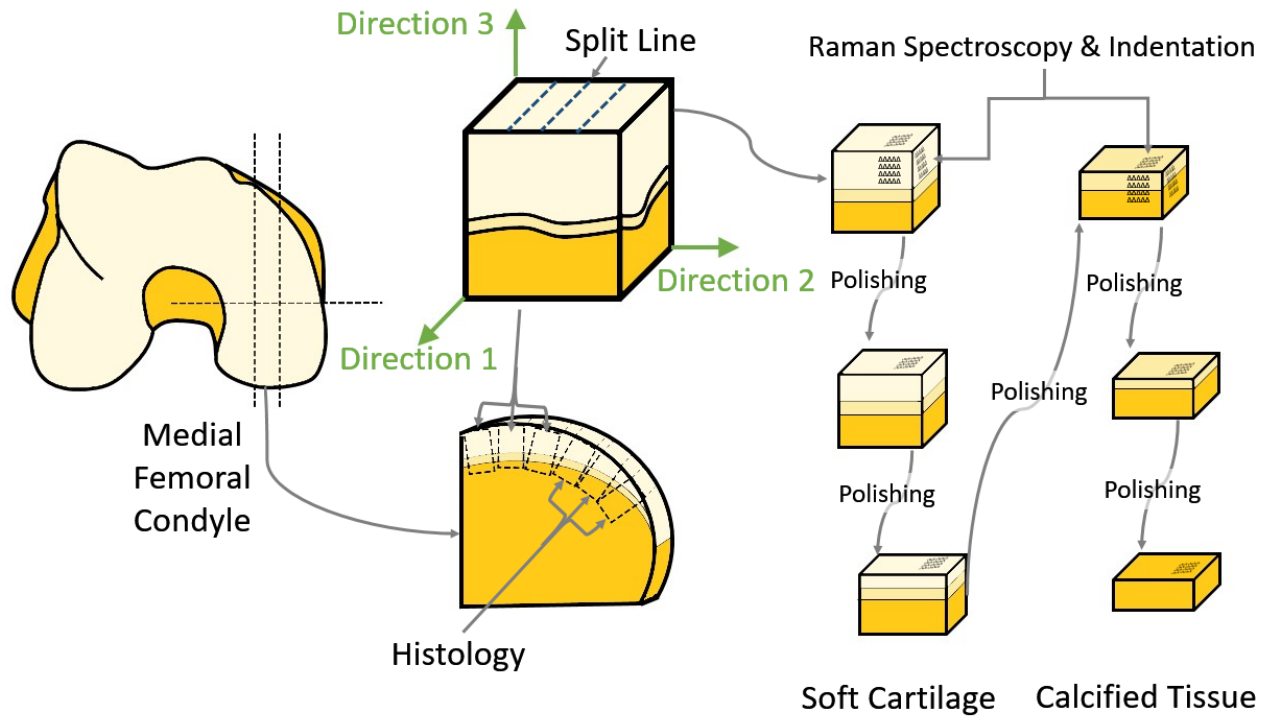


Figure 21 – Sample excise location, orientation, and testing sequence for soft articular cartilage and calcified tissue samples. Notional locations and directions for Indentation and Raman spectra arrays are depicted as dots on the samples. Bone depicted in gold, calcified cartilage in tan, and soft articular cartilage in white

### 5.3.2 X-Ray and Magnetic Resonance Imaging

Prior to dissection, a clinical X-ray (Medical Imaging Technologies, Quantum DR-1 CTM DR) was used at 3V to image each intact joint in the anteroposterior and lateral projection orientations. Images were reviewed for signs of trauma and osteoarthritis by an X-ray technician. Non-osseous tissues were removed and joints were wrapped in gauze with phosphate-buffered saline (PBS) and secured at the isocenter of a 7T Biospec MRI scanner (Bruker Medical GmbH, Ettlingen, Germany) for imaging experiments. MRI was performed in the coronal plane through

the most distal aspect of the medial condyle in the load bearing and the contact region of the joint. The acquired images share the same matrix size of 256 x 256 with field of view 100 x 100 mm and slice thickness of 2 mm. T2 weighted images were acquired using Multi Slice Multi Echo sequence in 21 slices with TE/TR = 8.74 msec / 2206 msec, Echo images = 8 with fat suppression option on and total acquisition time = 13 min. T1 $\rho$  images were acquired in a single slice at the contact region with TE/TR = 34.96 msec / 2578 msec, NEX = 2, NR = 6 and fat suppression. The spinlock strength was 19.99  $\mu$ T with spinlock duration = 10, 45, 80, 115, 150, and 185 msec and total acquisition time was 16 min.

#### 5.3.4 Histology, Secondary Harmonic Generation, and Two Photon Fluorescence Imaging

On the same samples used for mechanical testing, the prevalence of type II collagen in cartilage was investigated using SHG and TPF (Coherent Chameleon Ultra II laser tuned to 800 nm wavelength). A dichroic mirror was used to separate the output onto a non-descanned QUASAR Detection Unit with two detectors enabling the observation of SHG and two photon emissions separately. Imaging was performed on cartilage cubes without staining or contrast agents. Collagen I and II orientation was observed from the SHG signal by using Image J [236] applying the Orientation J plugin using the finite difference gradient method.

#### 5.3.5 Raman Spectroscopy Imaging

Raman spectroscopy was performed on cartilage cubes with an upright InVia microscope (Renishaw plc, Wotton-under-Edge, UK). The sample was excited by a 785 nm laser (Innovative Photonic Solutions, I0785SR0090B-IS1) without polarizations filters. An immersion 63x microscope objective with a NA of 0.9 (Leica) provided an approximately 1  $\mu$ m spot size on

samples submerged in PBS containing protease inhibitors. A 1200 l/mm grating and a charge coupled device (CCD) camera yielded a spectral resolution of approximately  $1\text{ cm}^{-1}$  for wavelengths from 620 to  $1711\text{ cm}^{-1}$ . The system was calibrated using both internal and external silicon standards, by setting the primary silicon peak to  $520\text{ cm}^{-1}$ .

Preprocessing of Raman spectra obtained in non-calcified tissues was performed as outlined elsewhere [125], [186] and in Chapter 3 of this work [232]. Briefly, cosmic rays were identified and removed, a linear baseline was subtracted, intensity was normalized, and outliers were detected and removed. The intensities observed at  $1578$ ,  $1488$  and  $782\text{ cm}^{-1}$  were summed for DNA, those at  $1380$ ,  $1342$  and  $1068\text{ cm}^{-1}$  were summed for chondroitin sulfate, those at  $1271$ ,  $1246$ ,  $920$ ,  $857$  and  $816\text{ cm}^{-1}$  were summed to represent collagen and those at  $1555$ ,  $1127$  and  $1004\text{ cm}^{-1}$  were summed for non-collagenous proteins. Raman maps were created of soft cartilage sections at  $50\text{ }\mu\text{m} \times 50\text{ }\mu\text{m}$  spacing on the two surfaces perpendicular to the articular surface, on the articular surface,  $\sim 500\text{ }\mu\text{m}$  below the articular surface (middle zone) and  $\sim 500\text{ }\mu\text{m}$  above the calcified cartilage (deep zone).

### 5.3.6 Soft Tissue Microindentation

Microindentation was performed on a Hysitron TI-950 nanoindenter. Indent arrays were five indents wide and spanned the full distance from articular surface to zone of calcified cartilage on both the parallel (direction 1), and transverse (direction 2) to split line directions. Additionally, 25 indents were placed in the longitudinal direction (direction 3) on the articular cartilage gliding surface, on a surface cut and polished  $500\text{ }\mu\text{m}$  below the articular surface (middle zone) and on a surface cut and polished  $500\text{ }\mu\text{m}$  above the calcified cartilage (deep zone). Indent arrays were

placed  $\sim 10$  times the contact radius from the tissue corner to avoid edge effects [237]. Indents were performed using a cono-spherical probe ( $R = 250.1 \mu\text{m}$ ) and were spaced at  $250 \times 250 \mu\text{m}$  in displacement control to a max indentation depth of  $12.5 \mu\text{m}$ . Tests at multiple load rates were performed using a trapezoidal load hold unload function. The displacement rates were 1, 4, and  $8 \mu\text{m/s}$ , hold time was 60 seconds, and unload rate was  $1 \mu\text{m/s}$ . Indentation was accomplished at large indentation depths and we assumed a perfect spherical geometry for the indenter. To determine the point of initial surface contact, we followed the method outlined by Guo [192] and explained in Chapter 3 using a  $1 \mu\text{m}$  lift and a  $20 \mu\text{N}$  preload.

Also as explained in Chapter 3, articular cartilage can be modeled as a nonlinear biphasic material with a Poisson's ratio near zero as proposed by Soltz and Ateshian [28] and applied to indentation by Burris *et al.* [30], [36], [148], [149]. Here we apply the resulting nonlinear biphasic “Hertz Burris Theory” (HBT) to obtain measures of tensile modulus ( $E_t$ ), equilibrium contact modulus ( $E_{co}$ ) and permeability ( $k$ ). To compensate for finite loading rates, we performed indentation tests at multiple loading and determined the portion of the load supported by the fluid, or fluid load fraction for each test. These combined tests at multiple rates were then used to find material properties applicable to all loading rates [36].

## 5.4 Results

During X-ray imaging, a patellar fracture and narrow joint space were identified on specimen C170123 but the remainder of the joints were radiographically normal. Visual observations of osteoarthritis status were recorded and synovial fluid was extracted the results of which are listed in Table 1.

Specimen	Medial Condyle	Lateral Condyle	Patella Femoral Groove	Patella	Synovial Fluid	X-Ray
C161473	None	Moderate	None	None	Yellow	Normal
C170123	None	None	None	None	Red	Broken Patella
C170125	None	None	None	Severe	Low Volume	Normal
C170243	None	Moderate	None	None	Light Pink	Normal

*Table 1 – Summary of observations during dissection of knees, all samples were obtained from the medial femoral condyle. Visual observation of the pervasiveness of cartilage damage (Minor, Moderate, Severe), coloration of the synovial fluid, and assessment of fracture via X-ray are indicated.*

For soft articular cartilage, results of indentation in the 1 and 2 directions where distance from the articular surface is normalized by the cartilage thickness are shown in Figure 22. The compressive and tensile moduli increased at greater distances from the articular surface for both the 1 and 2 directions for all samples. Greater intra-sample differences were observed between zones than was observed between samples from separate individuals (*i.e.* Direction 1  $E_{c0}$  average coefficient of variance 0.38 vs. 0.56). For all distances from the articular surface, the tensile modulus exceeded the compressive modulus ( $E_t/E_{c0}$  min = 1.5, mean = 1.9, max = 3.3). The permeability was highest and showed the greatest variability near the articular surface then decreased throughout the cartilage thickness. In agreement with the trends observed in averaged data, these heat maps representing compressive modulus, tensile modulus, and permeability show functional gradients in  $E_t$  and  $E_{c0}$  and  $k$  with increasing distance from the

articular surface (Figure 23). This Moreover, this map demonstrates the unique ability of microindentation to provide spatially resolved measures of time-dependent material properties over the full tissue thickness osteochondral region.

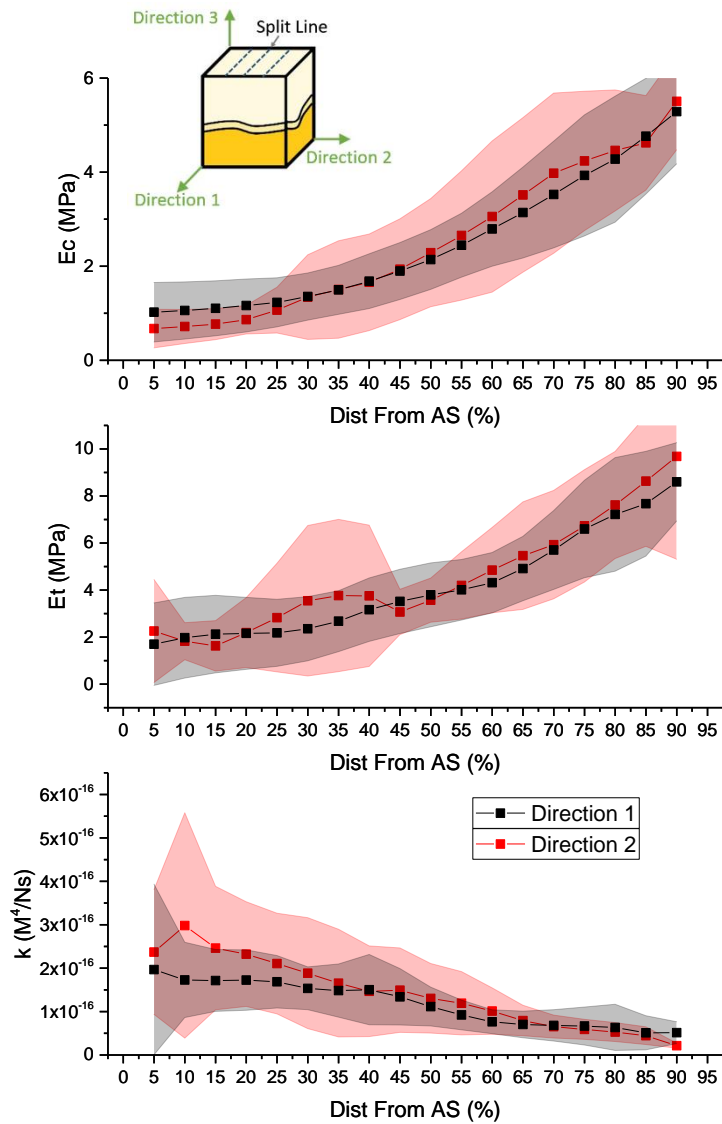
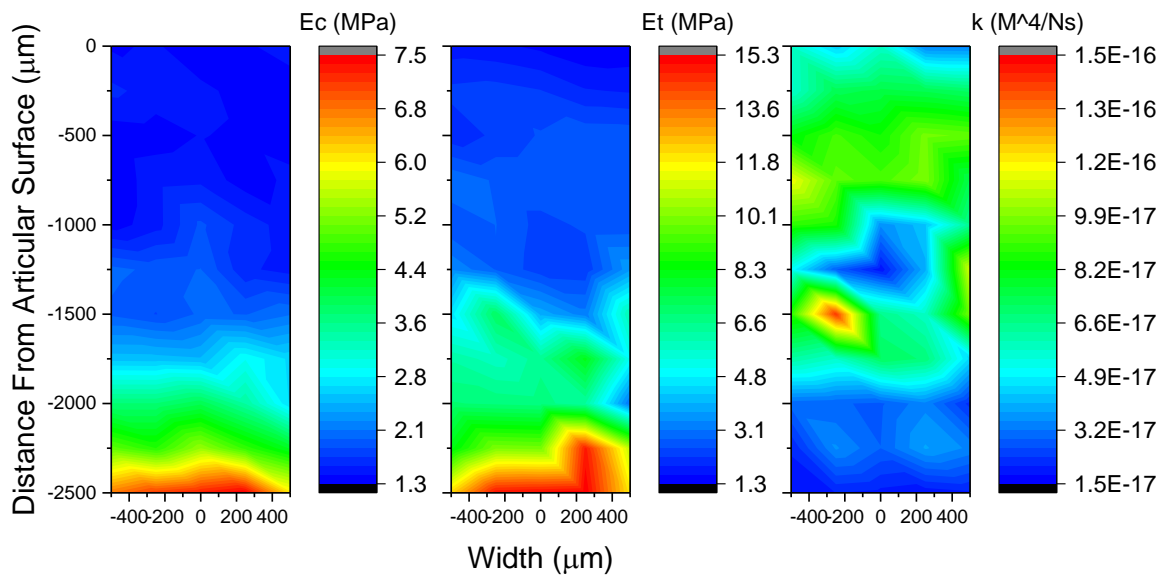


Figure 22 – Compressive modulus, tensile modulus, and permeability indicate pronounced zonal differences in material properties in both the split line (Direction 1) and perpendicular to the split line (Direction 2) directions. The compressive and tensile moduli increased while permeability decreased with increasing distance from the articular surface.



*Figure 23 – Heat maps of nonlinear biphasic mechanical properties of a representative sample in Direction 2 demonstrate the ability of microindentation to measure property variation over large areas.*

The ratios of indentation moduli in three orthogonal directions clearly demonstrate anisotropy throughout the soft articular cartilage (Figure 24). For an isotropic material, this ratio is equal to one (green line) and statistical significance is indicated as a departure from isotropic behavior. In the superficial region, the cartilage appears softest in the longitudinal direction (D3) whereas for middle and deep zones this observation is reversed. The compressive modulus parallel to the split line direction (Direction 1) is greater than in the direction perpendicular to the split line (Direction 2) with the most pronounced difference occurring in the superficial region.



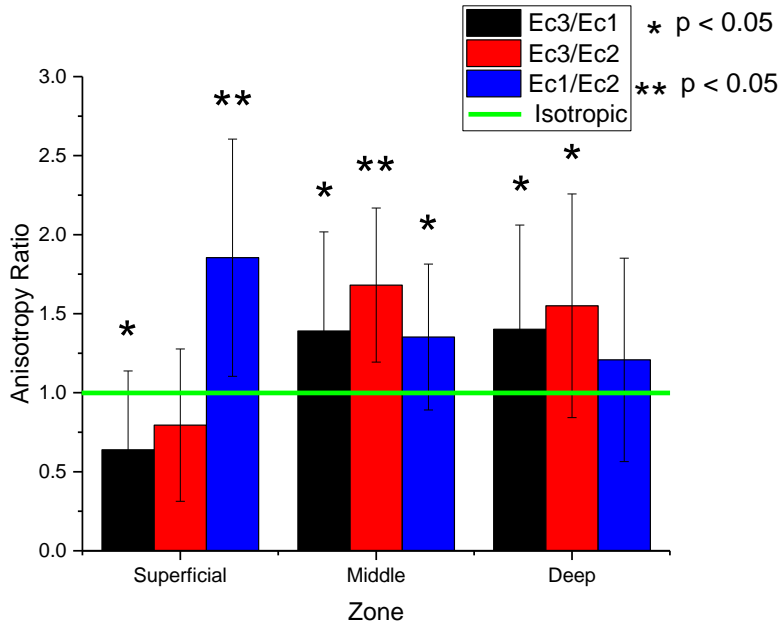


Figure 24 – Ratio of compressive moduli in three orthogonal directions for superficial middle and deep zone cartilage indicate that the tissue is anisotropic. This anisotropy varies in strength and direction depending on the zone tested. The behavior of an isotropic material is indicated as a green line and all statistical comparisons are made to isotropic behavior.

MRI imaging generated T2 maps of the articular cartilage within locations where mechanical testing was performed Figure 25. Mean values for the T2 and T1p were computed for the medial femoral condyle and tibial plateau where increased T2 and T1p signals can be used to assess potential signs of early arthritis Figure 26.

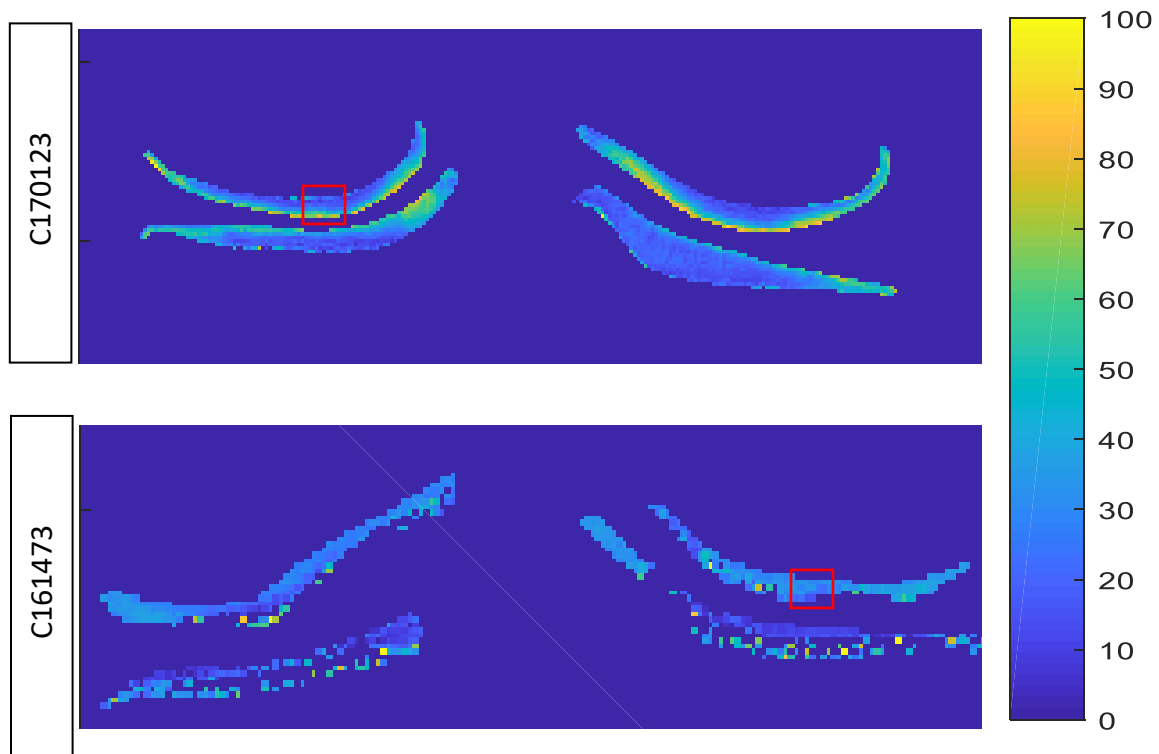
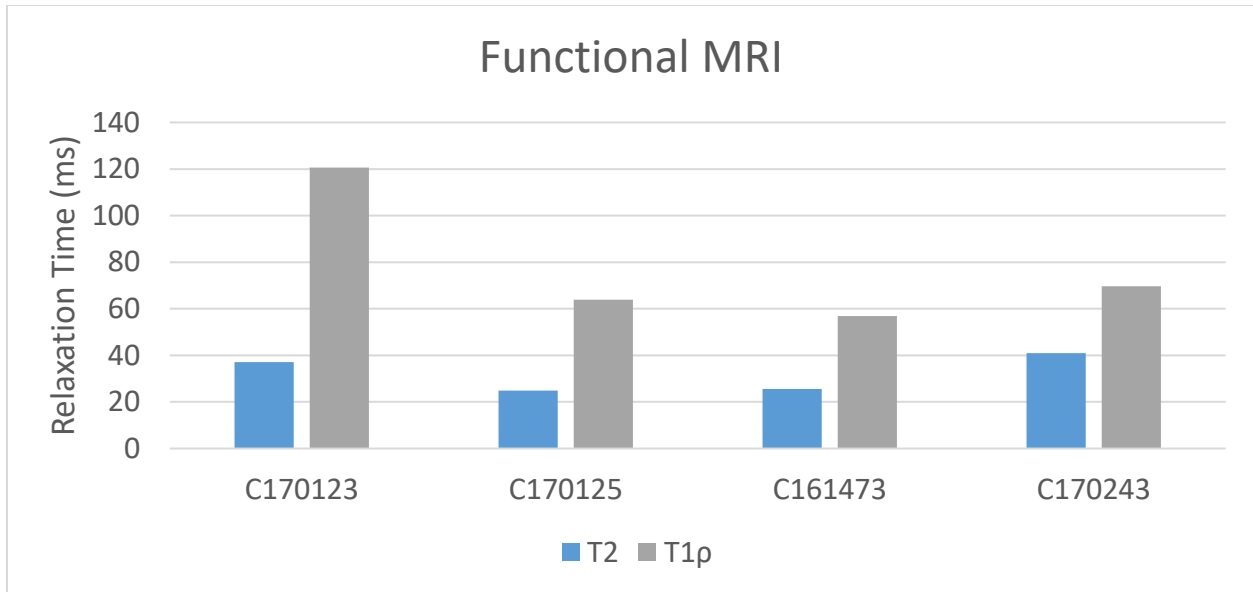
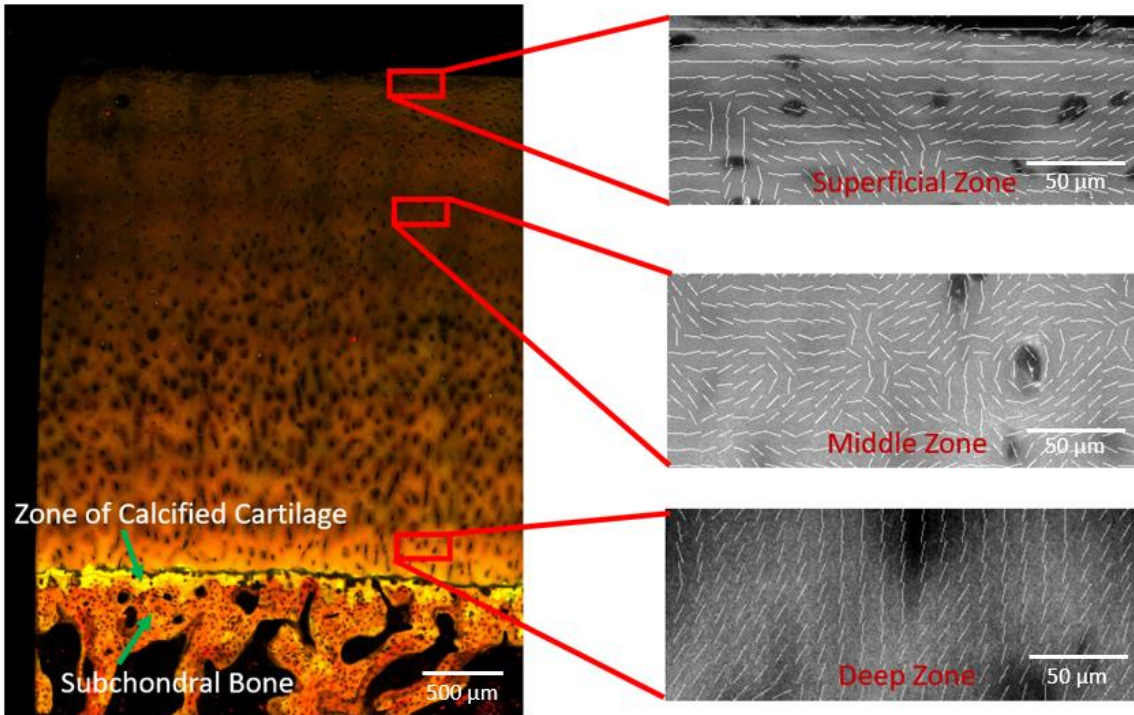


Figure 25 – Map of T2 relaxation time (ms) at a location approximately corresponding to the location where mechanical testing was performed (red boxes) for knees with the highest (top) and lowest (bottom) average values of T2.



*Figure 26 – Average T2 and T1ρ relaxation times (ms) obtained for the femoral condyle and tibial plateau in locations approximately corresponding to locations of mechanical testing. Images from knees C170123 and C161473 indicated the highest and the lowest likelihood of osteoarthritis respectively.*

SHG imaging of cartilage demonstrated changes in collagen type II orientation through the cartilage thickness (Figure 27). The zone of calcified cartilage produces an SHG signal consistent with presence of type II collagen. These images also produce an easily discernable change in TPF signal between the zone of calcified cartilage and the subchondral bone. Further, soft cartilage zones can be identified by processing the images to identify the predominant fiber direction.



*Figure 27 – SHG and TPF images reveal the zonal structure of cartilage and subchondral bone. For image on the left SHG is artificially colored red and TPF is artificially colored green. The demarcation between calcified cartilage and subchondral bone is identifiable based on a change in the strength of the TPF signal. Soft cartilage zones are distinguishable based on collagen orientation as identified using NIH imageJ software (Right side of image SHG is shown in grayscale and dominant fiber direction is shown as white line segments).*

Raman spectroscopy revealed variation in the concentration (and relative concentrations) of chemical species with distance from the articular surface. Both Collagen and GAG signal intensity increased with increasing distance from the articular surface. An example of representative sample illustrating the variation in the ratio of chondroitin sulfate to collagen signal is shown in Figure 28.

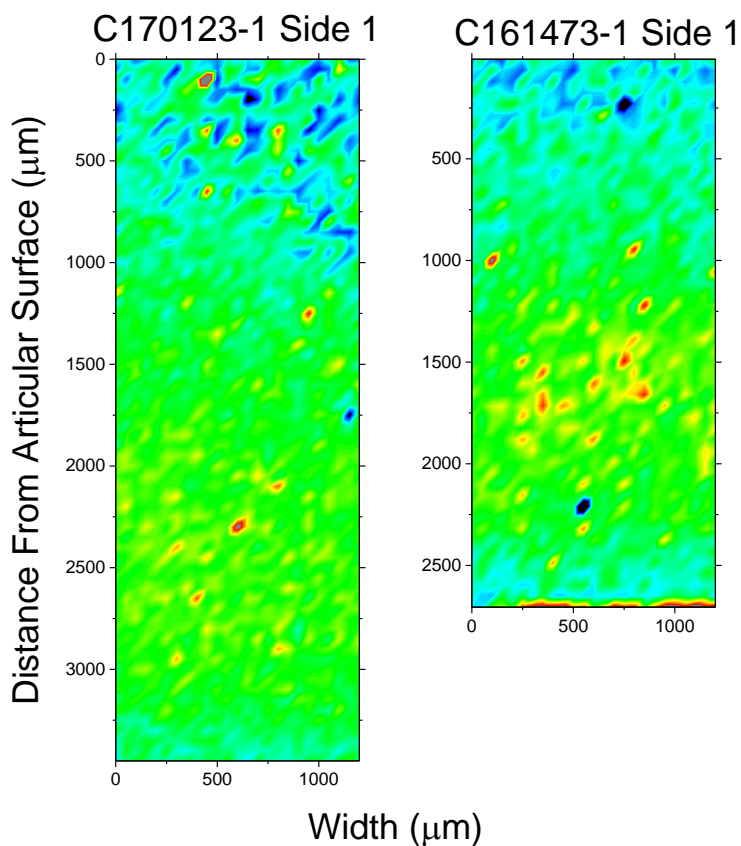


*Figure 28 – Raman maps showing variation in distribution of chemical constituents as a function of distance from the articular surface for two samples. The ratio of chondroitin sulfate peaks ( $1380$ ,  $1342$  and  $1068\text{ cm}^{-1}$ ) to collagen peaks ( $1271$ ,  $1246$ ,  $920$ ,  $857$  and  $816\text{ cm}^{-1}$ ) shown above.*

## 5.5 Discussion

The osteochondral unit is a complex combination of tissues that present marked heterogeneity in chemistry and structure. In a healthy state these tissues collaborate to support mechanical loading while maintain tissue viability. As we seek to repair damaged tissue, it is

important to restore the function of the articular cartilage, calcified cartilage, and subchondral bone so that they can work together as a complete osteochondral unit. One of the difficulties encountered in attempting to repair or replace these tissues is that they have complex mechanical behavior that is integral to their physiological function. It is important to quantify the mechanical complexities of these tissues to provide targets for replacement materials and to assess the effectiveness of repair approaches.

We quantified the mechanical behavior of soft and hard tissues within the osteochondral unit and investigated the time-dependence as a function of distance from the articular surface. We observed that soft articular cartilage has a pronounced time-dependence in all zones. The superficial region was softest in both tension and compression and had the highest permeability. This causes this zone to have the most rapid deformation in response to load. In contrast, the deep zone had the highest moduli, the lowest permeability, and the slowest time-dependent response. These findings are in agreement with research performed on bulk samples for compressive modulus [15], [30], tensile modulus [28], [36], [42], and permeability [28]. Additionally, the zonal changes observed here agree with work on long term compressive modulus [238] and zonal mechanical properties obtained via indentation for animal models in Chapter 3 [215].

Another mechanical complexity presented by the soft articular cartilage was material anisotropy. It has been widely observed that collagen fibers are not randomly distributed throughout the zonal articular cartilage but instead form arch-like Benninghoff structures [115], [239], this finding was confirmed in this dissertation via SHG imaging. Additionally, when viewed

perpendicular to the articular surface, the cartilage possesses a preferential collagen fiber direction which can be identified as split lines [191]. It has been hypothesized that this organized collagen fiber alignment is critical to physiological function [191], [239]. We observed that the mechanical properties of articular cartilage do vary with orientation and that higher moduli were present when indentation was performed in the predominant collagen fiber direction. This indicates that cartilage is at a minimum an orthotropic material with zonal variation in directional stiffness. These findings are in qualitative agreement with observations from AFM testing [10] and expand prior observations to a length scale at which measurements are consistent with bulk properties.

## 5.6 Limitations

During the dissection and testing process, the samples experienced multiple freeze thaw cycles that may have resulted in changes in the measured mechanical properties of the tissues. Additionally, because the system used to perform mechanical testing was not capable of performing indentation at extremely rapid loading rates multiple tests were required to obtain measures of tensile modulus and permeability leading to increased variability in these measures. Further, this testing was limited to four individuals with three samples from each individual and further work should be performed to obtain measures from a statistically representative number of individuals for application to broader populations.

Measuring the anisotropic properties of materials via indentation testing alone presents various challenges. While theoretical models have been developed to populate compliance matrices for material properties using indentation testing [175], [176], [240], testing in three



orthogonal directions does not supply sufficient independent measures (three measures) to fully quantify material behavior even for a transversely isotropic material (five independent elastic constants) let alone a fully anisotropic material (21 independent elastic constants). Current anisotropic indentation models are further limited to providing information regarding compressive properties but indentation testing may also be able to produce important information regarding anisotropy of permeability and tensile modulus or Poisson's ratio. Fortunately, even with these limitations, indentation testing can be used to place limits on the directionally dependent behavior and provide valuable information regarding comparative stiffness in different directions.

## 5.7 Conclusions

This study measured the variation of time-dependent mechanical properties as a function of distance from the articular surface for skeletally mature human tissues. Additionally we investigated the anisotropy of these mechanical properties and observed a relationship between these mechanical properties and the predominant collagen fiber orientation. This helps illuminate the structure function relationship of the cartilage constituents with their physiological function. The properties measured in this work provide important design targets for tissue engineers seeking to create constructs that reproduce the mechanical behavior of healthy native articular cartilage. Additionally the zonal and directional variations in mechanical properties provide important inputs for computational finite element models seeking model physiological conditions.

## Chapter 6 – Discussion and Conclusion

### 6.1 Major Findings

As we seek to recreate the mechanosensory cues experienced by cells, or develop computational models mirroring the behavior of native tissue, it is important that we understand the time, length scale, and directionally dependent mechanical behavior of cartilage, and other biological materials. Further, measuring the mechanical behavior of tissues offers the opportunity to assess disease progression. This dissertation explored the mechanical behavior of articular cartilage by focusing on three broad aspects of mechanical behavior: the underlying causes of time-dependent deformation for zonal cartilage, tissue microstructure resulting in an indentation size effect, and the mechanical anisotropy of soft (non-calcified) tissues within the osteochondral unit. This work provides information vital to creating tissue constructs and finite element models that mimic native tissue behavior.

In the first portion of this effort [Chapter 3], we used microindentation to map the time-dependent properties of untreated and trypsin treated cartilage throughout each cartilage zone. Unlike conventional approaches that combine viscoelastic and poroelastic behaviors into a single framework, we deconvoluted the mechanical response into separate contributions to time-dependent behavior. Poroelastic effects in all cartilage zones dominated the time-dependent behavior of articular cartilage, and a model that incorporates tension-compression nonlinearity best represents mechanical behavior. Tensile and compressive modulus increased and the permeability decreased with distance from the articular surface. Further, trypsin treatment resulted in decreased moduli and increased permeability.

Next in Chapter 4, we found that the indentation modulus of porous materials, including articular cartilage, is a strong function of contact radius. Softer moduli were obtained at small contact radii when compared to bulk measures for all tested materials. In contrast to agarose, this discrepancy in modulus persisted for untreated and trypsin treated cartilage even after compensation for indentation rate, matrix compaction, and surface roughness. This phenomenon was modeled as a soft thin film on a stiffer substrate and the apparent film thickness was found to be related to the collagen matrix prevalence, matrix organization, pervasiveness of sGAGs. This phenomenon may result from the fundamental matrix size of these materials and relief of internal residual stress at a newly liberated surface. These factors result in departure from continuum mechanics assumptions and produce apparent stiffness measures that varied by multiple orders of magnitude. These differences in modulus should be accounted for when analyzing small-scale interactions of biological tissues and may play an important role in the behavior of cells in both healthy and damaged tissue.

In Chapter 5, we found that the time-dependent mechanical properties of articular cartilage change with distance from the articular surface for skeletally mature human tissues. Additionally we observed that the elastic anisotropy of articular cartilage varies zonally. This variation in anisotropic properties appears to be related to the predominant collagen fiber orientation. This finding represents a potential link between the underlying cartilage structure and organization and the physiological function of the tissue. The properties measured here provide important time-dependent material property targets for tissue engineers and computational modelers seeking to recreate native tissues.

## 6.2 Significance of Work

This body of work indicates that cartilage possesses complex structural hierarchy and composition that results in variation in mechanical response based upon loading rate, the length scale of the test, and the direction of loading. In contrast to the mechanical complexities we observed, articular cartilage is commonly treated as an isotropic homogeneous material with a purely elastic response to mechanical load. As researchers attempt to create tissue engineered constructs, assess disease state and progression, or generate computational models it is likely highly important to account for the more complex mechanical behaviors of articular cartilage. The success of these repair and modeling approaches may hinge on incorporation of these more complex aspects of cartilage mechanical properties. The collective efforts outlined in this dissertation represent critical advances toward developing repair approaches that can recreate the mechanical environment of native cells.

In Chapter 3 we observed that cartilage behaves consistent with nonlinear biphasic models and these results directly contradicted predictions of viscoelastic and linear biphasic theory [28], [194]–[196]. While this concept had been shown for full thickness cartilage [28], [30], [36], [149], this work extended this observation to zonal cartilage and used this framework to establish material properties as a function of distance from the articular surface. The material properties established here for zonal cartilage are consistent with those for full cartilage samples fluid load fraction [9], permeability [28], compressive [15], [28], [30], [42] and tensile moduli [28], [36], [41], [42]. These property variations with distance may result from zonal differences in chemistry and structure. As anticipated trypsin treatment substantially increased permeability

which can be directly attributed to the absence of GAGs [134]. Additionally we observed decreased in tensile and compressive modulus consistent with relief of osmotic pressure resulting from GAG depletion as has been observed previously [19], [198]. GAG depletion is clinically relevant because it parallels tissue changes in osteoarthritis, would likely result in increased compressive strain and fluid flow which may attribute to cell death and further progression of the disease [58]–[60]. This work produced direct measures of tensile modulus and permeability of cartilage with intact zonal structure that represents a new contribution to the understanding of the mechanical properties of articular cartilage.

In Chapter 4 we investigated potential causes of modulus variation of biphasic materials with the length scale of testing [15], [35], [36]. We equalized effects from poroelastic indentation rate, matrix compaction, and surface roughness of the samples and found that the size effects persisted for trypsin treated and untreated cartilage but was corrected for agarose. Two factors likely contribute to this difference in observed indentation modulus for cartilage samples. The first is that the pore size of the tested material is on the same length scale as the test resulting in departure from continuum mechanics assumptions inherent in indentation analytical approaches [35]. We also proposed a second mechanism resulting from the relief of osmotic residual stress when a surface is newly liberated in a porous material. These two phenomena were modeled as a soft thin film. This film thickness was correlated with variations in pore size, collagen fiber arrangement [197], [241], and chemical composition of the matrix [115], [125], [186]. We found that a newly liberated surface might result in the creation of an apparent soft layer of material spanning multiple microns for articular cartilage. Altered mechanical behavior may affect the

behavior of cells in the immediate vicinity of damaged tissue [222] potentially resulting in chondrocyte necrosis [98], [223], [224]. This low modulus at small length scales and marked departure from continuum mechanics may have profound implications for the behavior of chondrocytes because their interactions with the extracellular matrix are at length scales less than 10  $\mu\text{m}$ .

In Chapter 5, we found that the time-dependent mechanical properties of articular cartilage from skeletally mature human subjects varied with distance from the articular surface in a manner similar to the trends observed in Chapter 3. The superficial zone presents much lower moduli in both tension and compression than the deep zone and has much higher permeability. In addition to the zonal property variation, we observed that articular cartilage is elastically anisotropic in agreement with previous research [41], [43], [240]. This anisotropy appears to be related to the predominant direction of the collagen fiber matrix. For example in the superficial zone, we observed higher moduli in the split line direction than in the transverse to split line direction. This link between the predominate collagen fiber direction and the mechanical behavior helps to link the zonal structure [231] with the physiological function of these tissues and strengthens the argument that the Benninghoff arrangement of collagen [239] is integral to load transfer within the tissue [110].

This work adds to a growing body of literature that demonstrates that the mechanical behavior of biological tissues is remarkably complex. This complexity can be observed in the time-dependent response, variations in behavior at different length scale, and material anisotropy. These multifaceted mechanical behaviors are increasingly being tied to the underlying chemistry

and the physical structure of the tissue. This structure function relationship presents both great challenges in characterizing materials but also great opportunities as we seek to develop novel materials we can draw upon inspiration from natural materials that so elegantly meet their functional requirements.

#### 6.4 Recommendations and Future Directions

To extend these findings there are important aspects which demand additional investigation. While these methods have been exploratory, it would be highly beneficial to test cartilage from a statistically representative number of healthy skeletally mature human subjects. Additionally, trypsin treatment may have resulted in degradation of the collagen network and removal of GAGs that may not precisely mimic disease, evaluating arthritic tissue would provide valuable insight. These tests were performed on tissues obtained from the femoral condyles but that location is not the only location affected by arthritis and there is great potential to contrast behavior from multiple anatomical sights that are more and less prone to arthritis. Further, these methods are not limited to articular cartilage. The approaches used in this work are applicable to testing many biological tissues that present a complex mechanical response.

In expanding the analytical tools used to perform assessment of these tissues, there are a few areas for advancement. First, due to load rate limitations of the indenter, a more direct method of assessing material properties would be desirable by extending the nonlinear biphasic indentation model to dynamic mechanical analysis or by incorporating a ramp correction factor. Additionally, this work has found that for the tested materials a single cause of time-dependent deformation was the dominant mechanism. However, it is likely that both viscoelasticity and

poroelasticity occur simultaneously and for some classes of materials these effects may be similar in magnitude. Preliminary work has been done to create a poroviscoelastic model [188] it would be valuable to extend this model to account for tension compression non-linearity, and to incorporate plastic behavior to better model materials like hydrated bone which undergo both time-dependent and permanent deformation. Additionally, anisotropic indentation models should be extended to enable measurement of material permeability and tensile modulus of nonlinear biphasic materials. Currently, anisotropic models are limited to comparison of elastic modulus only and extension will likely require incorporation of finite element modeling to enable extraction of additional anisotropic properties. These extensions provide a wonderful opportunity to create frameworks vital to fully characterizing the mechanical behavior of biological materials.

## 6.5 Concluding Remarks

This work focused on three major tasks. First, we quantified the time-dependent mechanical behavior of articular cartilage and biomimetic materials. Various models were applied to the experimental results and a process was established which provides clear criteria for selection of the appropriate material model. Second, the mechanical properties of cartilage were quantified via indentation at multiple length scales. A thin film model was proposed as a means to explain the discrepancies in testing observed at varying length scales. This model helps inform our understanding of the chemical and structural arrangement of biological materials at very small length scales. Third, this work has investigated the anisotropic behavior of soft osteochondral tissues in physiologically relevant conditions. While this work has primarily been



focused on testing articular cartilage the methods and approaches established here are applicable to a wide range of biological materials. These methods, focused on small-scale indentation, provide the opportunity to measure material properties for biological materials that frequently have significant variability at sub millimeter length scales. Understanding material behavior will prove invaluable in the design of biomaterials to repair or replace native tissues.

## Bibliography

- [1] R. C. Lawrence *et al.*, “Estimates of the prevalence of arthritis and other rheumatic conditions in the United States: Part II,” *Arthritis Rheum.*, vol. 58, no. 1, pp. 26–35, Jan. 2008.
- [2] R. C. Lawrence *et al.*, “Estimates of the prevalence of arthritis and selected musculoskeletal disorders in the United States,” *Arthritis Rheum.*, vol. 41, no. 5, pp. 778–799, May 1998.
- [3] C. G. Helmick *et al.*, “Estimates of the prevalence of arthritis and other rheumatic conditions in the United States: Part I,” *Arthritis Rheum.*, vol. 58, no. 1, pp. 15–25, Jan. 2008.
- [4] E. A. Aisenbrey and S. J. Bryant, “Mechanical loading inhibits hypertrophy in chondrogenically differentiating hMSCs within a biomimetic hydrogel,” *J Mater Chem B*, vol. 4, no. 20, pp. 3562–3574, 2016.
- [5] N. J. Steinmetz, E. A. Aisenbrey, K. K. Westbrook, H. J. Qi, and S. J. Bryant, “Mechanical loading regulates human MSC differentiation in a multi-layer hydrogel for osteochondral tissue engineering,” *Acta Biomater.*, vol. 21, pp. 142–153, Jul. 2015.
- [6] I. M. El-Sherbiny and M. H. Yacoub, “Hydrogel scaffolds for tissue engineering: Progress and challenges,” *Glob. Cardiol. Sci. Pract.*, vol. 2013, no. 3, pp. 316–342, Nov. 2013.
- [7] F. Yang, C. G. Williams, D. Wang, H. Lee, P. N. Manson, and J. Elisseeff, “The effect of incorporating RGD adhesive peptide in polyethylene glycol diacrylate hydrogel on osteogenesis of bone marrow stromal cells,” *Biomaterials*, vol. 26, no. 30, pp. 5991–5998, Oct. 2005.

- [8] S. K. Seidlits *et al.*, "The effects of hyaluronic acid hydrogels with tunable mechanical properties on neural progenitor cell differentiation," *Biomaterials*, vol. 31, no. 14, pp. 3930–3940, May 2010.
- [9] S. Park, R. Krishnan, S. B. Nicoll, and G. A. Ateshian, "Cartilage Interstitial Fluid Load Support in Unconfined Compression," *J. Biomech.*, vol. 36, no. 12, pp. 1785–1796, Dec. 2003.
- [10] M. A. McLeod, R. E. Wilusz, and F. Guilak, "Depth-dependent anisotropy of the micromechanical properties of the extracellular and pericellular matrices of articular cartilage evaluated via atomic force microscopy," *J. Biomech.*, vol. 46, no. 3, pp. 586–592, Feb. 2013.
- [11] S. S. Chen, Y. H. Falcovitz, R. Schneiderman, A. Maroudas, and R. L. Sah, "Depth-dependent compressive properties of normal aged human femoral head articular cartilage: relationship to fixed charge density," *Osteoarthritis Cartilage*, vol. 9, no. 6, pp. 561–569, Aug. 2001.
- [12] R. M. Schinagl, D. Gurskis, A. C. Chen, and R. L. Sah, "Depth-dependent confined compression modulus of full-thickness bovine articular cartilage," *J. Orthop. Res.*, vol. 15, no. 4, pp. 499–506, Jul. 1997.
- [13] T. J. Klein, M. Chaudhry, W. C. Bae, and R. L. Sah, "Depth-dependent biomechanical and biochemical properties of fetal, newborn, and tissue-engineered articular cartilage," *J. Biomech.*, vol. 40, no. 1, pp. 182–190, 2007.
- [14] S. M. Elmore, L. Sokoloff, G. Norris, and P. Carmeci, "Nature of 'imperfect' elasticity of articular cartilage," *J. Appl. Physiol.*, vol. 18, no. 2, pp. 393–396, Mar. 1963.

- [15] S. Park, C. T. Hung, and G. A. Ateshian, "Mechanical response of bovine articular cartilage under dynamic unconfined compression loading at physiological stress levels," *Osteoarthritis Cartilage*, vol. 12, no. 1, pp. 65–73, Jan. 2004.
- [16] W. C. Hayes and L. F. Mockros, "Viscoelastic properties of human articular cartilage.," *J. Appl. Physiol.*, vol. 31, no. 4, pp. 562–568, Oct. 1971.
- [17] D. R. M. Schinagl, M. K. Ting, J. H. Price, and R. L. Sah, "Video microscopy to quantitate the inhomogeneous equilibrium strain within articular cartilage during confined compression," *Ann. Biomed. Eng.*, vol. 24, no. 4, pp. 500–512, Jul. 1996.
- [18] M. A. Soltz and G. A. Ateshian, "Interstitial Fluid Pressurization During Confined Compression Cyclical Loading of Articular Cartilage," *Ann. Biomed. Eng.*, vol. 28, no. 2, pp. 150–159, Feb. 2000.
- [19] G. E. Kempson, H. Muir, C. Pollard, and M. Tuke, "The tensile properties of the cartilage of human femoral condyles related to the content of collagen and glycosaminoglycans," *Biochim. Biophys. Acta BBA - Gen. Subj.*, vol. 297, no. 2, pp. 456–472, Feb. 1973.
- [20] G. E. Kempson, "Relationship between the tensile properties of articular cartilage from the human knee and age.," *Ann. Rheum. Dis.*, vol. 41, no. 5, pp. 508–511, Oct. 1982.
- [21] M. B. Schmidt, V. C. Mow, L. E. Chun, and D. R. Eyre, "Effects of proteoglycan extraction on the tensile behavior of articular cartilage," *J. Orthop. Res.*, vol. 8, no. 3, pp. 353–363, May 1990.

- [22] V. Roth and V. C. Mow, "The intrinsic tensile behavior of the matrix of bovine articular cartilage and its variation with age.," *J Bone Jt. Surg Am*, vol. 62, no. 7, pp. 1102–1117, Oct. 1980.
- [23] A. Maroudas, "Transport of solutes through cartilage: permeability to large molecules.," *J. Anat.*, vol. 122, no. Pt 2, pp. 335–347, Nov. 1976.
- [24] J. M. Mansour and V. C. Mow, "The permeability of articular cartilage under compressive strain and at high pressures," *J. Bone Jt. Surg.*, vol. 58, no. 4, pp. 509–516, Jun. 1976.
- [25] C. W. McCutchen, "The frictional properties of animal joints," *Wear*, vol. 5, no. 1, pp. 1–17, Jan. 1962.
- [26] A. K. Williamson, A. C. Chen, and R. L. Sah, "Compressive properties and function—composition relationships of developing bovine articular cartilage," *J. Orthop. Res.*, vol. 19, no. 6, pp. 1113–1121, Nov. 2001.
- [27] A. Maroudas, "Physicochemical Properties of Cartilage in the Light of Ion Exchange Theory," *Biophys. J.*, vol. 8, no. 5, pp. 575–595, May 1968.
- [28] M. A. Soltz and G. A. Ateshian, "A Conewise Linear Elasticity Mixture Model for the Analysis of Tension-Compression Nonlinearity in Articular Cartilage," *J. Biomech. Eng.*, vol. 122, no. 6, pp. 576–586, Jul. 2000.
- [29] V. C. Mow, S. C. Kuei, W. M. Lai, and C. G. Armstrong, "Biphasic Creep and Stress Relaxation of Articular Cartilage in Compression: Theory and Experiments," *J. Biomech. Eng.*, vol. 102, no. 1, pp. 73–84, Feb. 1980.

- [30] A. C. Moore, B. K. Zimmerman, X. Chen, X. L. Lu, and D. L. Burris, "Experimental characterization of biphasic materials using rate-controlled Hertzian indentation," *Tribol. Int.*, vol. 89, pp. 2–8, Sep. 2015.
- [31] G. J. Miller and E. F. Morgan, "Use of microindentation to characterize the mechanical properties of articular cartilage: comparison of biphasic material properties across length scales," *Osteoarthritis Cartilage*, vol. 18, no. 8, pp. 1051–1057, Aug. 2010.
- [32] R. K. June, C. P. Neu, J. R. Barone, and D. P. Fyhrie, "Polymer mechanics as a model for short-term and flow-independent cartilage viscoelasticity," *Mater. Sci. Eng. C*, vol. 31, no. 4, pp. 781–788, May 2011.
- [33] S. Park, K. D. Costa, and G. A. Ateshian, "Microscale frictional response of bovine articular cartilage from atomic force microscopy," *J. Biomech.*, vol. 37, no. 11, pp. 1679–1687, Nov. 2004.
- [34] S. Park, K. D. Costa, G. A. Ateshian, and K.-S. Hong, "Mechanical properties of bovine articular cartilage under microscale indentation loading from atomic force microscopy," *Proc. Inst. Mech. Eng. [H]*, vol. 223, no. 3, pp. 339–347, Mar. 2009.
- [35] M. Stolz, R. Raiteri, A. U. Daniels, M. R. VanLandingham, W. Baschong, and U. Aebi, "Dynamic Elastic Modulus of Porcine Articular Cartilage Determined at Two Different Levels of Tissue Organization by Indentation-Type Atomic Force Microscopy," *Biophys. J.*, vol. 86, no. 5, pp. 3269–3283, May 2004.

- [36] E. D. Bonnevie, V. J. Baro, L. Wang, and D. L. Burris, "Fluid load support during localized indentation of cartilage with a spherical probe," *J. Biomech.*, vol. 45, no. 6, pp. 1036–1041, Apr. 2012.
- [37] W. C. Hayes, L. M. Keer, G. Herrmann, and L. F. Mockros, "A mathematical analysis for indentation tests of articular cartilage," *J. Biomech.*, vol. 5, no. 5, pp. 541–551, Sep. 1972.
- [38] A. F. Mak, W. M. Lai, and V. C. Mow, "Biphasic indentation of articular cartilage—I. Theoretical analysis," *J. Biomech.*, vol. 20, no. 7, pp. 703–714, Jan. 1987.
- [39] V. C. Mow, M. C. Gibbs, W. M. Lai, W. B. Zhu, and K. A. Athanasiou, "Biphasic indentation of articular cartilage—II. A numerical algorithm and an experimental study," *J. Biomech.*, vol. 22, no. 8, pp. 853–861, Jan. 1989.
- [40] R. K. Korhonen *et al.*, "Comparison of the equilibrium response of articular cartilage in unconfined compression, confined compression and indentation," *J. Biomech.*, vol. 35, no. 7, pp. 903–909, Jul. 2002.
- [41] N. O. Chahine, C. C.-B. Wang, C. T. Hung, and G. A. Ateshian, "Anisotropic strain-dependent material properties of bovine articular cartilage in the transitional range from tension to compression," *J. Biomech.*, vol. 37, no. 8, pp. 1251–1261, Aug. 2004.
- [42] C.-Y. Huang, A. Stankiewicz, G. A. Ateshian, and V. C. Mow, "Anisotropy, inhomogeneity, and tension–compression nonlinearity of human glenohumeral cartilage in finite deformation," *J. Biomech.*, vol. 38, no. 4, pp. 799–809, Apr. 2005.

- [43] J. S. Jurvelin, M. D. Buschmann, and E. B. Hunziker, "Mechanical anisotropy of the human knee articular cartilage in compression," *Proc. Inst. Mech. Eng. [H]*, vol. 217, no. 3, pp. 215–219, Mar. 2003.
- [44] J. Mizrahi, A. Maroudas, Y. Lanir, I. Ziv, and T. J. Webber, "The 'instantaneous' deformation of cartilage: effects of collagen fiber orientation and osmotic stress," *Biorheology*, vol. 23, no. 4, pp. 311–330, 1986.
- [45] M. E. Stender, R. A. Regueiro, and V. L. Ferguson, "A poroelastic finite element model of the bone–cartilage unit to determine the effects of changes in permeability with osteoarthritis," *Comput. Methods Biomech. Biomed. Engin.*, vol. 20, no. 3, pp. 319–331, Feb. 2017.
- [46] M. Galli, K. S. C. Comley, T. A. V. Shean, and M. L. Oyen, "Viscoelastic and poroelastic mechanical characterization of hydrated gels," *J. Mater. Res.*, vol. 24, no. 03, pp. 973–979, 2009.
- [47] Y. Hu, X. Zhao, J. J. Vlassak, and Z. Suo, "Using indentation to characterize the poroelasticity of gels," *Appl. Phys. Lett.*, vol. 96, no. 12, p. 121904, Mar. 2010.
- [48] V. C. Mow and R. Huiskes, *Basic Orthopaedic Biomechanics & Mechano-biology*. Lippincott Williams & Wilkins, 2005.
- [49] "An educational look inside the body - Cartilage," *dancehealthier*. .
- [50] "A fiber reinforced poroelastic model of nanoindentation of porcine costal cartilage: A combined experimental and finite element approach." [Online]. Available:



<http://www.sciencedirect.com/science/article/pii/S1751616108000799>. [Accessed: 14-Mar-2016].

- [51] A. P. Newman, "Articular Cartilage Repair," *Am. J. Sports Med.*, vol. 26, no. 2, pp. 309–324, Mar. 1998.
- [52] "– ARTHRITIS: A NATIONAL EPIDEMIC." [Online]. Available: <https://www.gpo.gov/fdsys/pkg/CHRG-108shrg94318/html/CHRG-108shrg94318.htm>. [Accessed: 18-Oct-2016].
- [53] D. D. Anderson *et al.*, "POST-TRAUMATIC OSTEOARTHRITIS: IMPROVED UNDERSTANDING AND OPPORTUNITIES FOR EARLY INTERVENTION," *J. Orthop. Res. Off. Publ. Orthop. Res. Soc.*, vol. 29, no. 6, pp. 802–809, Jun. 2011.
- [54] K. L. Cameron, M. S. Hsiao, B. D. Owens, R. Burks, and S. J. Svoboda, "Incidence of physician-diagnosed osteoarthritis among active duty United States military service members," *Arthritis Rheum.*, vol. 63, no. 10, pp. 2974–2982, Oct. 2011.
- [55] D. L. Scher, P. J. Belmont, S. Mountcastle, and B. D. Owens, "The incidence of primary hip osteoarthritis in active duty US military servicemembers," *Arthritis Care Res.*, vol. 61, no. 4, pp. 468–475, Apr. 2009.
- [56] U. M. Kujala, J. Kaprio, and S. Sarno, "Osteoarthritis of weight bearing joints of lower limbs in former elite male athletes," *BMJ*, vol. 308, no. 6923, pp. 231–234, Jan. 1994.
- [57] E. B. Hunziker, "Articular cartilage repair: basic science and clinical progress. A review of the current status and prospects," *Osteoarthritis Cartilage*, vol. 10, no. 6, pp. 432–463, Jun. 2002.

- [58] W. Hunter, "Of the structure and diseases of articulating cartilages, by William Hunter, surgeon," *Philos. Trans.*, vol. 42, no. 462–471, pp. 514–521, 1742.
- [59] M. Brittberg, "The History of the Treatment of Cartilage Injuries," in *Techniques in Cartilage Repair Surgery*, A. A. Shetty, S.-J. Kim, N. Nakamura, and M. Brittberg, Eds. Springer Berlin Heidelberg, 2014, pp. 3–16.
- [60] E. Gautier, D. Kolker, and R. P. Jakob, "Treatment of cartilage defects of the talus by autologous osteochondral grafts," *J. Bone Joint Surg. Br.*, vol. 84–B, no. 2, pp. 237–244, Mar. 2002.
- [61] D. O. Clegg *et al.*, "Glucosamine, Chondroitin Sulfate, and the Two in Combination for Painful Knee Osteoarthritis," *N. Engl. J. Med.*, vol. 354, no. 8, pp. 795–808, Feb. 2006.
- [62] T. E. McAlindon, M. P. LaValley, J. P. Gulin, and D. T. Felson, "Glucosamine and chondroitin for treatment of osteoarthritis: a systematic quality assessment and meta-analysis," *JAMA*, vol. 283, no. 11, pp. 1469–1475, Mar. 2000.
- [63] J. Y. Reginster *et al.*, "Long-term effects of glucosamine sulphate on osteoarthritis progression: a randomised, placebo-controlled clinical trial," *The Lancet*, vol. 357, no. 9252, pp. 251–256, Jan. 2001.
- [64] P. J. Livesley, M. Doherty, M. Needoff, and A. Moulton, "Arthroscopic lavage of osteoarthritic knees," *J. Bone Joint Surg. Br.*, vol. 73–B, no. 6, pp. 922–926, Nov. 1991.
- [65] R. W. Chang, J. Falconer, S. David Stulberg, W. J. Arnold, L. M. Manheim, and A. R. Dyer, "A randomized, controlled trial of arthroscopic surgery versus closed-needle joint lavage for

- patients with osteoarthritis of the knee," *Arthritis Rheum.*, vol. 36, no. 3, pp. 289–296, Mar. 1993.
- [66] J. N. Gibson, M. D. White, V. M. Chapman, and R. K. Strachan, "Arthroscopic lavage and debridement for osteoarthritis of the knee," *J. Bone Joint Surg. Br.*, vol. 74–B, no. 4, pp. 534–537, Jul. 1992.
- [67] J. B. Moseley, N. P. Wray, D. Kuykendall, K. Willis, and G. Landon, "Arthroscopic Treatment of Osteoarthritis of the Knee: A Prospective, Randomized, Placebo-Controlled Trial Results of a Pilot Study," *Am. J. Sports Med.*, vol. 24, no. 1, pp. 28–34, Jan. 1996.
- [68] H. K. Kim, M. E. Moran, and R. B. Salter, "The potential for regeneration of articular cartilage in defects created by chondral shaving and subchondral abrasion. An experimental investigation in rabbits.," *J Bone Jt. Surg Am*, vol. 73, no. 9, pp. 1301–1315, Oct. 1991.
- [69] S. R. Tew, A. P. Kwan, A. Hann, B. M. Thomson, and C. W. Archer, "The reactions of articular cartilage to experimental wounding: role of apoptosis," *Arthritis Rheum.*, vol. 43, no. 1, pp. 215–225, Jan. 2000.
- [70] N. Mitchell and N. Shepard, "Effect of patellar shaving in the rabbit," *J. Orthop. Res.*, vol. 5, no. 3, pp. 388–392, Jan. 1987.
- [71] E. B. Hunziker and T. M. Quinn, "Surgical Removal of Articular Cartilage Leads to Loss of Chondrocytes from Cartilage Bordering the Wound Edge," *J Bone Jt. Surg Am*, vol. 85, no. suppl 2, pp. 85–92, Apr. 2003.
- [72] W. Tabib, P. Beaufils, J. L. Blin, J. Trémoulet, and P. Hardy, "[Arthroscopic meniscectomy with Ho-Yag laser versus mechanical meniscectomy. Mid-term results of a randomized

- prospective study of 80 meniscectomies],” *Rev. Chir. Orthopédique Réparatrice Appar. Mot.*, vol. 85, no. 7, pp. 713–721, Nov. 1999.
- [73] D. S. Menche *et al.*, “A comparison of abrasion burr arthroplasty and subchondral drilling in the treatment of full-thickness cartilage lesions in the rabbit,” *Arthrosc. J. Arthrosc. Relat. Surg.*, vol. 12, no. 3, pp. 280–286, Jun. 1996.
- [74] O. Ma, B. Cl, and M. Be, “Patellofemoral arthrosis: the treatment options,” *Am. J. Orthop. Belle Mead NJ*, vol. 27, no. 4, pp. 263–270, Apr. 1998.
- [75] “Spongialization: A New Treatment for Diseased Patellae. : Clinical Orthopaedics and Related Research,” *LWW*. [Online]. Available: [http://journals.lww.com/corr/Fulltext/1979/10000/Spongialization\\_\\_A\\_New\\_Treatment\\_for\\_Diseased.14.aspx](http://journals.lww.com/corr/Fulltext/1979/10000/Spongialization__A_New_Treatment_for_Diseased.14.aspx). [Accessed: 13-Nov-2015].
- [76] J. R. Steadman, W. G. Rodkey, K. K. Briggs, and J. J. Rodrigo, “The microfracture technique to treat full thickness articular cartilage defects of the knee,” *Orthop.*, vol. 28, no. 1, pp. 26–32, Jan. 1999.
- [77] H. A. Breinan, S. D. Martin, H. Hu-Ping, and M. Spector, “Healing of canine articular cartilage defects treated with microfracture, a type-II collagen matrix, or cultured autologous chondrocytes,” *J. Orthop. Res.*, vol. 18, no. 5, pp. 781–9, Sep. 2000.
- [78] G. Knutsen *et al.*, “Autologous Chondrocyte Implantation Compared with Microfracture in the Knee,” *J Bone Jt. Surg Am*, vol. 86, no. 3, pp. 455–464, Mar. 2004.
- [79] K. Mithoefer *et al.*, “The Microfracture Technique for the Treatment of Articular Cartilage Lesions in the Knee,” *J Bone Jt. Surg Am*, vol. 87, no. 9, pp. 1911–1920, Sep. 2005.

- [80] J. R. Steadman, W. G. Rodkey, S. B. Singleton, and K. K. Briggs, "Microfracture technique for full-thickness chondral defects: Technique and clinical results," *Oper. Tech. Orthop.*, vol. 7, no. 4, pp. 300–304, Oct. 1997.
- [81] J. R. Steadman, K. K. Briggs, J. J. Rodrigo, M. S. Kocher, T. J. Gill, and W. G. Rodkey, "Outcomes of microfracture for traumatic chondral defects of the knee: Average 11-year follow-up," *Arthrosc. J. Arthrosc. Relat. Surg.*, vol. 19, no. 5, pp. 477–484, May 2003.
- [82] G. Knutsen *et al.*, "A Randomized Trial Comparing Autologous Chondrocyte Implantation with Microfracture," *J. Bone Jt. Surg.*, vol. 89, no. 10, pp. 2105–2112, Oct. 2007.
- [83] J. D. Harris, R. A. Siston, X. Pan, and D. C. Flanigan, "Autologous Chondrocyte Implantation," *J Bone Jt. Surg Am*, vol. 92, no. 12, pp. 2220–2233, Sep. 2010.
- [84] S. M. Kurtz, E. Lau, K. Ong, K. Zhao, M. Kelly, and K. J. Bozic, "Future Young Patient Demand for Primary and Revision Joint Replacement: National Projections from 2010 to 2030," *Clin. Orthop. Relat. Res.*, vol. 467, no. 10, pp. 2606–2612, Apr. 2009.
- [85] T. Dixon, M. Shaw, S. Ebrahim, and P. Dieppe, "Trends in hip and knee joint replacement: socioeconomic inequalities and projections of need," *Ann. Rheum. Dis.*, vol. 63, no. 7, pp. 825–830, Jul. 2004.
- [86] V. Wylde, S. Hewlett, I. D. Learmonth, and P. Dieppe, "Persistent pain after joint replacement: Prevalence, sensory qualities, and postoperative determinants," *PAIN®*, vol. 152, no. 3, pp. 566–572, Mar. 2011.
- [87] G. Labek, M. Thaler, W. Janda, M. Agreiter, and B. Stöckl, "Revision rates after total joint replacement," *J Bone Jt. Surg Br*, vol. 93–B, no. 3, pp. 293–297, Mar. 2011.

- [88] C. G. Armstrong, A. S. Bahrani, and D. L. Gardner, "In vitro measurement of articular cartilage deformations in the intact human hip joint under load," *J. Bone Joint Surg. Am.*, vol. 61, no. 5, pp. 744–755, Jul. 1979.
- [89] T. Macirowski, S. Tepic, and R. W. Mann, "Cartilage stresses in the human hip joint," *J. Biomech. Eng.*, vol. 116, no. 1, pp. 10–18, Feb. 1994.
- [90] F. Eckstein, B. Lemberger, T. Stammberger, K. H. Englmeier, and M. Reiser, "Patellar cartilage deformation in vivo after static versus dynamic loading," *J. Biomech.*, vol. 33, no. 7, pp. 819–825, Jul. 2000.
- [91] F. Eckstein, M. Tieschky, S. Faber, K. H. Englmeier, and M. Reiser, "Functional analysis of articular cartilage deformation, recovery, and fluid flow following dynamic exercise in vivo," *Anat. Embryol. (Berl.)*, vol. 200, no. 4, pp. 419–424, Oct. 1999.
- [92] C. Herberhold *et al.*, "In situ measurement of articular cartilage deformation in intact femoropatellar joints under static loading," *J. Biomech.*, vol. 32, no. 12, pp. 1287–1295, Dec. 1999.
- [93] M. J. Kääh, K. Ito, J. M. Clark, and H. P. Nötzli, "Deformation of articular cartilage collagen structure under static and cyclic loading," *J. Orthop. Res.*, vol. 16, no. 6, pp. 743–751, Nov. 1998.
- [94] A. M. Ahmed and D. L. Burke, "In-Vitro of Measurement of Static Pressure Distribution in Synovial Joints—Part I: Tibial Surface of the Knee," *J. Biomech. Eng.*, vol. 105, no. 3, pp. 216–225, Aug. 1983.

- [95] T. D. Brown and D. T. Shaw, "In vitro contact stress distributions in the natural human hip," *J. Biomech.*, vol. 16, no. 6, pp. 373–384, Jan. 1983.
- [96] W. A. Hodge *et al.*, "Contact pressures from an instrumented hip endoprosthesis," *J. Bone Joint Surg. Am.*, vol. 71, no. 9, pp. 1378–1386, Oct. 1989.
- [97] L. S. Matthews, D. A. Sonstegard, and J. A. Henke, "Load bearing characteristics of the patello-femoral joint," *Acta Orthop. Scand.*, vol. 48, no. 5, pp. 511–516, 1977.
- [98] F. Shapiro, S. Koide, and M. J. Glimcher, "Cell origin and differentiation in the repair of full-thickness defects of articular cartilage," *J Bone Jt. Surg Am*, vol. 75, no. 4, pp. 532–553, Apr. 1993.
- [99] W.-J. Li *et al.*, "A three-dimensional nanofibrous scaffold for cartilage tissue engineering using human mesenchymal stem cells," *Biomaterials*, vol. 26, no. 6, pp. 599–609, Feb. 2005.
- [100] C. V. Gemmiti and R. E. Guldberg, "Fluid Flow Increases Type II Collagen Deposition and Tensile Mechanical Properties in Bioreactor-Grown Tissue-Engineered Cartilage," *Tissue Eng.*, vol. 12, no. 3, pp. 469–479, Mar. 2006.
- [101] N. J. Steinmetz and S. J. Bryant, "The effects of intermittent dynamic loading on chondrogenic and osteogenic differentiation of human marrow stromal cells encapsulated in RGD-modified poly(ethylene glycol) hydrogels," *Acta Biomater.*, vol. 7, no. 11, pp. 3829–3840, Nov. 2011.
- [102] T. Boland, T. Xu, B. Damon, and X. Cui, "Application of inkjet printing to tissue engineering," *Biotechnol. J.*, vol. 1, no. 9, pp. 910–917, Sep. 2006.

- [103] X. Cui and T. Boland, "Human microvasculature fabrication using thermal inkjet printing technology," *Biomaterials*, vol. 30, no. 31, pp. 6221–6227, Oct. 2009.
- [104] T. Xu *et al.*, "Viability and electrophysiology of neural cell structures generated by the inkjet printing method," *Biomaterials*, vol. 27, no. 19, pp. 3580–3588, Jul. 2006.
- [105] X. Cui, K. Breitenkamp, M. g. Finn, M. Lotz, and D. D. D'Lima, "Direct Human Cartilage Repair Using Three-Dimensional Bioprinting Technology," *Tissue Eng. Part A*, vol. 18, no. 11–12, pp. 1304–1312, Jun. 2012.
- [106] C. I. Fiedler *et al.*, "Enhanced mechanical properties of photo-clickable thiol–ene PEG hydrogels through repeated photopolymerization of in-swollen macromer," *Soft Matter*, vol. 12, no. 44, pp. 9095–9104, Nov. 2016.
- [107] C. Hirsch, "A contribution to the pathogenesis of chondromalacia of the patella: a physical, histologic and chemical study," Kungl. boktryckeriet, PA Norstedt & söner, 1944.
- [108] B. F. Matthews, "Composition of Articular Cartilage in Osteoarthritis," *Br. Med. J.*, vol. 2, no. 4837, pp. 660–661, Sep. 1953.
- [109] A. Maroudas, H. Muir, and J. Wingham, "The correlation of fixed negative charge with glycosaminoglycan content of human articular cartilage," *Biochim. Biophys. Acta BBA - Gen. Subj.*, vol. 177, no. 3, pp. 492–500, May 1969.
- [110] H. Muir, P. Bullough, and A. Maroudas, "The Distribution of Collagen in Human Articular Cartilage with Some of Its Physiological Implications," *Bone Jt. J.*, vol. 52–B, no. 3, pp. 554–563, Aug. 1970.
- [111] L. Sokoloff, *The Joints and Synovial Fluid*. Academic Press, 2014.



- [112] Y. H. An and H. E. Gruber, "Introduction to Experimental Bone and Cartilage Histology," in *Handbook of Histology Methods for Bone and Cartilage*, Y. H. A. MD and K. L. M. BSc, Eds. Humana Press, 2003, pp. 3–31.
- [113] J. C. Y. Hu and K. A. Athanasiou, "Structure and Function of Articular Cartilage," in *Handbook of Histology Methods for Bone and Cartilage*, Y. H. A. MD and K. L. M. BSc, Eds. Humana Press, 2003, pp. 73–95.
- [114] N. Schmitz, S. Laverty, V. B. Kraus, and T. Aigner, "Basic methods in histopathology of joint tissues," *Osteoarthritis Cartilage*, vol. 18, Supplement 3, pp. S113–S116, Oct. 2010.
- [115] L. C. U. Junqueira, G. Bignolas, and R. R. Brentani, "Picrosirius staining plus polarization microscopy, a specific method for collagen detection in tissue sections," *Histochem. J.*, vol. 11, no. 4, pp. 447–455, Jul. 1979.
- [116] A. R. Poole, I. Pidoux, A. Reiner, L. H. Tang, H. Choi, and L. Rosenberg, "Localization of proteoglycan monomer and link protein in the matrix of bovine articular cartilage: An immunohistochemical study.," *J. Histochem. Cytochem.*, vol. 28, no. 7, pp. 621–635, Jul. 1980.
- [117] R. Hagg, P. Bruckner, and E. Hedbom, "Cartilage Fibrils of Mammals are Biochemically Heterogeneous: Differential Distribution of Decorin and Collagen IX," *J. Cell Biol.*, vol. 142, no. 1, pp. 285–294, Jul. 1998.
- [118] T. Douglas, S. Heinemann, S. Bierbaum, D. Scharnweber, and H. Worch, "Fibrillogenesis of Collagen Types I, II, and III with Small Leucine-Rich Proteoglycans Decorin and Biglycan," *Biomacromolecules*, vol. 7, no. 8, pp. 2388–2393, Aug. 2006.

- [119] E. Georgiou, T. Theodossiou, V. Hovhannisyan, K. Politopoulos, G. S. Rapti, and D. Yova, "Second and third optical harmonic generation in type I collagen, by nanosecond laser irradiation, over a broad spectral region," *Opt. Commun.*, vol. 176, no. 1–3, pp. 253–260, Mar. 2000.
- [120] M.-A. Houle *et al.*, "Analysis of forward and backward Second Harmonic Generation images to probe the nanoscale structure of collagen within bone and cartilage," *J. Biophotonics*, vol. 8, no. 11–12, pp. 993–1001, Nov. 2015.
- [121] O. del Barco and J. M. Bueno, "Second harmonic generation signal in collagen fibers: role of polarization, numerical aperture, and wavelength," *J. Biomed. Opt.*, vol. 17, no. 4, pp. 0450051–0450058, 2012.
- [122] E. Werkmeister, N. De Isla, P. Netter, J.-F. Stoltz, and D. Dumas, "Collagenous Extracellular Matrix of Cartilage Submitted to Mechanical Forces Studied by Second Harmonic Generation Microscopy," *Photochem. Photobiol.*, vol. 86, no. 2, pp. 302–310, Mar. 2010.
- [123] A. T. Yeh *et al.*, "Nonlinear optical microscopy of articular cartilage," *Osteoarthritis Cartilage*, vol. 13, no. 4, pp. 345–352, Apr. 2005.
- [124] N. Colthup, *Introduction to Infrared and Raman Spectroscopy*. Elsevier, 2012.
- [125] A. Bonifacio *et al.*, "Chemical imaging of articular cartilage sections with Raman mapping, employing uni- and multi-variate methods for data analysis," *The Analyst*, vol. 135, no. 12, p. 3193, 2010.

- [126] M. Kazanci, P. Roschger, E. P. Paschalis, K. Klaushofer, and P. Fratzl, "Bone osteonal tissues by Raman spectral mapping: Orientation–composition," *J. Struct. Biol.*, vol. 156, no. 3, pp. 489–496, Dec. 2006.
- [127] S. Gamsjaeger *et al.*, "Cortical bone composition and orientation as a function of animal and tissue age in mice by Raman spectroscopy," *Bone*, vol. 47, no. 2, pp. 392–399, Aug. 2010.
- [128] A. J. Makowski, C. A. Patil, A. Mahadevan-Jansen, and J. S. Nyman, "Polarization control of Raman spectroscopy optimizes the assessment of bone tissue," *J. Biomed. Opt.*, vol. 18, no. 5, pp. 055005–055005, 2013.
- [129] E. Bär, "Elastizitätsprüfungen der Gelenkknorpel," *Wilhelm Roux Arch. Für Entwicklungsmechanik Org.*, vol. 108, no. 4, pp. 739–760, Dec. 1926.
- [130] E. Gocke, "Elastizitätsstudien am jungen und alten gelenkknorpel," *Verhundl Dtsch. Orthop Ges*, vol. 22, pp. 130–147, 1927.
- [131] G. E. Kempson, M. A. R. Freeman, and S. A. V. Swanson, "The determination of a creep modulus for articular cartilage from indentation tests on the human femoral head," *J. Biomech.*, vol. 4, no. 4, pp. 239–250, Jul. 1971.
- [132] J. M. Coletti, W. H. Akeson, and S. L.-Y. Woo, "A Comparison of the Physical Behavior of Normal Articular Cartilage and the Arthroplasty Surface," *J Bone Jt. Surg Am*, vol. 54, no. 1, pp. 147–160, Jan. 1972.
- [133] K. A. Athanasiou, A. Agarwal, and F. J. Dzida, "Comparative study of the intrinsic mechanical properties of the human acetabular and femoral head cartilage," *J. Orthop. Res. Off. Publ. Orthop. Res. Soc.*, vol. 12, no. 3, pp. 340–349, May 1994.

- [134] M. S. Laasanen *et al.*, "Biomechanical properties of knee articular cartilage," *Biorheology*, vol. 40, no. 1,2,3, pp. 133–140, Jan. 2003.
- [135] V. C. Mow and X. E. Guo, "MECHANO-ELECTROCHEMICAL PROPERTIES OF ARTICULAR CARTILAGE: Their Inhomogeneities and Anisotropies," *Annu. Rev. Biomed. Eng.*, vol. 4, no. 1, pp. 175–209, 2002.
- [136] V. C. Mow, M. H. Holmes, and W. Michael Lai, "Fluid transport and mechanical properties of articular cartilage: A review," *J. Biomech.*, vol. 17, no. 5, pp. 377–394, Jan. 1984.
- [137] R. H. Pritchard, P. Lava, D. Debruyne, and E. M. Terentjev, "Precise determination of the Poisson ratio in soft materials with 2D digital image correlation," *Soft Matter*, vol. 9, no. 26, p. 6037, 2013.
- [138] E. M. C. Jones, M. N. Silberstein, S. R. White, and N. R. Sottos, "In Situ Measurements of Strains in Composite Battery Electrodes during Electrochemical Cycling," *Exp. Mech.*, vol. 54, no. 6, pp. 971–985, Jul. 2014.
- [139] J. T. Henderson, G. Shannon, A. I. Veress, and C. P. Neu, "Direct Measurement of Intranuclear Strain Distributions and RNA Synthesis in Single Cells Embedded within Native Tissue," *Biophys. J.*, vol. 105, no. 10, pp. 2252–2261, Nov. 2013.
- [140] H. Hertz, "On the contact of elastic solids," *J Reine Angew Math*, vol. 92, no. 110, pp. 156–171, 1881.
- [141] H. Hertz, "On hardness," *Verh Ver Beförd. Gewerbe Fleisses*, vol. 61, p. 410, 1882.

- [142] W. c. Oliver and G. m. Pharr, "An improved technique for determining hardness and elastic modulus using load and displacement sensing indentation experiments," *J. Mater. Res.*, vol. 7, no. 06, pp. 1564–1583, 1992.
- [143] W. c. Oliver and G. m. Pharr, *J. Mater. Res.*, vol. 19, no. 01, pp. 3–20, 2004.
- [144] A. C. Fischer-Cripps, "Contact Mechanics," in *Nanoindentation*, Springer New York, 2011, pp. 1–19.
- [145] M. Galli, E. Fornasiere, J. Cugnoni, and M. L. Oyen, "Poroviscoelastic characterization of particle-reinforced gelatin gels using indentation and homogenization," *J. Mech. Behav. Biomed. Mater.*, vol. 4, no. 4, pp. 610–617, May 2011.
- [146] E. G. Herbert, P. Sudharshan Phani, and K. E. Johanns, "Nanoindentation of viscoelastic solids: A critical assessment of experimental methods," *Curr. Opin. Solid State Mater. Sci.*, vol. 19, no. 6, pp. 334–339, Dec. 2015.
- [147] J. M. Mattice, A. G. Lau, M. L. Oyen, and R. W. Kent, "Spherical indentation load-relaxation of soft biological tissues," *J. Mater. Res.*, vol. 21, no. 08, pp. 2003–2010, 2006.
- [148] E. D. Bonnevie, V. J. Baro, L. Wang, and D. L. Burris, "In Situ Studies of Cartilage Microtribology: Roles of Speed and Contact Area," *Tribol. Lett.*, vol. 41, no. 1, pp. 83–95, Sep. 2010.
- [149] A. C. Moore and D. L. Burris, "An analytical model to predict interstitial lubrication of cartilage in migrating contact areas," *J. Biomech.*, vol. 47, no. 1, pp. 148–153, Jan. 2014.
- [150] L. Sokoloff, "Elasticity of articular cartilage: effect of ions and viscous solutions," *Science*, vol. 141, no. 3585, pp. 1055–1057, 1963.

- [151] L. Sokoloff, "Elasticity of aging cartilage.," in *Federation proceedings*, 1965, vol. 25, pp. 1089–1095.
- [152] R. Chadwick, "Axisymmetric Indentation of a Thin Incompressible Elastic Layer," *SIAM J. Appl. Math.*, vol. 62, no. 5, pp. 1520–1530, Jan. 2002.
- [153] E. K. Dimitriadis, F. Horkay, J. Maresca, B. Kachar, and R. S. Chadwick, "Determination of Elastic Moduli of Thin Layers of Soft Material Using the Atomic Force Microscope," *Biophys. J.*, vol. 82, no. 5, pp. 2798–2810, May 2002.
- [154] M. V. Swain and J. Menčík, "Mechanical property characterization of thin films using spherical tipped indenters," *Thin Solid Films*, vol. 253, no. 1, pp. 204–211, Dec. 1994.
- [155] R. Saha and W. D. Nix, "Effects of the substrate on the determination of thin film mechanical properties by nanoindentation," *Acta Mater.*, vol. 50, no. 1, pp. 23–38, Jan. 2002.
- [156] M. L. Oyen, R. F. Cook, J. A. Emerson, and N. R. Moody, "Indentation responses of time-dependent films on stiff substrates," *J. Mater. Res.*, vol. 19, no. 08, pp. 2487–2497, Aug. 2004.
- [157] D. M. Ebenstein and L. A. Pruitt, "Nanoindentation of biological materials," *Nano Today*, vol. 1, no. 3, pp. 26–33, Aug. 2006.
- [158] C. Li, L. A. Pruitt, and K. B. King, "Nanoindentation differentiates tissue-scale functional properties of native articular cartilage," *J. Biomed. Mater. Res. A*, vol. 78A, no. 4, pp. 729–738, 2006.
- [159] O. Franke *et al.*, "Mechanical properties of hyaline and repair cartilage studied by nanoindentation," *Acta Biomater.*, vol. 3, no. 6, pp. 873–881, Nov. 2007.

- [160] D. M. Ebenstein, A. Kuo, J. J. Rodrigo, A. H. Reddi, M. Ries, and L. Pruitt, "A nanoindentation technique for functional evaluation of cartilage repair tissue," *J. Mater. Res.*, vol. 19, no. 01, pp. 273–281, 2004.
- [161] S. Gupta, J. Lin, P. Ashby, and L. Pruitt, "A fiber reinforced poroelastic model of nanoindentation of porcine costal cartilage: A combined experimental and finite element approach," *J. Mech. Behav. Biomed. Mater.*, vol. 2, no. 4, pp. 326–338, Aug. 2009.
- [162] M. Taffetani, M. Griebel, D. Gastaldi, S. M. Klisch, and P. Vena, "Poroviscoelastic finite element model including continuous fiber distribution for the simulation of nanoindentation tests on articular cartilage," *J. Mech. Behav. Biomed. Mater.*, vol. 32, pp. 17–30, Apr. 2014.
- [163] O. Franke, M. Göken, M. A. Meyers, K. Durst, and A. M. Hodge, "Dynamic nanoindentation of articular porcine cartilage," *Mater. Sci. Eng. C*, vol. 31, no. 4, pp. 789–795, May 2011.
- [164] M. Taffetani, R. Gottardi, D. Gastaldi, R. Raiteri, and P. Vena, "Poroelastic response of articular cartilage by nanoindentation creep tests at different characteristic lengths," *Med. Eng. Phys.*, vol. 36, no. 7, pp. 850–858, Jul. 2014.
- [165] B. Doyran *et al.*, "Nanoindentation modulus of murine cartilage: a sensitive indicator of the initiation and progression of post-traumatic osteoarthritis," *Osteoarthr. Cartil. OARS Osteoarthr. Res. Soc.*, Aug. 2016.
- [166] G. Binnig, C. F. Quate, and C. Gerber, "Atomic Force Microscope," *Phys. Rev. Lett.*, vol. 56, no. 9, pp. 930–933, Mar. 1986.
- [167] W. Zhong, G. Overney, and D. Tománek, "Limits of Resolution in Atomic Force Microscopy Images of Graphite," *EPL Europhys. Lett.*, vol. 15, no. 1, p. 49, 1991.

- [168] I. N. Sneddon, "The relation between load and penetration in the axisymmetric boussinesq problem for a punch of arbitrary profile," *Int. J. Eng. Sci.*, vol. 3, no. 1, pp. 47–57, May 1965.
- [169] P. KUMAR *et al.*, "Role of uppermost superficial surface layer of articular cartilage in the lubrication mechanism of joints," *J. Anat.*, vol. 199, no. Pt 3, pp. 241–250, Sep. 2001.
- [170] M. Loparic *et al.*, "Micro- and Nanomechanical Analysis of Articular Cartilage by Indentation-Type Atomic Force Microscopy: Validation with a Gel-Microfiber Composite," *Biophys. J.*, vol. 98, no. 11, pp. 2731–2740, Jun. 2010.
- [171] H. T. Nia *et al.*, "High-Bandwidth AFM-Based Rheology Reveals that Cartilage is Most Sensitive to High Loading Rates at Early Stages of Impairment," *Biophys. J.*, vol. 104, no. 7, pp. 1529–1537, Apr. 2013.
- [172] J. R. Willis, "Hertzian contact of anisotropic bodies," *J. Mech. Phys. Solids*, vol. 14, no. 3, pp. 163–176, May 1966.
- [173] V. A. Sveklo, "Boussinesq type problems for the anisotropic half-space," *J. Appl. Math. Mech.*, vol. 28, no. 5, pp. 1099–1105, Jan. 1964.
- [174] D. Shi, Y. Lin, and T. C. Ovaert, "Indentation of an Orthotropic Half-Space by a Rigid Ellipsoidal Indenter," *J. Tribol.*, vol. 125, no. 2, pp. 223–231, Mar. 2003.
- [175] J. G. Swadener, J.-Y. Rho, and G. M. Pharr, "Effects of anisotropy on elastic moduli measured by nanoindentation in human tibial cortical bone," *J. Biomed. Mater. Res.*, vol. 57, no. 1, pp. 108–112, Oct. 2001.



- [176] J. G. Swadener and G. M. Pharr, "Indentation of elastically anisotropic half-spaces by cones and parabolae of revolution," *Philos. Mag. A*, vol. 81, no. 2, pp. 447–466, Feb. 2001.
- [177] J. B. Choi *et al.*, "Zonal changes in the three-dimensional morphology of the chondron under compression: The relationship among cellular, pericellular, and extracellular deformation in articular cartilage," *J. Biomech.*, vol. 40, no. 12, pp. 2596–2603, 2007.
- [178] "Alterations in the permeability of articular cartilage by proteolytic enzymes - Lotke - 1972 - Arthritis & Rheumatology - Wiley Online Library." [Online]. Available: <http://onlinelibrary.wiley.com/doi/10.1002/art.1780150312/abstract>. [Accessed: 06-Aug-2016].
- [179] D. D. Chan, L. Cai, K. D. Butz, S. B. Trippel, E. A. Nauman, and C. P. Neu, "In vivo articular cartilage deformation: noninvasive quantification of intratissue strain during joint contact in the human knee," *Sci. Rep.*, vol. 6, Jan. 2016.
- [180] W. Kim, V. L. Ferguson, M. Borden, and C. P. Neu, "Application of Elastography for the Noninvasive Assessment of Biomechanics in Engineered Biomaterials and Tissues," *Ann. Biomed. Eng.*, vol. 44, no. 3, pp. 705–724, Mar. 2016.
- [181] D. J. Griffin, J. Vicari, M. R. Buckley, J. L. Silverberg, I. Cohen, and L. J. Bonassar, "Effects of enzymatic treatments on the depth-dependent viscoelastic shear properties of articular cartilage," *J. Orthop. Res.*, vol. 32, no. 12, pp. 1652–1657, Dec. 2014.
- [182] A. F. Mak, "The Apparent Viscoelastic Behavior of Articular Cartilage—The Contributions From the Intrinsic Matrix Viscoelasticity and Interstitial Fluid Flows," *J. Biomech. Eng.*, vol. 108, no. 2, pp. 123–130, May 1986.

- [183] W. Wilson, C. C. van Donkelaar, B. van Rietbergen, K. Ito, and R. Huiskes, "Stresses in the local collagen network of articular cartilage: a poroviscoelastic fibril-reinforced finite element study," *J. Biomech.*, vol. 37, no. 3, pp. 357–366, Mar. 2004.
- [184] V. L. Ferguson, A. J. Bushby, and A. Boyde, "Nanomechanical properties and mineral concentration in articular calcified cartilage and subchondral bone," *J. Anat.*, vol. 203, no. 2, pp. 191–202, Aug. 2003.
- [185] H. S. Gupta *et al.*, "Two different correlations between nanoindentation modulus and mineral content in the bone–cartilage interface," *J. Struct. Biol.*, vol. 149, no. 2, pp. 138–148, Feb. 2005.
- [186] M. S. Bergholt *et al.*, "Raman Spectroscopy Reveals New Insights into the Zonal Organization of Native and Tissue-Engineered Articular Cartilage," *ACS Cent. Sci.*, vol. 2, no. 12, pp. 885–895, Dec. 2016.
- [187] Y. C. Fung and P. Tong, *Classical and Computational Solid Mechanics*. World Scientific Publishing Co Inc, 2001.
- [188] D. G. T. Strange, T. L. Fletcher, K. Tonsomboon, H. Brawn, X. Zhao, and M. L. Oyen, "Separating poroviscoelastic deformation mechanisms in hydrogels," *Appl. Phys. Lett.*, vol. 102, no. 3, p. 031913, Jan. 2013.
- [189] A. Maroudas and M. Venn, "Chemical composition and swelling of normal and osteoarthrotic femoral head cartilage. II. Swelling.," *Ann. Rheum. Dis.*, vol. 36, no. 5, pp. 399–406, Oct. 1977.

- [190] A. Bashir, M. L. Gray, and D. Burstein, "Gd-DTPA2- as a measure of cartilage degradation," *Magn. Reson. Med.*, vol. 36, no. 5, pp. 665–673, Nov. 1996.
- [191] P. Bullough and J. Goodfellow, "The Significance of the Fine Structure of Articular Cartilage," *Bone Jt. J.*, vol. 50–B, no. 4, pp. 852–857, Nov. 1968.
- [192] S. Guo and B. B. Akhremitchev, "Packing Density and Structural Heterogeneity of Insulin Amyloid Fibrils Measured by AFM Nanoindentation," *Biomacromolecules*, vol. 7, no. 5, pp. 1630–1636, May 2006.
- [193] "Calibration of atomic-force microscope tips," *Rev. Sci. Instrum.*, vol. 64, no. 7, pp. 1868–1873, Jul. 1993.
- [194] L. K. Agbezuge and H. Deresiewicz, "On the indentation of a consolidating half-space," *Isr J Technol*, vol. 12, pp. 322–338, 1974.
- [195] J. S. Jurvelin, M. D. Buschmann, and E. B. Hunziker, "Optical and mechanical determination of poisson's ratio of adult bovine humeral articular cartilage," *J. Biomech.*, vol. 30, no. 3, pp. 235–241, Mar. 1997.
- [196] P. Kiviranta, J. Rieppo, R. K. Korhonen, P. Julkunen, J. Töyräs, and J. S. Jurvelin, "Collagen network primarily controls Poisson's ratio of bovine articular cartilage in compression," *J. Orthop. Res.*, vol. 24, no. 4, pp. 690–699, Apr. 2006.
- [197] A. R. Gannon, T. Nagel, A. P. Bell, N. C. Avery, and D. J. Kelly, "The changing role of the superficial region in determining the dynamic compressive properties of articular cartilage during postnatal development," *Osteoarthr. Cartil. OARS Osteoarthr. Res. Soc.*, vol. 23, no. 6, pp. 975–984, Jun. 2015.

- [198] A. Lawrence, X. Xu, M. D. Bible, S. Calve, C. P. Neu, and A. Panitch, "Synthesis and characterization of a lubricin mimic (mLub) to reduce friction and adhesion on the articular cartilage surface," *Biomaterials*, vol. 73, pp. 42–50, Dec. 2015.
- [199] H. J. Mankin, H. Dorfman, L. Lippiello, and A. Zarins, "Biochemical and metabolic abnormalities in articular cartilage from osteo-arthritic human hips. II. Correlation of morphology with biochemical and metabolic data," *J. Bone Joint Surg. Am.*, vol. 53, no. 3, pp. 523–537, Apr. 1971.
- [200] A. Bashir, M. L. Gray, J. Hartke, and D. Burstein, "Nondestructive imaging of human cartilage glycosaminoglycan concentration by MRI," *Magn. Reson. Med.*, vol. 41, no. 5, pp. 857–865, May 1999.
- [201] A. Williams, L. Sharma, C. A. McKenzie, P. V. Prasad, and D. Burstein, "Delayed gadolinium-enhanced magnetic resonance imaging of cartilage in knee osteoarthritis: findings at different radiographic stages of disease and relationship to malalignment," *Arthritis Rheum.*, vol. 52, no. 11, pp. 3528–3535, Nov. 2005.
- [202] J. Kastelic, A. Galeski, and E. Baer, "The Multicomposite Structure of Tendon," *Connect. Tissue Res.*, vol. 6, no. 1, pp. 11–23, Jan. 1978.
- [203] N. M. Hancox, *Biology of Bone*. CUP Archive, 1972.
- [204] U. G. K. Wegst, H. Bai, E. Saiz, A. P. Tomsia, and R. O. Ritchie, "Bioinspired structural materials," *Nat. Mater.*, vol. 14, no. 1, pp. 23–36, Jan. 2015.

- [205] E. B. Hunziker, T. M. Quinn, and H.-J. Häuselmann, "Quantitative structural organization of normal adult human articular cartilage," *Osteoarthritis Cartilage*, vol. 10, no. 7, pp. 564–572, Jul. 2002.
- [206] A. j. Bushby, V. I. Ferguson, and A. Boyde, "Nanoindentation of bone: Comparison of specimens tested in liquid and embedded in polymethylmethacrylate," *J. Mater. Res.*, vol. 19, no. 01, pp. 249–259, Jan. 2004.
- [207] J.-Y. Rho, L. Kuhn-Spearing, and P. Zioupos, "Mechanical properties and the hierarchical structure of bone," *Med. Eng. Phys.*, vol. 20, no. 2, pp. 92–102, Mar. 1998.
- [208] R. C. Paietta, S. E. Campbell, and V. L. Ferguson, "Influences of spherical tip radius, contact depth, and contact area on nanoindentation properties of bone," *J. Biomech.*, vol. 44, no. 2, pp. 285–290, Jan. 2011.
- [209] M. L. Oyen, V. L. Ferguson, A. K. Bembey, A. J. Bushby, and A. Boyde, "Composite bounds on the elastic modulus of bone," *J. Biomech.*, vol. 41, no. 11, pp. 2585–2588, Aug. 2008.
- [210] D. W. Hutmacher, "Scaffolds in tissue engineering bone and cartilage," *Biomaterials*, vol. 21, no. 24, pp. 2529–2543, Dec. 2000.
- [211] A. Maroudas, "Balance between swelling pressure and collagen tension in normal and degenerate cartilage," *Nature*, vol. 260, no. 5554, pp. 808–809, Apr. 1976.
- [212] M. M. Chui, R. J. Phillips, and M. J. McCarthy, "Measurement of the Porous Microstructure of Hydrogels by Nuclear Magnetic Resonance," *J. Colloid Interface Sci.*, vol. 174, no. 2, pp. 336–344, Sep. 1995.

- [213] J. A. Greenwood, K. L. Johnson, and E. Matsubara, "A surface roughness parameter in Hertz contact," *Wear*, vol. 100, no. 1, pp. 47–57, Dec. 1984.
- [214] S. A. Chizhik, K. Wierzcholski, A. V. Trushko, M. A. Zhytkova, and A. Miszczak, "Properties of Cartilage on Micro- and Nanolevel," *Adv. Tribol.*, vol. 2010, p. e243150, Jan. 2011.
- [215] J. A. Wahlquist *et al.*, "Indentation Mapping Reveals Poroelastic, but not Viscoelastic, Properties Spanning Native Zonal Articular Cartilage," *Rev.*, 2017.
- [216] J. A. Greenwood and J. B. P. Williamson, "Contact of Nominally Flat Surfaces," *Proc. R. Soc. Lond. Math. Phys. Eng. Sci.*, vol. 295, no. 1442, pp. 300–319, Dec. 1966.
- [217] J. A. Greenwood and J. H. Tripp, "The Elastic Contact of Rough Spheres," *J. Appl. Mech.*, vol. 34, no. 1, pp. 153–159, Mar. 1967.
- [218] S. M. T. Chan, C. P. Neu, G. DuRaine, K. Komvopoulos, and A. H. Reddi, "Atomic force microscope investigation of the boundary-lubricant layer in articular cartilage," *Osteoarthritis Cartilage*, vol. 18, no. 7, pp. 956–963, Jul. 2010.
- [219] C. Walter, T. Antretter, R. Daniel, and C. Mitterer, "Finite element simulation of the effect of surface roughness on nanoindentation of thin films with spherical indenters," *Surf. Coat. Technol.*, vol. 202, no. 4–7, pp. 1103–1107, Dec. 2007.
- [220] M. Stevanovic, M. M. Yovanovich, and J. R. Culham, "Modeling contact between rigid sphere and elastic layer bonded to rigid substrate," *IEEE Trans. Compon. Packag. Technol.*, vol. 24, no. 2, pp. 207–212, Jun. 2001.

- [221] J. G. Swadener, E. P. George, and G. M. Pharr, "The correlation of the indentation size effect measured with indenters of various shapes," *J. Mech. Phys. Solids*, vol. 50, no. 4, pp. 681–694, Apr. 2002.
- [222] T. S. Atkinson, R. C. Haut, and N. J. Altiero, "Impact-Induced Fissuring of Articular Cartilage: An Investigation of Failure Criteria," *J. Biomech. Eng.*, vol. 120, no. 2, pp. 181–187, Apr. 1998.
- [223] C.-T. Chen, N. Burton-Wurster, C. Borden, K. Hueffer, S. E. Bloom, and G. Lust, "Chondrocyte necrosis and apoptosis in impact damaged articular cartilage," *J. Orthop. Res.*, vol. 19, no. 4, pp. 703–711, Jul. 2001.
- [224] J. L. Lewis, L. B. Deloria, M. Oyen-Tiesma, R. C. Thompson, M. Ericson, and T. R. Oegema, "Cell death after cartilage impact occurs around matrix cracks," *J. Orthop. Res.*, vol. 21, no. 5, pp. 881–887, Sep. 2003.
- [225] W. R. Jones, H. Ping Ting-Beall, G. M. Lee, S. S. Kelley, R. M. Hochmuth, and F. Guilak, "Alterations in the Young's modulus and volumetric properties of chondrocytes isolated from normal and osteoarthritic human cartilage," *J. Biomech.*, vol. 32, no. 2, pp. 119–127, Feb. 1999.
- [226] U. Pohl, J. Holtz, R. Busse, and E. Bassenge, "Crucial role of endothelium in the vasodilator response to increased flow in vivo," *Hypertens. Dallas Tex 1979*, vol. 8, no. 1, pp. 37–44, Jan. 1986.
- [227] S. S. Margulies and L. E. Thibault, "A proposed tolerance criterion for diffuse axonal injury in man," *J. Biomech.*, vol. 25, no. 8, pp. 917–923, Aug. 1992.

- [228] R. J. Lories and F. P. Luyten, "The bone–cartilage unit in osteoarthritis," *Nat. Rev. Rheumatol.*, vol. 7, no. 1, pp. 43–49, Jan. 2011.
- [229] S. R. Goldring and M. B. Goldring, "Changes in the osteochondral unit during osteoarthritis: structure, function and cartilage-bone crosstalk," *Nat. Rev. Rheumatol.*, vol. 12, no. 11, pp. 632–644, Nov. 2016.
- [230] V. C. Mow and X. E. Guo, "Mechano-Electrochemical Properties Of Articular Cartilage: Their Inhomogeneities and Anisotropies," *Annu. Rev. Biomed. Eng.*, vol. 4, no. 1, pp. 175–209, 2002.
- [231] L. C. Hughes, C. W. Archer, and I. ap Gwynn, "The ultrastructure of mouse articular cartilage: collagen orientation and implications for tissue functionality. A polarised light and scanning electron microscope study and review," *Eur. Cell. Mater.*, vol. 9, pp. 68–84, 2005.
- [232] J. A. Wahlquist, X. Xu, F. W. DelRio, M. A. Randolph, C. P. Neu, and V. L. Ferguson, "The influence of contact radius on the indentation response of poroelastic materials," *Rev.*, 2017.
- [233] P. L. Mente and J. L. Lewis, "Elastic modulus of calcified cartilage is an order of magnitude less than that of subchondral bone," *J. Orthop. Res.*, vol. 12, no. 5, pp. 637–647, Sep. 1994.
- [234] S. Akizuki, V. C. Mow, F. Müller, J. C. Pita, D. S. Howell, and D. H. Manicourt, "Tensile properties of human knee joint cartilage: I. Influence of ionic conditions, weight bearing, and fibrillation on the tensile modulus," *J. Orthop. Res.*, vol. 4, no. 4, pp. 379–392, Jan. 1986.
- [235] R. R. Regatte, S. V. S. Akella, J. h. Lonner, J. b. Kneeland, and R. Reddy, "T1 $\rho$  relaxation mapping in human osteoarthritis (OA) cartilage: Comparison of T1 $\rho$  with T2," *J. Magn. Reson. Imaging*, vol. 23, no. 4, pp. 547–553, Apr. 2006.



- [236] C. A. Schneider, W. S. Rasband, and K. W. Eliceiri, "NIH Image to ImageJ: 25 years of image analysis," *Nat. Methods*, vol. 9, no. 7, pp. 671–675, Jul. 2012.
- [237] D. S. S. Joseph E. Jakes, "The edge effect in nanoindentation," *Philos. Mag.*, vol. 91, no. 7–9, pp. 1387–1399, 2011.
- [238] R. M. Schinagl, D. Gurskis, A. C. Chen, and R. L. Sah, "Depth-dependent confined compression modulus of full-thickness bovine articular cartilage," *J. Orthop. Res.*, vol. 15, no. 4, pp. 499–506, 1997.
- [239] A. Benninghoff, "Form und Bau der Gelenkknorpel in ihren Beziehungen zur Funktion," *Z. Für Zellforsch. Mikrosk. Anat.*, vol. 2, no. 5, pp. 783–862, Nov. 1925.
- [240] G. Franzoso and P. K. Zysset, "Elastic anisotropy of human cortical bone secondary osteons measured by nanoindentation," *J. Biomech. Eng.*, vol. 131, no. 2, p. 021001, 2009.
- [241] A. R. Gannon, T. Nagel, and D. J. Kelly, "The role of the superficial region in determining the dynamic properties of articular cartilage," *Osteoarthritis Cartilage*, vol. 20, no. 11, pp. 1417–1425, Nov. 2012.